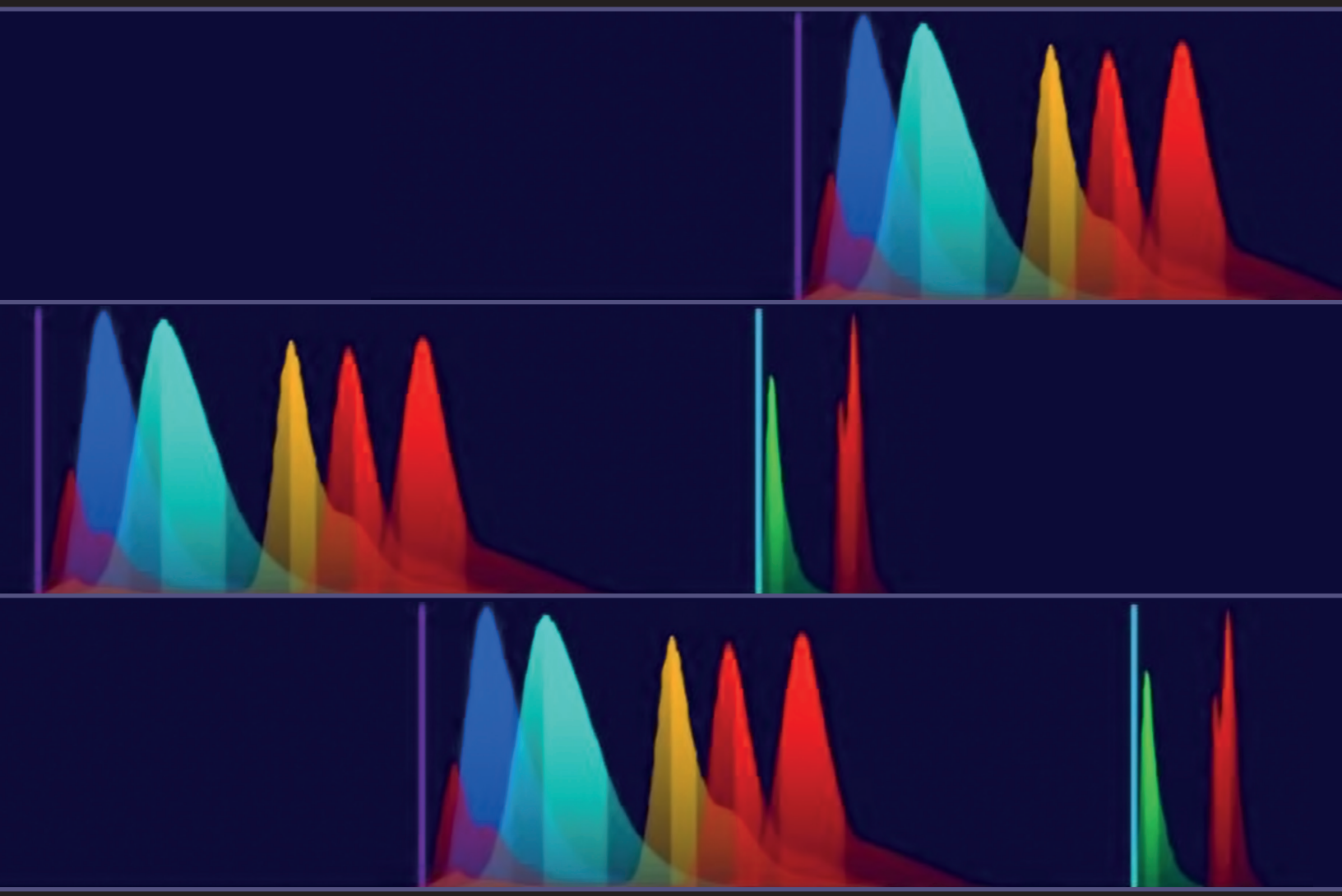

Demystifying Panel Design
for Immunophenotyping

ARTICLE COLLECTION

WILEY

CURRENT PROTOCOLS
A Wiley Brand

Cytometry PART A
ISAC
Journal of Quantitative Cell Science

Sponsored by:
ThermoFisher SCIENTIFIC
The world leader in serving science

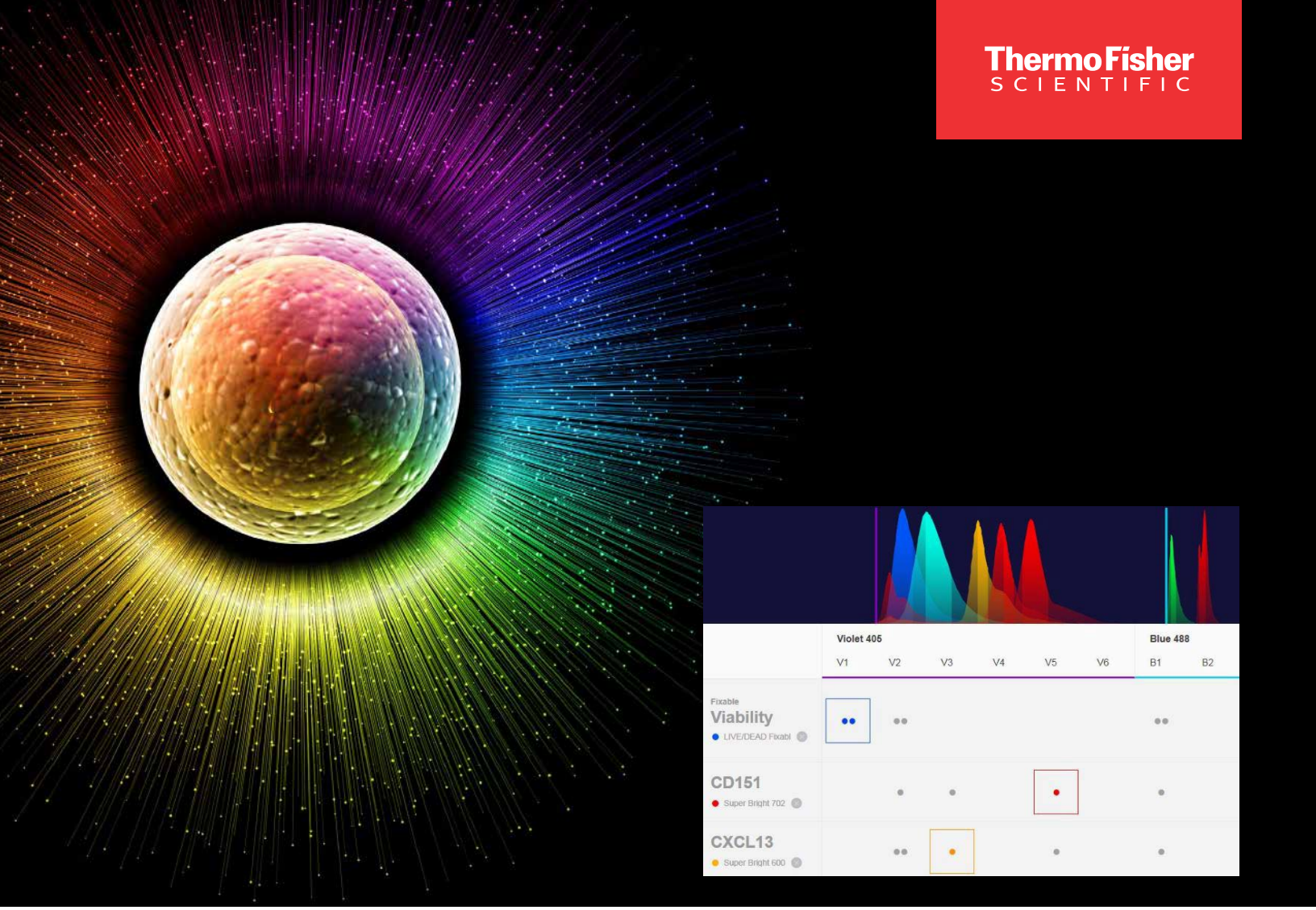

The flow cytometry panel builder

Empowering spectral flow cytometry solutions for life science researchers

Enable your multicolor flow cytometry with the Invitrogen™ Flow Cytometry Panel Builder.

With this tool, you can:

- Create a new immunophenotyping experiment or add antibodies and reagents to an older panel
- Insert antibodies already used in your experiment
- View fluorochrome spectra to quantify emission spectral overlap
- Export a Microsoft™ Excel™ document with your antibody choices or order directly

Build your custom panel now at **thermofisher.com/spectral**

invitrogen

Contents

Introduction

BY JEREMY PETRAVICZ, PH.D., EDITOR, *CURRENT PROTOCOLS*

Few things in the world of flow cytometry can appear more daunting to the novice user than the design of immunophenotyping panels for use in their experiments. A flow cytometry panel can be defined as a collection of fluorescent dyes and/or antibody markers designed to identify the types of cells present in an experimental sample. For example, if a researcher wants to distinguish various types of immune cells that are activated in response to a drug treatment, a panel can be designed to distinguish major cell types such as T- or B-cells, NK cells or macrophages. With advances in flow cytometry such as spectral flow cytometry and the wide range of fluorophores available to researchers, that same panel could be redesigned or optimized to now identify subpopulations of cells or various states of activation to increase the depth of information acquired. However, the task of determining what markers to employ and how to optimize them for detection of the cell types of interest and in some cases their biological state can seem overwhelming.

The creation of an optimized flow cytometry panel must consider several factors during its formulation. Knowing the biological question at hand and the cell types to be tested, the type of equipment that will be employed (conventional versus spectral flow cytometer), the properties of the available fluorophores (full spectra, brightness), and prevalence of individual cellular markers (high versus low abundance) all factor into the design and optimization of the panel. To aid researchers and demystify the process we have assembled this article collection, along with online resources, as a primer on effective immunophenotyping panel design from conception to optimization.

Our initial two articles appeared in *Current Protocols*. First, Ferrer-Font et al (2020) provides an overview and step-by-step guide to the design processes and critical parameters to be considered during panel creation. While the focus of the discussion is on panel design for spectral flow cytometry, the principles outlined can be applied to conventional flow cytometry as well. Following is Tembhare et al (2017) describing a procedure for creating a panel to screen samples for resident immunophenotypes and DNA-ploidy identification simultaneously.

Our remaining articles each detail the construction and validation of optimized multicolor immunofluorescence panels (OMIPs) as published in the journal *Cytometry Part A*, allowing the reader to see the principles of panel design in action. We begin with Payne et al (2020) that describes a 28-color panel to screen lymphocyte subsets in human peripheral blood mononuclear cells. The panel was designed to reduce repeated sample runs across multiple panels down to one panel, but still have high immunophenotyping resolution. Next, Hertoghs et al (2020) presents a 27-color panel for identifying changes in immune cell populations during an immunization and challenge regimen for malaria vaccine development. Third, Ohne et al (2020) describes a 14-color panel to identify the presence and activation status of innate lymphoid cell (ILC) subsets from human peripheral blood and tonsillar cells. Lastly, Nogimori et al (2021) presents a 31-color panel to simultaneously immunophenotype multiple cell populations including, but not limited to, T-cells, B-cells, NK cells and dendritic cells. This panel was specifically designed to identify subpopulations as well as allow for dynamic characterization of changes on the individual to population level to these cell types.

By introducing readers to the process of panel design and optimization underlying effective immunophenotyping by flow cytometry, we hope to empower users to develop panels that address their specific research or diagnostic goals. For more information and resources for panel design, we encourage you to visit the Thermo Fisher Scientific Flow Cytometry Panel Builder website and explore the online tools provided there.

References

Ferrer-Font, Laura, et al. „Panel design and optimization for high-dimensional immunophenotyping assays using spectral flow cytometry.“ *Curr. Protoc. Cytom.* 92.1 (2020): e70. https://doi.org/10.1002/cpcy.70

Tembhare, P., Badrinath, Y., Ghogale, S., and Subramanian, P.G. 2017. Method for DNA ploidy analysis along with immunophenotyping for rare populations in a sample using FxCycle violet. *Curr. Protoc. Cytom.* 80: 6.38.1- 6.38.15. https://doi.org/10.1002/cpcy.15

Payne, K., Li, W., Salomon, R. and Ma, C.S. (2020), OMIP-063: 28-Color Flow Cytometry Panel for Broad Human Immunophenotyping. *Cytometry*, 97: 777-781. https://doi.org/10.1002/cyto.a.24018

Hertoghs, N., Schwedhelm, K.V., Stuart, K.D., McElrath, M.J. and De Rosa, S.C. (2020), OMIP-064: A 27-Color Flow Cytometry Panel to Detect and Characterize Human NK Cells and Other Innate Lymphoid Cell Subsets, MAIT Cells, and γδ T Cells. *Cytometry*, 97: 1019-1023. https://doi.org/10.1002/cyto.a.24031

Ohne, Y. (2020), OMIP-066: Identification of Novel Subpopulations of Human Group 2 Innate Lymphoid Cells in Peripheral Blood. *Cytometry*, 97: 1028-1031. https://doi.org/10.1002/cyto.a.24046

Nogimori, T, Sugawara, Y, Higashiguchi, M, Murakami, H, Akita, H, Takahama, S, et al. OMIP 078: A 31-parameter panel for comprehensive immunophenotyping of multiple immune cells in human peripheral blood mononuclear cells. *Cytometry*. 2021; 99: 893– 898. https://doi.org/10.1002/cyto.a.24490

Panel Design and Optimization for High-Dimensional Immunophenotyping Assays Using Spectral Flow Cytometry

Laura Ferrer-Font,[1,3,4] Christophe Pellefigues,[1,3] Johannes U. Mayer,[1] Sam J. Small,[1] Maria C. Jaimes,[2] and Kylie M. Price[1,4]

[1]Malaghan Institute of Medical Research, Wellington, New Zealand
[2]Cytek Biosciences, Fremont, California
[3]These authors contributed equally to this work
[4]Corresponding authors: *lferrer@malaghan.org.nz*; *kprice@malaghan.org.nz*

Technological advances in fluorescence flow cytometry and an ever-expanding understanding of the complexity of the immune system have led to the development of large (20+ parameters) flow cytometry panels. However, as panel complexity and size increase, so does the difficulty involved in designing a high-quality panel, accessing the instrumentation capable of accommodating large numbers of parameters, and analyzing such high-dimensional data. A recent advancement is spectral flow cytometry, which in contrast to conventional flow cytometry distinguishes the full emission spectrum of each fluorophore across all lasers, rather than identifying only the peak of emission. Fluorophores with a similar emission maximum but distinct off-peak signatures can therefore be accommodated within the same flow cytometry panel, allowing greater flexibility in terms of panel design and fluorophore detection. Here, we highlight the specific characteristics of spectral flow cytometry and aim to guide users through the process of building, designing, and optimizing high-dimensional spectral flow cytometry panels using a comprehensive step-by-step protocol. Special considerations are also given for using highly overlapping dyes, and a logical selection process for optimal marker-fluorophore assignment is provided.

Keywords: fluorescent antibodies • high-dimensional panel design • immunophenotyping • optimization • spectral flow cytometry

BASIC PROTOCOL

Flow cytometry has rapidly evolved over the past few decades after being first introduced as a one-laser system capable of measuring one fluorescence parameter in the late 1960s (Dittrich & Göhde, 1969). In 1979, an improved dual-laser multi-parameter flow cytometer was developed that could measure, quantify, and sort mammalian cells (Steinkamp, Orlicky, & Crissman, 1979). Thereafter, multi-laser flow cytometers developed at a rapid pace, with three lasers and 10 parameters by the late 1990s (Roederer et al., 1997), four lasers and 19 parameters by 2004 (Perfetto, Chattopadhyay, & Roederer, 2004), and five lasers most recently, which has allowed successful detection of 28 fluorescent parameters (Brummelman et al., 2019).

CURRENT PROTOCOLS
A Wiley Brand

Current Protocols in Cytometry e70, Volume 92
Published in Wiley Online Library (wileyonlinelibrary.com).
doi: 10.1002/cpcy.70

In parallel, the development of spectral flow cytometry began in 1979 (Wade, Rhyne, Woodruff, Bloch, & Bartholomew, 1979) and saw significant developments in the 2000s at Purdue University (Grégori et al., 2012; Robinson, Rajwa, Gregori, Jones, & Patsekin, 2005), with many different prototypes being trialed (Nolan, Condello, Duggan, Naivar, & Novo, 2013), before a commercial instrument was released by Sony in 2012 (Futamura et al., 2015). Whereas conventional flow cytometers record portions of the light spectrum specific for the peak emission of each fluorophore using relevant optical filters, spectral cytometers record small segments of light across the full emission pattern of each molecule (Futamura et al., 2015; Schmutz, Valente, Cumano, & Novault, 2016). Thus, dyes not designed for standard optical configurations or fluorophores that have identical peaks of emission but different off-peak spectra can be efficiently differentiated using the unmixing algorithms of spectral cytometry (Keenan, Timlin, Van Benthem, & Haaland, 2002).

Most flow cytometers measure incident photons using photomultiplier tubes (PMTs), which are costly, high-gain detectors whose quantum efficiency steeply declines after 650 nm. The recent use of avalanche photodiodes (APDs), which have a high quantum efficiency ranging from 400 to 1100 nm, markedly improves performance in the red and near-infrared ranges (Lawrence, Varadi, Entine, Podniesinski, & Wallace, 2008). The sensitivity of APDs is comparable to that of PMTs over a broad spectral range at a significantly lower cost. In 2017, Cytek Biosciences released the Aurora spectral flow cytometer, which combines spectral flow cytometry with improved detection using APDs. The base unit from Cytek offers three lasers (three lasers: 405, 488, and 640 nm) and 48 fluorescence channels that use dispersive optics to distribute the collected light across a large detector array, thus allowing the full spectrum from each particle to be measured (Nolan et al., 2013). Additional instrument configurations were later developed, incorporating a 561-nm yellow-green laser (released in 2018) and/or a 355-nm UV laser (five lasers, released in 2019). The five-laser configuration consists of 64 fluorescent detectors and currently expands the multiplexing capability to 40 fluorophores. Previous constraints on the design of high-dimensional flow cytometry panels, which arose from the limited ability to combine and separately detect different fluorophores, have therefore been replaced by limitations on the availability of dyes with distinct fluorescent spectra (Robinson, 2019).

Although spectral flow cytometry has significantly increased the flexibility of fluorophore selection and detection, considerations around panel design from conventional flow cytometry still apply. These considerations include prior knowledge of the biology of the assay, the instrumentation, the expression levels of the markers of interest, the brightness of the selected fluorophores, and careful optimization of the antibody panel. This Basic Protocol summarizes these points and outlines a number of specific considerations for spectral flow cytometry. Furthermore, it features a simple step-by-step guide for successful design and optimization of a high-dimensional spectral cytometry panel. This protocol was built around the three-laser Aurora but can easily be adapted to any spectral flow cytometer with other specifications. Although the design of spectral flow cytometry panels follows similar steps to those described for conventional flow cytometry (see Current Protocols article; Ashhurst, Smith, & King, 2017; Brummelman et al., 2019), important differences and additional considerations apply for spectral flow cytometry, as described in this protocol (for an overview, see Fig. 1).

Step 1: Determine the experimental question

Determine the experimental question that you will address using spectral cytometry. Important metrics to consider are as follows:

- Which readouts are needed to test your hypothesis? Which readouts are more critical than others (e.g., *mean fluorescence intensity, counts…*)?

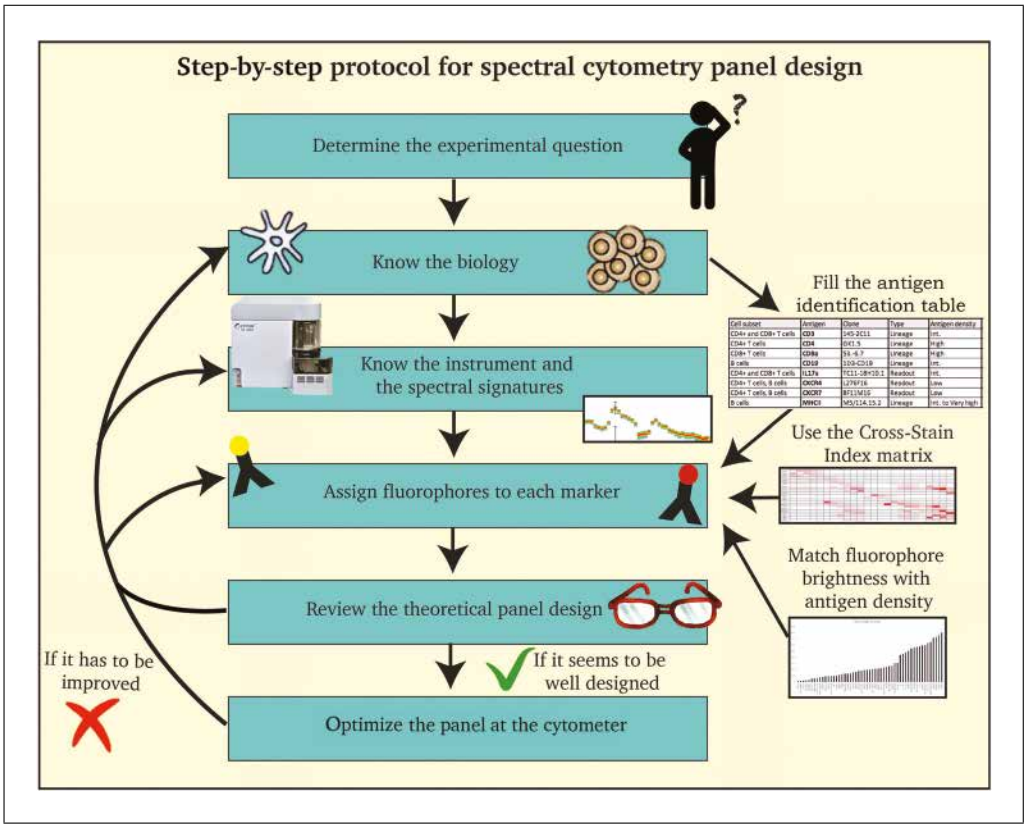

Figure 1 Overview of a step-by-step protocol that illustrates the design of a high-dimensional spectral flow cytometry panel.

- Which tissues will have to be analyzed? What limitations are associated with the tissue (e.g., *digestion, tissue stability, autofluorescence*)?
- How will you need to process the samples to obtain the readout of interest (e.g., *fixation, permeabilization, stimulation*)?

Step 2: Design the panel

For proper panel design, it is imperative to know which markers are necessary to accurately define the cell types of interest and which markers are important for the functional readout needed to address the experimental question. To facilitate collection of this information, we suggest defining a cell identification table (Table 1) to do the following:

- Record the cell populations that need to be analyzed.
- Define the lineage markers that are required to identify the cells of interest.
- Highlight co-expressed markers.

The cell identification table allows us to visualize all the cells of interest for the new panel. The antigens should then be listed in a second table, called an antigen identification table (Table 2). Columns should be filled by following these steps:

a. Define if the markers to be used are for readout or lineage definition.
b. Decide on the clone to be used (based on previous experience or publications).
c. Note the expected antigen density (low, medium, or high), if known.
d. Record the availability of fluorophore-conjugated antibodies for each marker of interest. Commercial websites as well as specialized search engines such as *https://www.biocompare.com* or *https://www.fluorofinder.com* are useful tools to interrogate. If a certain clone is only available with a few fluorophores, list these fluorophores in the table. Otherwise, note it as "common" and add only unusual fluorophores (e.g., APC-Cy5.5 or BV750).

Table 1 Cell Identification Table

Cell type	Lineage	Co-expression phenotype
Basophils	eYFP^{+}	CD45^{lo} CD200R3^{+} CD11b$^{\pm}$ CD90^{lo}
Macrophages	CD45^{+} CD64^{+} CD11b^{+}	CD11c$^{\pm}$ MHCII$^{\pm}$ CD206$^{\pm}$ CD301$^{\pm}$ Ly6C$^{\pm}$
Macrophages (inflammatory)	CD45^{+} CD64^{+} CD11b^{+} Ly6C^{hi}	
Macrophages (dermal resident)	CD45^{+} CD64^{+} CD11b^{+} Ly6C$^{-/lo}$ CD206^{hi} MHCII^{lo}	
Macrophages (monocyte derived)	CD45^{+} CD64^{+} CD11b^{+} Ly6C$^{-/lo}$ CD206^{-} MHCII^{+}	
Dendritic cells	CD45^{+} CD64^{-} CD11c^{+} MHCII^{+}	CD11b$^{\pm}$ CD206$^{\pm}$ CD301$^{\pm}$ Ly6C$^{\pm}$
Neutrophils	CD45^{+} CD11b^{+} Ly6G^{+}	Ly6C+
Eosinophils	CD45^{+} CD11b^{+} SiglecF^{+} SSC^{hi}	Ly6C+
B cells	CD45^{+} CD19^{+} MHCII^{+}	
CD4^{+} T cells	CD45^{+} CD3^{+} TCRβ^{+} NK1.1^{-} CD4^{+}	CD90^{+} TCRγδ^{-} CD25$^{\pm}$
CD8^{+} T cells	CD45^{+} CD3^{+} TCRβ^{+} NK1.1^{-} CD8^{+}	CD90^{+} TCRγδ^{-}
DN T cells	CD45^{+} CD3^{+} TCRβ^{+} NK1.1^{-} CD4^{-} CD8^{-}	CD90^{+} TCRγδ^{-}
γδ T cells	CD45^{+} CD3^{+} TCRγδ^{+} TCRβ^{-} CD90^{+}	TCRβ^{-}
DETCs	CD45^{+} CD3^{vhi} TCRγδ^{vhi} TCRβ^{-} CD90^{vhi}	TCRβ^{-}
NKT cells	CD45^{+} CD3^{+} TCRβ^{+} NK1.1^{+}	CD90$^{\pm}$ CD8$^{\pm}$ CD4$^{\pm}$ CD11b$^{\pm}$ Ly6C$^{\pm}$
NK cells	CD45^{+} CD3^{-} TCRβ^{-} NK1.1^{+}	CD90$^{\pm}$ CD11b$^{\pm}$ Ly6C$^{\pm}$
Inflammatory monocytes	CD45^{+} CD64$^{lo/+}$ CD11b^{+} Ly6C^{hi}	
Mast cells	CD45^{+} CD200R3^{+} CD117^{+}	CD11b^{-} CD301^{+}
ILC2 cells	CD45^{+} Lin^{-} CD90^{+} CD25$^{lo/+}$	CD117$^{\pm}$
Lineage (part 1)	CD11b CD64 Ly6G CD11c MHCII SiglecF CD19	
Lineage (part 2)	CD3 CD4 CD8 TCRβ TCRγδ CD200R3 Ly6C	

Step 3: Define the fluorophores

Only dyes with unique spectral signatures should be used in the same panel. However, dyes with similar spectral signatures can be used at the risk of introducing spreading error (SE), which can be mitigated if they are used with markers that are not co-expressed. The spectral signatures of many fluorophores have been extensively defined by Cytek Biosciences for their one-, two-, three-, four-, and five-laser Auroras (*https://spectrum.cytekbio.com/*), and spectral signatures of additional fluorophores can be assessed using other online fluorescence spectra viewers (e.g., from BD, BioLegend, Thermo Fisher, Expedeon, or FluoroFinder) or by manually assessing the signature by acquiring single-stained controls on the Aurora.

Although visual inspection of full-spectrum signatures is sometimes sufficient to evaluate the uniqueness of a spectrum, when two spectra are similar, more advanced tools are needed to assess the pair's compatibility. As part of SpectroFlo^{TM} v2.2 software (Cytek Biosciences), a metric called the Similarity Index was developed. This index ranges from

Table 2 Antigen Identification Table

Antigen	Type	Clone	Antigen density	Fluorophores available
IL-4	Readout	Reporter	Low to high	AmCyan
IL-13	Readout	Reporter	Low to high	dsRed
MCPT8	Lineage	Reporter	High	YFP
CD45	Lineage	30F11	High	Common, APC-Cy5.5
CD64	Lineage	X54-5/7.1	Low	Common
CD11b	Lineage	M1/70	Low to very high	Common, AF594, BV570, BV750
Ly6C	Lineage	HK1.4	High	Common, BV570
CD206	Lineage	C068C2	High	Common, AF594
CD301	Lineage	LOM/14	Medium	Common, AF594
CD11c	Lineage	N418	Low	Common, AF594, BV570, BV750
MHCII	Lineage	M5/114.15.2	Very high	Common, AF594, BV570, BV750
Ly6G	Lineage	1A8	High	Common, AF594, BV570
SiglecF	Lineage	S17007L	Medium	APC, BV421, FITC, PE, SB436, PE-Dazzle594
CD3e	Lineage	145-2C11	Low to very high	Common, PE-Cy5
TCRb	Lineage	H57-597	Medium	Common, AF594, BV570, PE-Cy5
CD4	Lineage	RM4-5	High	Common, BV570, BV750, PE-Cy5
CD8a	Lineage	53-6.7	High	Common, BV570, BV750, PE-Cy5
TCRgd	Lineage	GL3	High	Common
CD90.2	Lineage	53-2.1	High	Common, BV570, PE-Cy5
NK1.1	Lineage	PK136	Medium	Common, BV570, PE-Cy5
CD19	Lineage	6D5	Medium	Common, AF594, BV570, PE-Cy5
CD200R3	Lineage	Ba13	Medium	APC, PE, PerCP-Cy5.5
CD117	Lineage	2B8	High	Common, PE-Cy5, BB700
CD25	Lineage	PC61	Low	Common, BB515, AF594, PE-Cy5

0 to 1. Two fluorophores that have totally distinct signatures will have a Similarity Index close to 0 (for example, FITC and APC), whereas two signatures that highly overlap will have a Similarity Index close to 1 (for example, PerCP-Cy5.5 and PerCP-eF710). Based on experimental data, the cut-off to use dyes in combination has been set at a Similarity Index of 0.98 (i.e., for FITC and BB515). Interestingly, with the addition of more lasers and hence more channels, the full-spectrum signature of the same dye shows more data points on a five-laser Aurora than on the three-laser model, so extra information is available to more accurately distinguish between similar spectral signatures. For example, the Similarity Index between APC and AF647 decreases from 0.94 to 0.9 with the addition of a 561-nm laser to the three-laser Aurora.

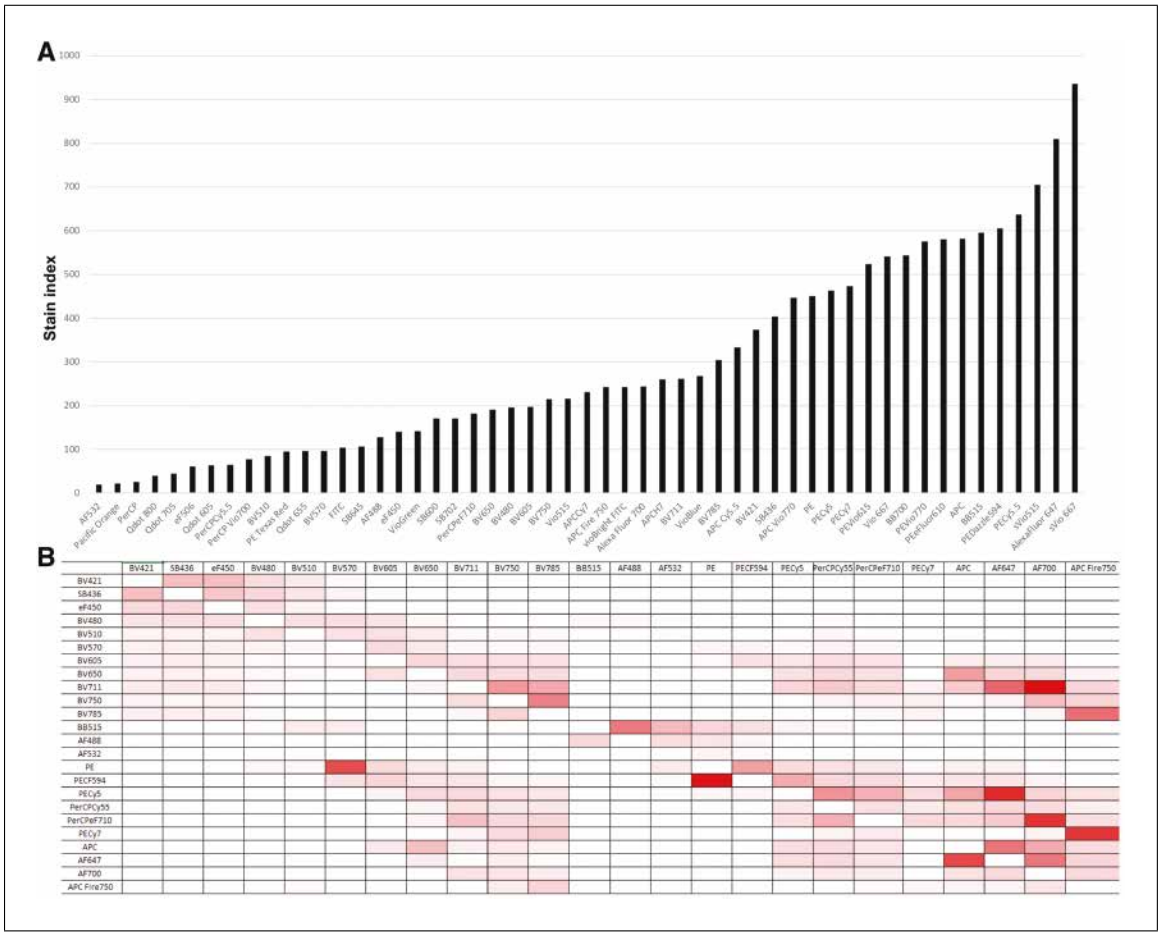

Figure 2 Overview of brightness and spillover between fluorophores that can be used on the three-laser Aurora spectral flow cytometer (Cytek Biosciences). (**A**) Stain Index (SI) of 53 commonly available dyes for the three-laser Aurora. A higher SI represents brighter fluorophores or lower background. (**B**) Cross-Stain Index (CSI) matrix for 24 unique-signature fluorophores that can be used in combination on a three-laser Aurora. Spillover is contributed by fluorophores listed in the rows, with spilling into the fluorophores listed in the columns (for example, PE-CF594 spreads strongly into PE). Combinations depicted in red should be assigned to non-co-expressed markers or used for dump or viability channels. Note that the SI and the CSI matrix will vary depending on the instrument and laser configuration and are shown here for the three-laser Aurora.

Once a panel of dyes is selected, another metric, called the Complexity Index, evaluates the overall similarity for all spectra within that selection. The Complexity Index takes the Similarity Index for each pair of dyes into account. The lower the Complexity Index, the higher the chance of obtaining optimal results with a given combination of fluorophores. For example, when selecting 10 different dyes for which the highest Similarity Index is 0.3, the Complexity Index would be 2.5. In contrast, if among these 10 dyes, the Similarity Index reaches 0.98 for two of them, the Complexity Index would increase to 26.

It is also critical to consider the brightness of the fluorophores when designing a panel. For this purpose, the Stain Index (SI) of different fluorophores, measured using conjugated antibodies with the same specificity, is a valuable metric (Fig. 2A). A commonly used marker is anti–human CD4, as it is available conjugated to a great variety of commercially available fluorophores. Ideally, the same clone should be used for this assessment, but there are often limitations based on commercial availability.

Spread is another important consideration for fluorophore selection and will be discussed in the next section. It is important to point out that with the addition of more lasers and more channels, the ability to better distinguish two dyes with a similar spectrum

Table 3 Panel Distribution Table for a Three-Laser Instrument[a]

nm	Violet	Fluorophore	Marker	Cells	Blue	Fluorophore	Marker	Cells	Red	Fluorophore	Marker	Cells
420	V1											
440	V2											
460	V3											
480	V4											
490	*488 nm*											
510	V5				B1							
530	V6				B2							
550	V7				B3							
570	V8				B4							
590	V9				B5							
610	V10				B6							

(*Continued*)

Table 3 Panel Distribution Table for a Three-Laser Instrument[a], *continued*

nm	Violet	Fluorophore	Marker	Cells	Blue	Fluorophore	Marker	Cells	Red	Fluorophore	Marker	Cells
640	*640 nm*											
660	V11				B7				R1			
680	V12				B8				R2			
700	V12				B9				R3			
720	V13				B10				R4			
740	V14				B11				R5			
760	V14				B12				R6			
780	V15				B13				R7			
800	V16				B14				R8			

[a]This table can be used to predict the spread induced for co-expressed markers. As a general rule, the closer the emission peaks of two fluorophores are, the more spreading error and spillover will be observed between them. The table is structured to represent all the detectors of a three-laser Aurora based on their wavelength detection range upon excitation by one of the three lasers. Each marker-fluorophore combination should be assigned to the row corresponding to the emission peak of the fluorophore. The main cell types expressing the marker should be annotated. Co-expressed markers should never be close in the same column, in order to avoid the emergence of spreading error. If possible, they should also not be in the same row, as dyes showing a broad excitation spectrum will tend to emit in the same wavelength after being excited by different lasers.

signature will generally improve. However, this can also result in additional spread being introduced.

Step 4: Assign fluorophores to each marker

The most difficult task in multicolor panel design is to match the most appropriate fluorophore with each marker of interest. Fluorophore brightness and availability, levels of marker expression and marker co-expression, and spectral spillover have to be considered. Always match the fluorophore brightness with antigen expression levels by combining brighter fluorophores with weaker expression levels and vice versa. The summary of SI values shown in Figure 2A provides a useful tool for fluorophore classification. Co-expressed markers and markers selected for functional readouts should be matched with fluorophores that receive minimal spread from other fluorophores in the panel. An indication of the SE between fluorophores can be found on the Cross-Stain Index (CSI) matrix in Figure 2B. Determining SE is crucial when building high-dimensional fluorescence panels. Factors that contribute to the amount of SE from a given fluorophore into another fluorescence detector have been well described (see Current Protocols article; Ashhurst et al., 2017; Nguyen, Perfetto, Mahnke, Chattopadhyay, & Roederer, 2013). It is important to note that the CSI matrix is highly specific to the instrument setup and the fluorophores used and needs to be modified if additional or alternative fluorophores or another instrument is used. SI values and the CSI can be found on the Cytek Biosciences website for each Aurora configuration (1 to 5 lasers; *https://cytekbio.com/blogs/resources/tagged/data-sheets*).

In order to facilitate the selection process, we suggest completing a panel distribution table (Table 3) using the following step-by-step strategy:

a. Note fluorescent reporter genes first, as they have a predefined fluorescent signature.
b. Assign very rare markers to the only fluorophore options available (e.g., CXCR5 to PE).
c. Assign the most common markers to rare fluorophores that have distinct spectral signatures in the panel (e.g., CD4 to BV750).
d. Assign the remaining markers to other fluorophores, considering their co-expression and spread.
e. Unless nonviable cells are to be interrogated further, the viability dye can be selected last, regardless of any spreading issues, due to the wide range of available fluorophores.

Step 5: Review the theoretical panel design

In order to theoretically validate the panel before proceeding to practical testing, it is advised to review the panel on a marker-by-marker and cell-by-cell basis with the help of the annotated tables (Tables 1 and 2) by asking the following questions:

a. Are fluorophores that induce high amounts of spread allocated to non-co-expressed markers?
b. Do the "readout" markers receive a minimal amount of spread?
c. Are fluorophore brightness and antigen expression levels well matched?

To address potential issues, markers that are available with multiple fluorophores can be swapped out to see if spillover can be reduced. Additionally, fluorophores that create (but do not receive) the most spillover can be designated to dump or viability channels.

COMMENTARY

Background Information

Panel design considerations for a spectral cytometer overlap heavily with good standard practices for panel design for a conventional cytometer (i.e., ranking antigens and matching fluorophore brightness with antigen expression levels). However, spectral cytometry provides greater flexibility in fluorophore

selection as well as additional tools to help with successful multi-parameter panel design, which are further outlined below.

Instrument setup

On the Aurora, the "Cytek Assay Settings" are designed to provide optimized gains for all detectors. This optimization has been done in order to provide the best resolution of most known fluorophores on antibody-stained cells. These gains are automatically adjusted after each daily quality-control (QC) check based on laser and detector performance relative to an ideal value, which is defined by the detection and optimal placement of proprietary fluorescent beads against predetermined target values. Due to use of APDs, output fluorescence intensity increases linearly with gain up to the maximum value of 4×10^6.

If the signal observed during testing is off scale using the optimized "Cytek Assay Settings," it is generally better to titrate down the antibody used than to modify the instrument settings. However, for special circumstances (such as fluorescent reporter-gene expression or when saturating antibody titers are needed), the gains can be adjusted to allow dim or bright signals to be detected accurately. It is recommended to adjust the gains by a fixed percentage for all the detectors of a specific laser (SpectroFlo™ v2.0 and above) instead of adjusting the gains of individual detectors. It is extremely important to note that changing the gains of any detector will alter the spectral profile of all the fluorophores. This generally implies that the differences in spectral signatures between fluorophores will decrease compared to the optimized default gain setting. Therefore, adjusting the gains away from the optimized default setting to enable detection of a specialized fluorophore might increase overall SE between other fluorophores and should only be done if absolutely necessary. Single-stained controls and all multi-stained samples will need to be acquired using the same settings, be it the "Cytek Assay Settings" or an adjusted version.

Using spectral signatures

Fluorophores emit light over a range of wavelengths, and in conventional flow cytometry, optical filters are used to capture peak fluorescence emission in a primary detector. When the emission profiles of two or more fluorophores overlap, the light emitted from one fluorophore appears in a non-primary detector (a detector intended for another fluorophore). This is referred to as spillover. Single-stained controls must be acquired to calculate the amount of spillover into each of the non-primary detectors. In conventional flow cytometry, spillover can be corrected by using a mathematical calculation called compensation.

In spectral cytometry, the full emission spectrum of each single-stained sample can be used to determine the contribution of each fluorophore in a mixed sample using spectral deconvolution (unmixing) algorithms in real time or post-acquisition (see Current Protocols article; Nolan & Condello, 2013). Here, the key to differentiating various fluorophores is distinct patterns or signatures across the full spectrum. Because the system measures the full range of emission (not only peak emission), two dyes with a similar emission maximum but different spectral signatures, such as APC and AF647, can be distinguished from each other (Fig. 3). It is a good practice to compare actual fluorophore spectral signatures obtained at the cytometer to the gold standard shown in the Aurora Fluorochrome Guide (*https://cytekbio.com/blogs/resources/tagged/data-sheets*) to ensure fluorophore identity and quality. Moreover, each laboratory can establish benchmark/gold-standard full-spectrum signatures for the most commonly used fluorophores. In SpectroFlo™ v2.2, that benchmark is automatically used to run QC on new controls by calculating the Similarity Index between the benchmark and the newly run control. The expectation is to obtain high agreement between the two spectra and hence a Similarity Index equal to or close to 1.

Fluorophore brightness and Stain Index (SI)

The SI is calculated using Equation 1 to help determine the relative brightness of a fluorophore on a given instrument (Nguyen et al., 2013):

$$SI = \frac{MFI_{Pos} - MFI_{Neg}}{SD_{Neg} \times 2}$$

Equation 1

Here, MFI_{Pos} and MFI_{Neg} are the MFI values of the positive and negative populations, respectively, and SD_{Neg} is the standard deviation of the negative population.

Absolute brightness depends on many attributes, namely the intrinsic fluorescence of the fluorophore, laser power, excitation wavelength, optical filters, and detector type. Therefore, the SI is heavily dependent on the cytometer used and its specific setup.

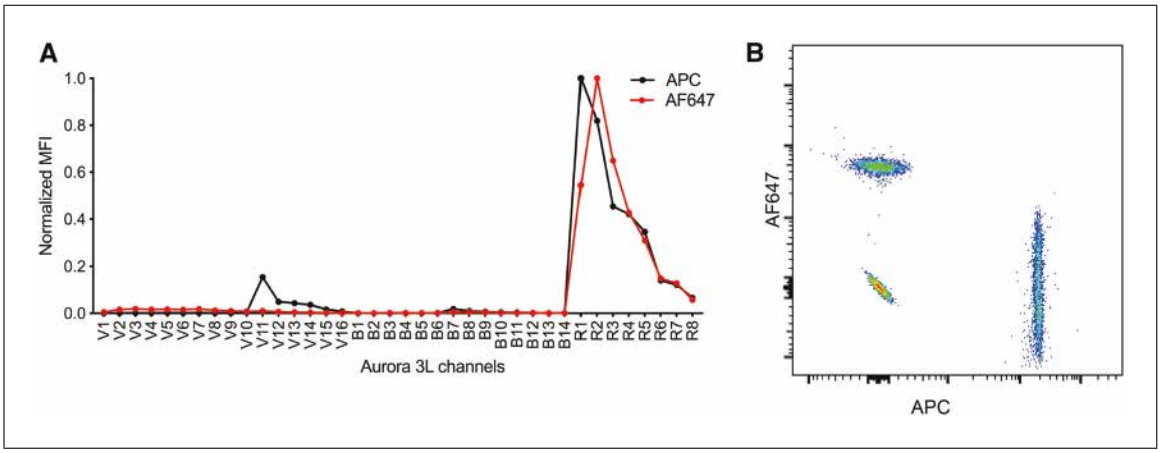

Figure 3 Different spectral signatures allow for separate detection of APC and AF647. (**A**) Spectral pattern comparison (APC vs AF647). Note the stronger violet emission for APC compared with AF647 and differences in the peak emission profile. (**B**) Dot plot showing that AF647- and APC-stained beads can be discriminated by spectral flow cytometry, at the expense of significant spreading error.

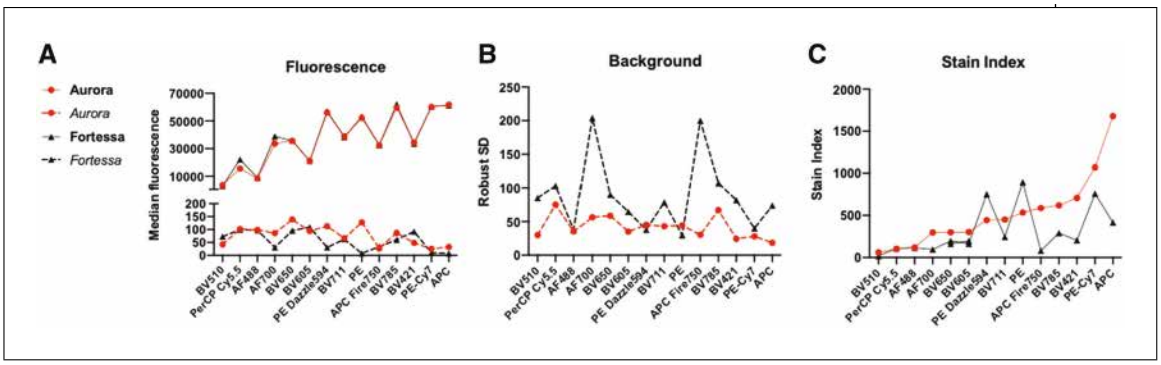

Figure 4 Brightness comparison of different fluorophores conjugated with anti-CD4 antibodies on human peripheral blood leukocytes. (**A**) Raw median fluorescence for antibody-positive (solid line) and antibody-negative (dashed line) populations. Background noise (standard deviation of the negative population) (**B**) and the Stain Index (SI) (**C**) were compared between 14 fluorophores detected on a three-laser Aurora (Cytek Biosciences) or a five-laser Fortessa (BD). Fluorophores are listed based on increasing SI according to the Aurora data. The median fluorescence measured on the Fortessa has been adjusted to match that measured on the three-laser Aurora using optimized defaults.

An example of potential differences is shown in Figure 4. We adjusted the mean fluorescence intensity (MFI) values of common fluorophores on a conventional cytometer to match those measured the Aurora using optimized defaults (Fig. 4A). This resulted in increased background noise for the negative population on the conventional cytometer (measured by the robust standard deviation, or rSD; Fig. 4B). The rSD was smaller on the Aurora in most channels and generally allowed better SI values (Fig. 4C). As previously reported (Lawrence et al., 2008), APDs perform better at wavelengths >650 nm, where the higher quantum efficiency contributes to better signal-to-noise ratios than for PMTs. This was also reflected in our measurements, resulting in a higher SI for dyes emitting in red and far-red channels (Fig. 4C).

Autofluorescence (AF)

AF is a natural characteristic of all cells, whereby biological substances and structures within the cell fluoresce. AF can be attributed to biomolecules such as NADH, folic acid, and retinol, which have emission maxima in the range of 450 to 500 nm, and to riboflavin, flavin coenzymes, and flavoproteins, which have emission maxima in the range of 520 to 540 nm (Monici, 2005). AF creates background that can impair the detection of dim markers emitting light at the same wavelengths. In spectral flow cytometry, the spectral profile of unstained cells can be collected and treated as an independent parameter (AF), which allows the AF signature to be extracted using the unmixing algorithm. Correcting for autofluorescent signatures can improve the signal-to-noise ratios (Fig. 5) and enables clearer distinction of fluorophores that have

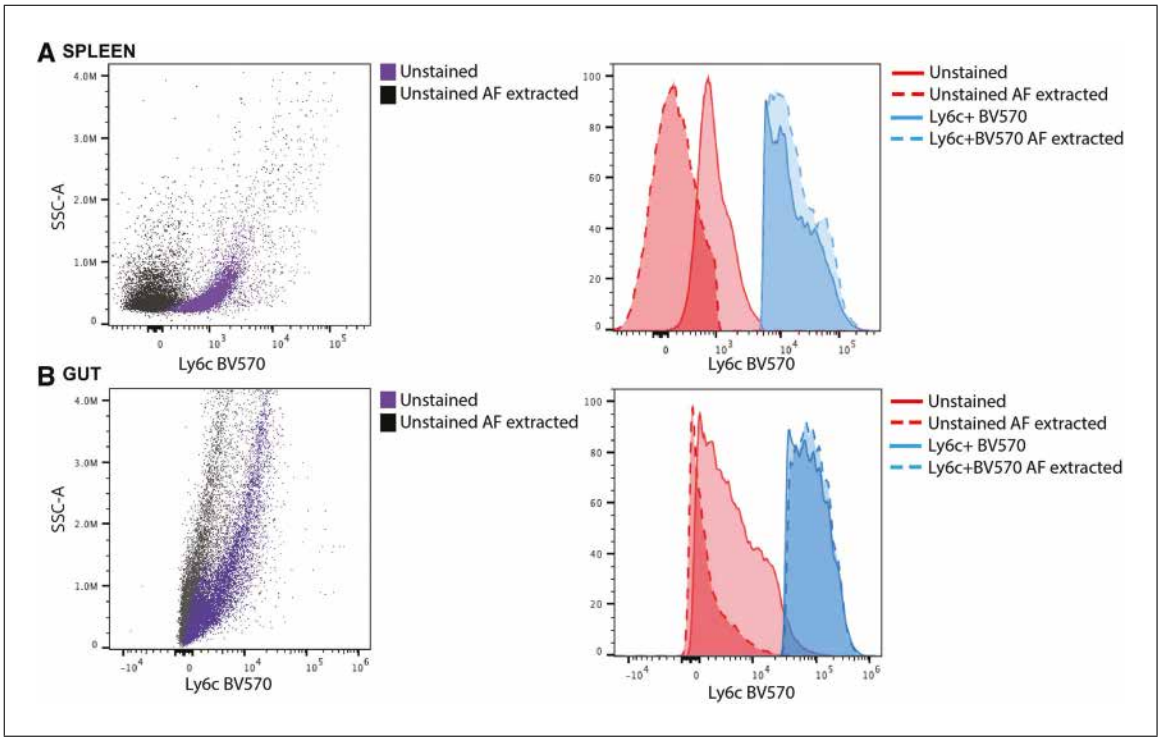

Figure 5 Autofluorescence correction reduces the background signal of the negative population. Comparison of autofluorescence (AF)-corrected (AF extracted) or uncorrected spleen (**A**) and gut (**B**) samples stained with anti-Ly6C BV570. Correction of AF improves the positive-signal resolution by lowering the background of the negative population with minimal effect on the positive signal.

been avoided in the past due to their peak emission in the AF range (e.g., AF532 and BV510). Furthermore, AF correction can improve the resolution of certain markers in highly autofluorescent tissues such as the brain, lung, skin, intestine, and tumors (Schmutz et al., 2016).

Critical Parameters

Antibody titration

Antibody titration is an absolute requirement for the development of a successful high-dimensional spectral cytometry panel. As with conventional flow cytometry, optimal antibody titration is necessary to reduce the amount of antibody used, reduce background signal by minimizing nonspecific binding, and compare samples accurately (see Current Protocols article; Hulspas, 2010). If a signal is too bright, the best practice is to use an antibody conjugated to a dimmer fluorophore. If this is not possible, it is better to titrate the antibody down to reduce the spread created in other channels (Mahnke & Roederer, 2007) than to change the instrument settings. However, antibodies used to assess functional readouts should not be titrated below saturation, as saturating concentrations are needed to avoid variability and ensure accurate detection between samples (Cossarizza et al., 2017).

Reporter genes

For accurate detection of fluorescent reporter-gene expression, single-stained controls should be derived from the reporter system under experimental conditions that induce the highest level of gene expression (e.g., stimulation), whereas all other single-stained controls should be derived from wild-type cells. Furthermore, fully stained wild-type cells serve as the fluorescence minus one (FMO) control for fully stained reporter-gene samples. It is important to ensure that fluorescent reporter-gene expression is on scale; otherwise, the gains will need to be adjusted. However, modifying the gains via the "Cytek Assay Settings" will impact all channels, resulting in suboptimal detection of the remaining fluorophores. An extreme example is shown in Figure 6, where dramatically reduced gains in the red- and blue-laser detectors resulted in distortion of the spectral signature and a strong increase in SE.

Tandem dyes

Many available fluorophores are tandem organic or polymer dyes, in which excitation of the donor fluorophore leads to emission by the acceptor dye of the tandem pair (Johansson & Macey, 2014). The resulting spectral profile is a hybrid between the excitation and

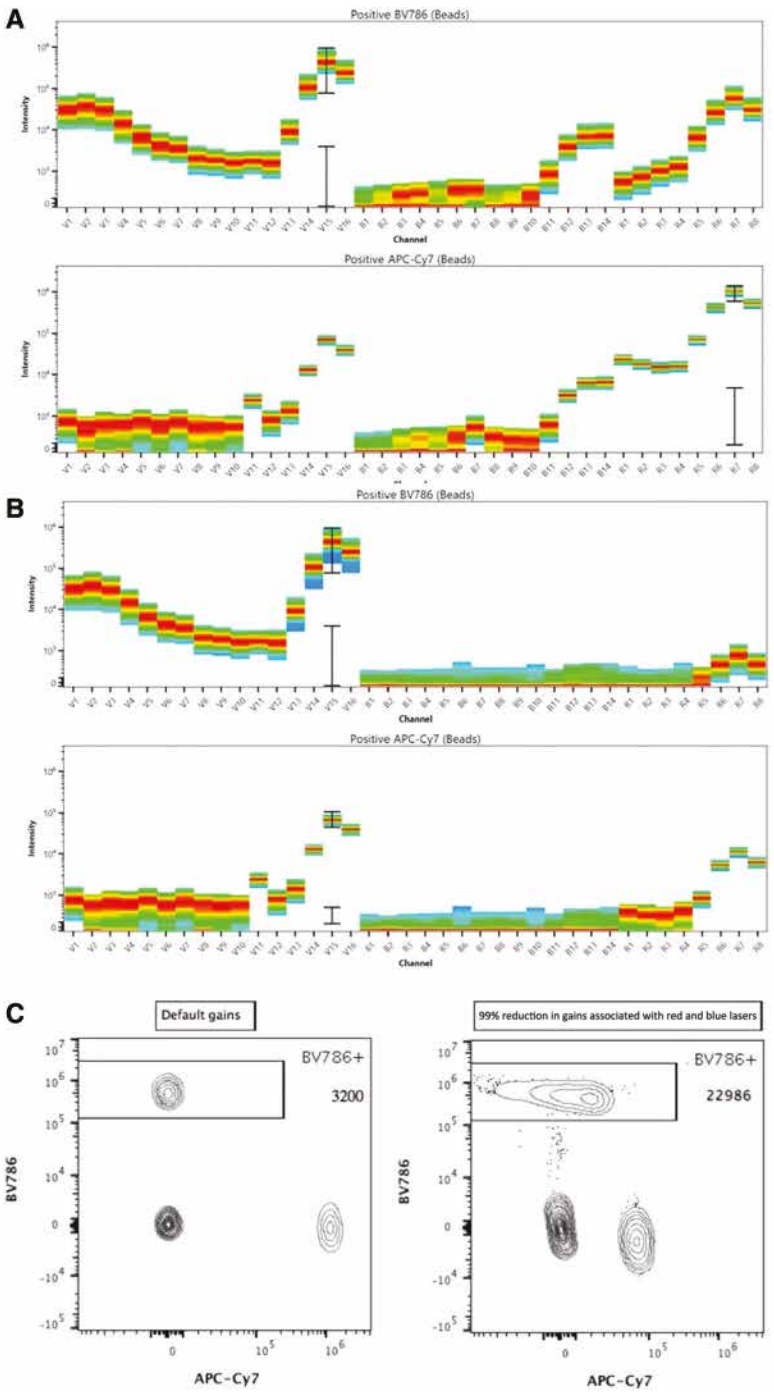

Figure 6 Modification of the detection gains will affect the spectral signature of interest and reduce its separation relative to other fluorophores. Compensation beads were stained with BV786- or APC-Cy7-conjugated antibodies, and their spectral profile was acquired on a three-laser Aurora system using vendor-established gains ("Cytek Assay Settings") (**A**) or after a 99% reduction of the gains of all detectors associated with the red and blue lasers (**B**). (**C**) Unmixing was performed for both datasets, and then single-stained bead preparations were acquired under default or reduced-gain conditions. The 84th percentile of the APC-Cy7 fluorescence detected on the BV786$^+$ beads after spillover compensation (a measure of the SE; Nguyen et al., 2013) is depicted on the dot plots. Note that the width basis for data display needed to be further adjusted after gain reduction to produce the single BUV786+ population.

emission spectra of the two dyes. However, spectral profiles of tandem dyes slowly degrade over time, differ in a lot-to-lot fashion (due to changing acceptor/donor ratios), and can also be affected by experimental conditions, such as fixation and incubation at 37°C (Johansson & Macey, 2014; Le Roy, Varin-Blank, Ajchenbaum-Cymbalista, & Letestu, 2009; Tario & Wallace, 2014). Therefore, single-stained controls need to use the same antibody lot and must be treated in the same manner as the experimental samples. New lots of tandem dyes need to be re-titrated to ensure consistent results.

Spreading error (SE)

SE is a large contributor to reduced signal resolution (Nguyen et al., 2013). To minimize SE, only fluorophores with unique spectral signatures should be selected. Although spectral flow cytometry can distinguish between dyes that have a very similar signature (Fig. 3), these fluorophores will introduce SE and should not be used to detect co-expressed markers. As in conventional flow cytometry, SE is a direct function of fluorescence intensity, and as such, panels should be designed so that fluorophores that contribute the most spread are paired with dimly expressed markers.

Dump channels

It is advisable to use fluorophores with identical spectral signatures for dump channels. Therefore, use of tandem dyes should be avoided. Fluorophores that produce SE (e.g., PerCP-Cy5.5) or fluorophores that emit in the AF range (e.g., BV510, V500, or eFluor506) are ideal candidates for use as dump-channel dyes, as the SE created by the positive signal will be excluded from further analysis. SE from other fluorophores into the dump channel should be avoided, as cells of interest could accidentally be excluded. The same rationale can also be applied for viability dye selection.

Spectral reference controls (SRCs)

SRCs are single-stained controls used for establishing reference vectors to enable successful linear unmixing to occur. SRCs should always be as bright as or brighter than experimental samples, ideally with a fluorescence intensity above 5×10^5 but below 4×10^6, which is the maximum value of the linear range of detection for Aurora spectral flow cytometers. It is recommended to use single-stained cells of a similar tissue as the experimental sample as SRCs if the positive signal observed is bright enough and the population of interest is not rare. It is essential to collect enough total events for the software to clearly distinguish the spectral fingerprint for both the positive and the negative populations. As a general rule, Cytek Biosciences recommends acquisition of 5000 events for beads and 1000 events for cells; however, it is important to have at least 500 events each in the positive and negative gates. Certain conditions, such as low antigen density or rare positive events, might greatly benefit from use of compensation beads (see Current Protocols article; Ashhurst et al., 2017). Either compensation beads or cells can be used as single-stained controls in the same experiment as long as the correct internal negative control is used (e.g., unstained compensation beads or cells with similar AF, respectively).

SRCs should also be treated the same way as fully stained samples, as fixation steps or pH variations can alter the spectral profiles of some fluorophores (see Current Protocols article; Ashhurst et al., 2017). Such treatments can also affect the fluorescent signature of compensation beads. One example is use of Brilliant Stain Buffer (BD), which is used to decrease the interactions of the Brilliant dyes among themselves and mitigate nonspecific signals in multicolor samples. However, this buffer also significantly alters the spectral profile of some latex beads (e.g., UltraComp beads; see Fig. 7) and should be avoided when staining them. Therefore, a good practice when using compensation beads is to compare the spectral profile obtained with that of cells stained with the same antibodies.

Unstained SRCs have to be acquired for every experiment, and it is advised to use a matched unstained control for unmixing each individual tissue if multiple tissues are analyzed, especially if AF correction is applied during the unmixing process.

The Aurora creates Raw and Unmixed FCS 3.1 files for each experiment. If an SRC did not yield an ideal signature at the time of recording the experiment (e.g., if the signal was not bright enough or did not include enough events), recorded data can be re-unmixed within the SpectroFlo™ software post-acquisition using different SRCs. Similarly, samples can be re-unmixed with or without AF extraction.

Once optimal SRCs have been defined for a panel, they can be recorded for future use in the reference library within the software. When the controls are recorded within the setup and QC module, the data defining the

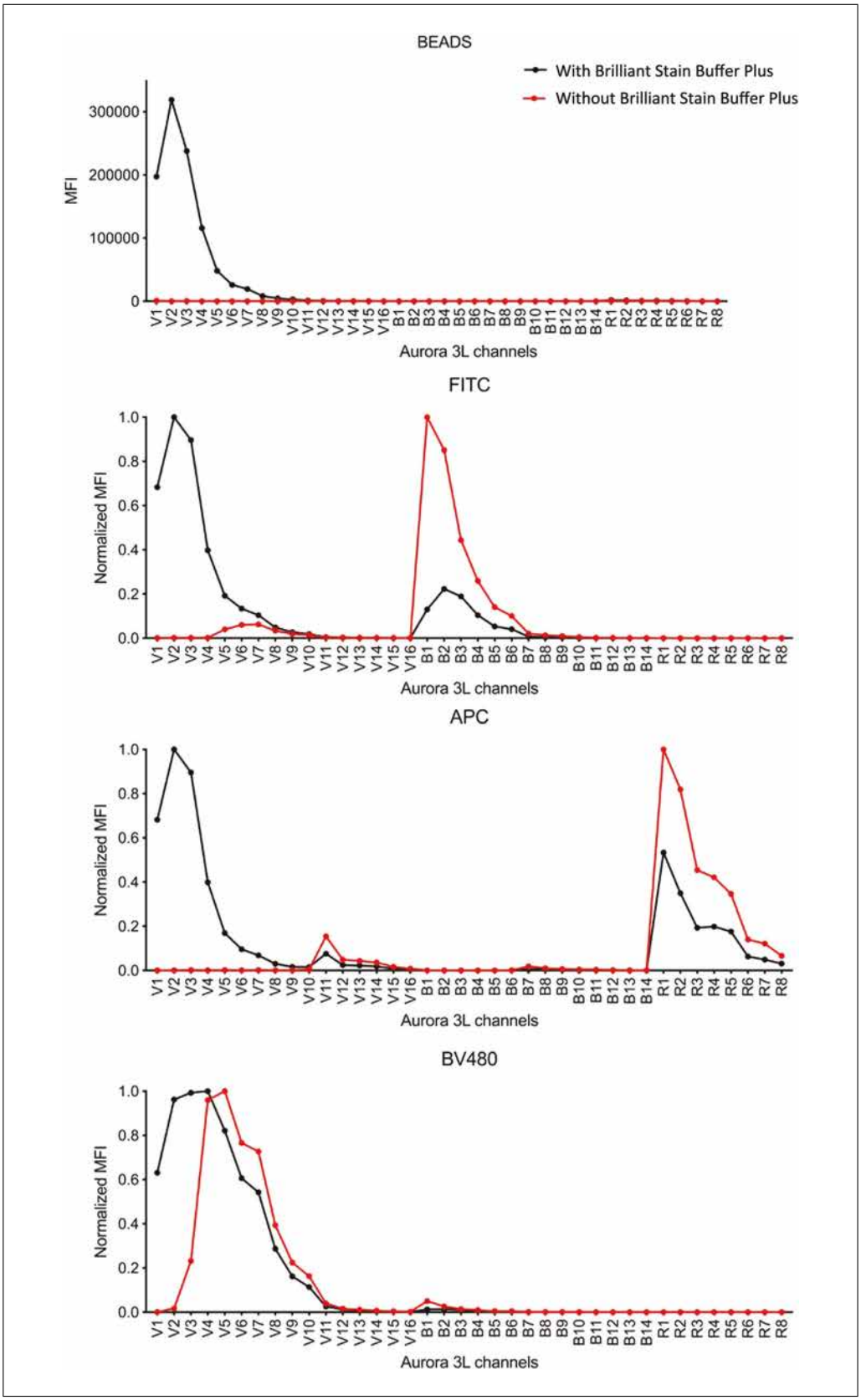

Figure 7 Compensation beads need to be stained without Brilliant Stain Buffer Plus™ to allow appropriate detection of single stains. UltraComp eBeads™ (Thermo Fisher) were stained either with or without Brilliant Stain Buffer Plus™ (BD Biosciences). Examples for beads and the fluorophores FITC, APC, and BV480 are shown.

controls are normalized to the detector gains and will be optimally adjusted during the daily setup process. Reference-library SRCs should be re-acquired after any system stability or QC performance issues and after any instrument maintenance. It is important to note that new SRCs must be recorded for each new antibody lot, as there is significant lot-to-lot variation in fluorophore spectral profiles, particularly for tandem dyes. Optimum reference-library SRCs can be very convenient to use when working with fluorescent proteins or when positive controls are laborious to obtain. These SRCs allow users to save a lot of time when frequently working with the same high-dimensional panels. The main risk of this feature is that users tend to rely on it too heavily, and they should be reminded to regularly re-acquire their reference-library SRCs. Indeed, outdated SRCs can lead to improper unmixing, increased SE, and spillover, resulting in poor resolution of populations or incorrect readouts.

Troubleshooting

Panel optimization is an important step for any multicolor panel design. One of the first steps is to compare how antibodies behave in combination to single-stained cells. By comparing the fluorescence intensity and SE of all single-stained cells to those of fully stained samples, one can easily assess whether the combination of antibodies in the multicolor panel decreases the resolution of a given fluorophore by, for example, introducing spillover or SE.

Analyzing an FMO control for each fluorophore in the panel is not required for the panel optimization step. Only those fluorophores creating spillover or SEs will require an FMO control to help with panel QC. FMO controls or good experimental controls (e.g., unstimulated cells or antigen-negative cells) are needed to reliably and reproducibly define the boundary between positive and negative readout signals across different cell populations and experiments. They are necessary for establishing gating boundaries between dimly expressed antigens and background and are an important tool for assessing panel performance.

If a conflicting pair of antibodies has been identified by assessing the single-stained cells or FMO controls, alterations should be made to the panel by changing the antibody concentration or modifying the antibody-fluorophore assignment. Small corrections to spillover can be made by altering the compensation matrix within SpectroFlo™ or in a third-party software of choice.

Understanding Results

As an example of how to accurately understand results, we describe the design of a 25-parameter panel, which includes use of triple-reporter (YFP/AmCyan/DsRed) Basoph8 × 4C13R mice with or without experimental treatment. Each step of the protocol identified in Figure 1 is described, and important considerations are highlighted.

Experimental question

The aim was to understand which cell types express IL-4 and IL-13 in the skin in a MC903-induced atopic dermatitis model using triple-reporter Basoph8 × 4C13R mice (Pellefigues et al., 2019). These mice express eYFP as a specific marker for basophils and report expression of the type 2 cytokines IL-4 and IL-13 as AmCyan and dsRed, respectively. The experimental readouts were expression of IL-4 (AmCyan) and IL-13 (dsRed) by the various immune cells identified.

Our analysis focused on the skin, a highly autofluorescent tissue requiring collagenase digestion to obtain single-cell suspensions. Prior analysis of splenocytes revealed that expression of certain epitopes (i.e., cKit, CD3, CD4) was decreased by digestion; therefore, bright fluorophores were needed to detect these markers. Furthermore, preliminary experiments revealed that reporter-fluorophore stability was strongly affected by fixation and permeabilization; therefore, only fresh cells were assessed.

Biology

Different subsets of T cells (including $CD4^+$, $CD8^+$, γδ, and dendritic epidermal T cells, or DETCs), mast cells, basophils, type 2 innate lymphoid (ILC2) cells, eosinophils, natural killer (NK) cells, natural killer T (NKT) cells, monocytes, and neutrophils have been shown to express IL-4 and/or IL-13 during allergic inflammation (Bao & Reinhardt, 2015; Chen et al., 2014; Sun et al., 2018; Vantourout & Hayday, 2013; von Bubnoff et al., 2010). To address whether these and other cell types express IL-4 or IL-13 in the skin after MC903 treatment, we wanted to quantify these cell subsets and various macrophage subpopulations, as they are known to be responsive to type 2 cytokines. We listed the lineage-defining phenotype of every cell subset of interest in a cell identification table (Table 1) and then listed all the antigens of choice in an

Table 4 Panel Distribution Table for a Five-Laser Instrument[a]

nm	*355-nm laser line*																				nm
355	UV	Fluor	Marker	Cells																	360
370	UV1																				370
390	UV2																				390
405	*405-nm laser line*				Violet	Fluor	Marker	Cells													410
430	UV3				V1																430
440	UV4				V2																450
460	UV5				V3																460
470	UV6				V4																470
488	*488-nm laser line*								Blue	Fluorophore	Marker	Cells									490
510	UV7				V5				B1												510
520					V6				B2												520
540	UV8				V7				B3												540
561	*561-nm laser line*												Green	Fluorophore	Marker	Cells					560
580	UV9				V8				B4				YG1								580
600					V9				B5				YG2								600

(*Continued*)

Table 4 Panel Distribution Table for a Five-Laser Instrument[a], *continued*

nm	*355-nm laser line*																				nm
615	UV10				V10				B6				YG3								615
640	*640-nm laser line*																Red	Fluorophore	Marker	Cells	640
660	UV11				V11				B7				YG4				R1				660
680									B8				YG5				R2				680
695	UV12				V12				B9				YG6				R3				695
720	UV13				V13				B10				YG7				R4				720
740									B11				YG8				R5				740
750	UV14				V14				B12				YG9								750
760																	R6				760
780	UV15				V15				B13				YG10				R7				780
810	UV16				V16				B14				YG10				R8				810

[a]This table can be used to predict the spread induced for co-expressed markers. As a general rule, the closer the emission peaks of two fluorophores are, the more spreading error and spillover will be observed between them. The table is structured to represent all the detectors of a five-laser Aurora based on their wavelength detection range upon excitation by one of the five lasers. Each marker-fluorophore combination should be assigned to the row corresponding to the emission peak of the fluorophore. The main cell types expressing the marker should be annotated. Co-expressed markers should never be close in the same column, in order to avoid the emergence of spreading error. If possible, they should also not be in the same row, as dyes showing a broad excitation spectrum will tend to emit in the same wavelength after being excited by different lasers.

Table 5 Completed Panel Distribution Table for a 25-Color Panel to Detect Type 2 Cytokine Expression by Skin Immune Cells[a]

nm	Violet	Dye	Marker	Cells	Dilution	Blue	Dye	Marker	Cells	Dilution	Red	Dye	Marker	Cells	Dilution
420	V1	BV421	SiglecF	Eosinophils	100										
440	V2														
460	V3	Pacific Blue	MHCII	DCs MACs	10,000										
480	V4														
490	*488 nm*														
510	V5	AmCyan	IL-4	Basophils, T cells	Reporter	B1	BB515	CD25	Lymphoids	100					
530	V6					B2	YFP	YFP	Basophils	Reporter					
550	V7	BV510	CD8a	CD8+ T cells	200	B3									
570	V8	BV570	CD11b	Myeloids	100	B4	PE	CD301	M2/DCs	100					
590	V9					B5	dsRed	IL-13	ILCs T cells	Reporter					
610	V10	BV605	TCRb	CD4+/CD8+ T cells	100	B6	PE-Dazzle 594	CD64	MACs	100					
640	*640 nm*														
660	V11	BV650	NK1.1	NKs	100	B7					R1	AF647	CD206	M2/DCs	800
680	V12					B8	PE-Cy5	CD3	T cells	600	R2	APC	CD200R3	Basophils Mast cells	100
700	V12					B9	BB700	cKit	Mast cells	200	R3	APC-Cy55	CD45	all	50
720	V13	BV711	Ly6G	Neutrophils	200	B10	PerCP-eF710	TCRgd	gd T cells	2000	R4	AF700	Ly6C	Monocytes	400
740	V14	BV750	CD4	CD4+ T cells	100	B11					R5				
780	V15	BV786	CD11c	DCs MACs	100	B12					R6	Zombie NIR	Dead	Dead	2000 in PBS
800	V16					B14	PE-Cy7	CD90.2	Lymphoids	2000	R8	APC-CH7	CD19	B cells	100

[a]Following the rules described in the Basic Protocol, the table was first filled with reporters (red) and then with essential or rare markers (orange), followed by different lineage markers of rare (yellow), intermediate (blue), or common (white) availability.

antigen identification table (Table 2) to annotate the associated cell subsets, clones, readout characteristics, antigen density, and fluorophore availability.

Instrument and spectral signatures

A three-laser Cytek Aurora was used for this experiment. By using online fluorescence spectra viewers, we were able to identify 25 fluorophores with distinct signatures that could be used in the panel.

Assignment of markers to fluorophores

We sequentially assigned fluorophores to the markers of interest in a panel distribution table (such as Table 3, or Table 4 if a five-laser Aurora were to be used). A completed panel distribution table can be found in Table 5, where the main steps of the fluorophore assignment sequence have been color coded.

Our primary readouts of interest were IL-4 (AmCyan) and IL-13 (dsRed) expression by different cell types. All of our cell types of interest expressed CD45, as they were leukocytes, so it was important to have a bright CD45 signal that did not spread in our readout channels. We chose APC-Cy5.5 because of its unique spectral signature and the rarity of this dye on the market. Similarly, we expected $CD4^+$ $CD3^+$ Th2 cells to be a major source of both IL-4 and IL-13. CD4 expression is quite selective and relatively high, so we assigned it to a less common fluorophore that creates and receives some spread (BV750). CD3 expression is very heterogeneous in the skin: αβ T cells show low expression after digestion, whereas DETCs show very high expression. We needed a dye bright enough to be able to detect the $CD3^{low}$ population and to gate on $CD3^-$ cells while keeping $CD3^{hi}$ cells on scale. Here, we chose PE-Cy5, which is moderately bright on the three-laser Cytek Aurora.

The commercial availability of anti-CD200R3 antibodies is sparse, and we were limited to either APC or PE. As basophils and mast cells express CD200R3 and can express IL-13, we chose APC for our panel so as not to create any spread in the IL-13 dsRed channel. We knew from the literature that cKit is strongly expressed by mast cells (Roediger et al., 2013), but preliminary testing showed that its expression was decreased upon digestion. We therefore assigned it to a bright marker (BB700) in order to have resilient identification of mast cells in our panel.

CD90.2 is strongly expressed in lymphoid cells. However, as the main positive lineage marker for ILC2 cells, it needed to have a very bright fluorophore that did not receive much spread from other channels. We chose to assign it to PE-Cy7. The other T-cell markers are well defined and semi-exclusive and could be assigned later, away from AmCyan or dsRed.

We also wanted to analyze the different macrophage subsets in the skin, which are not known to express type 2 cytokines. The expression of CD64 can be dim, so we chose to assign it to PE-Dazzle594, a very bright fluorophore. Macrophages also express CD11b at high levels, but it is also expressed by many other cell types at lower levels. However, only high expression of CD11b is lineage defining in our panel, so we chose to assign it to the dim BV570. Macrophages in the dermis are also known to express CD11c, which is a key lineage marker for dendritic cells. We assigned it to a bright dye (BV786), far from any interference with other macrophage markers.

Similarly, CD206 and CD301 expression defines type 2 subsets of macrophages and dendritic cells in the skin, but these markers are not expressed by other cells. We assigned them to AF647 and PE, based on availability. MHCII expression is critical to identify dendritic cells and is highly expressed. We assigned it to Pacific Blue, a dim marker. Ly6C expression is very high on inflammatory macrophages and monocytes, so it was assigned to AF700, far from other macrophage or monocyte markers.

More general markers, such as lineage-defining markers for eosinophils, neutrophils, NK cells, and B cells (SiglecF, Ly6G, NK1.1, CD19), were assigned to the remaining available fluorophores (BV421, BV711, BV650, and APC-H7, respectively). As these cell types could potentially express IL-4 and IL-13, they were assigned to fluorophores that were spectrally different from AmCyan and dsRed.

Other T-cell markers were then assigned based on availability (TCRβ BV605, TCRγδ PerCP-eF710, and CD8 BV510). Among one of the last markers to be assigned was CD25; it is dimly expressed on T cells and was thus assigned to BB515. Finally, the viability dye was assigned to Zombie NIR, based on the few free channels still available.

Panel review

Several pairs of dyes used in this panel are impacted by significant SE between them (such as AF647/APC and BB515/YFP). However, this effect was mitigated by assigning these fluorophores to non-co-expressed markers (e.g., CD206 and CD200R3 for AF647 and APC, respectively). Other difficult

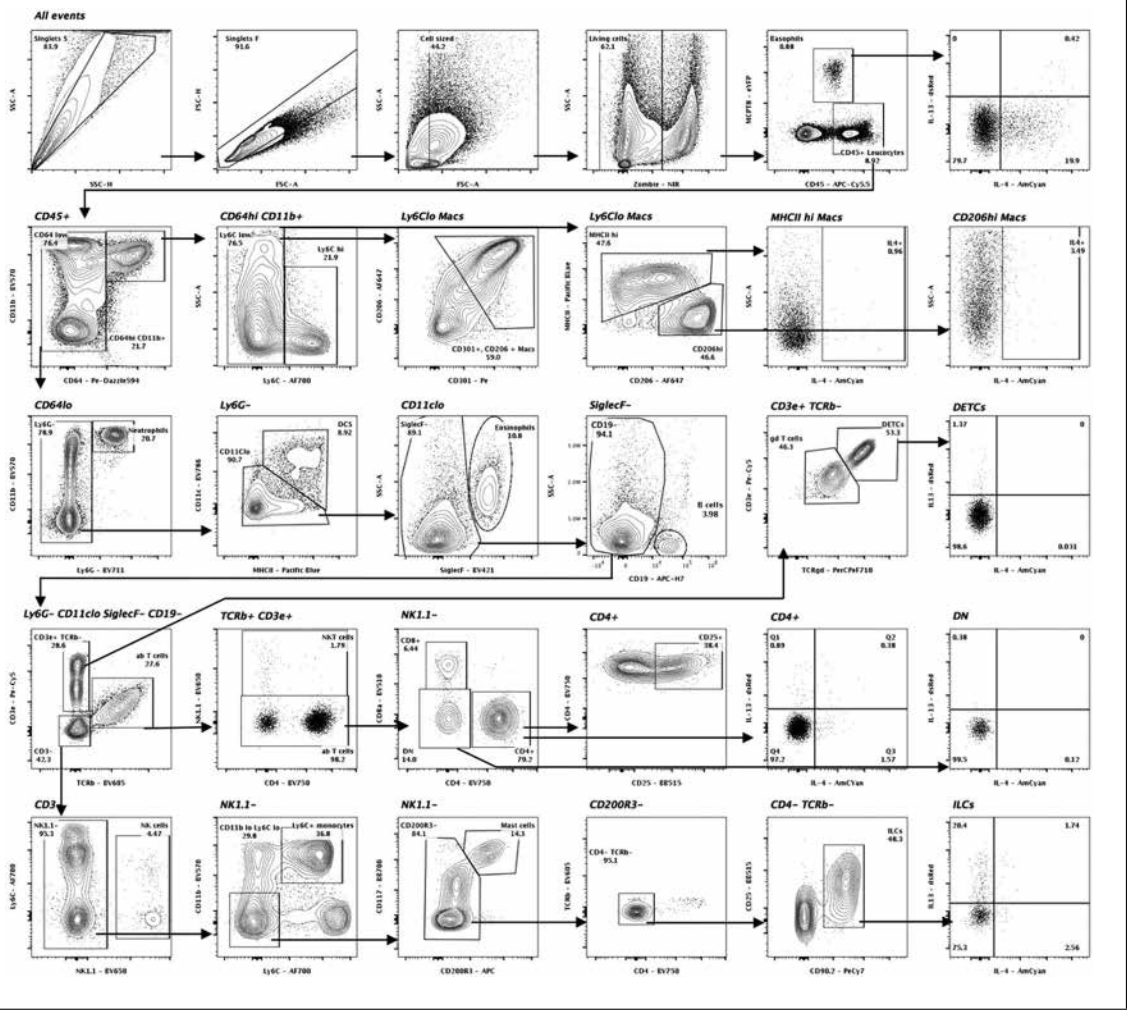

Figure 8 Gating strategy for the full 25-parameter staining panel for MC903-treated ear skin. $CD45^+$ leukocytes and YFP^+ basophils were gated from live single cells. $CD64^+$ $CD11b^+$ macrophages comprised a $Ly6C^+$ inflammatory subset and two $Ly6C^{lo}$ subsets, $MHCII^{hi}$ or $CD206^{hi}$. From the $CD64^{lo}$ population, neutrophils were identified as $CD11b^+$ $Ly6G^+$. In the $Ly6G^-$ population, dendritic cells were defined as $MHCII^+$ $CD11c^+$. Eosinophils were gated as $SiglecF^+$ SSC^{hi} cells from the $CD11c^{lo}$ subset, as were $CD19^+$ B cells. Within the $Ly6G^-$ $CD11c^{lo}$ $SiglecF^-$ $CD19^-$ population, $TCR\beta^+$ $CD3^+$ T cells and $CD3^+$ $TCR\beta^-$ T cells were identified. $\alpha\beta$T cells included $NK1.1^+$ NKT cells, $CD8^+$ T cells, $CD4^+$ T cells, and $CD4^-$ $CD8^-$ double-negative (DN) T cells. The $CD4^+$ subset further contained a population of $CD25^+$ T cells. The $TCR\beta^-$ population could be divided into two subsets of $\gamma\delta$T cells, including a CD3/CD90.2/$\gamma\delta TCR^{vhi}$ dendritic epidermal T-cell (DETC) population. $CD3^-$ subsets were gated as $NK1.1^+$ NK cells, $CD11b^+$ $Ly6C^+$ inflammatory monocytes, $CD11b^-$ $Ly6C^-$ $CD117^+$ $CD200R3^+$ mast cells, or lineage$^-$ $CD90.2^+$ $CD25^+$ ILC2 cells. The expression of IL-4 and IL-13 by relevant immune cells was separately analyzed.

combinations included PE/dsRed/PE-Dazzle 594, PE-Cy5/BB700/PerCP-eF710, and BV605/BV650/PE-Cy5, as the markers used with these combinations of fluorophores were known to be co-expressed on certain cell types. We took note of these particular fluorophore combinations and investigated their separation during the panel-testing phase.

Panel testing and optimization

Testing the panel on unstimulated ear skin revealed that all the populations could be resolved adequately by expert gating (Fig. 8). Our main readouts were expression of IL-4 (AmCyan) and IL-13 (dsRed) by the main skin leukocytes. In order to analyze the fluorescence of these reporters, Basoph8 × C57BL/6 samples were used as FMO-control groups to define the IL-4 and IL-13 expression boundary independently on each cell population using quadrant gates (Fig. 9).

However, during experimental inflammation of the skin, IL-4 expression on some macrophages was detected, creating SEs between IL-4 (AmCyan) and MHCII (Pacific Blue). We therefore reduced the

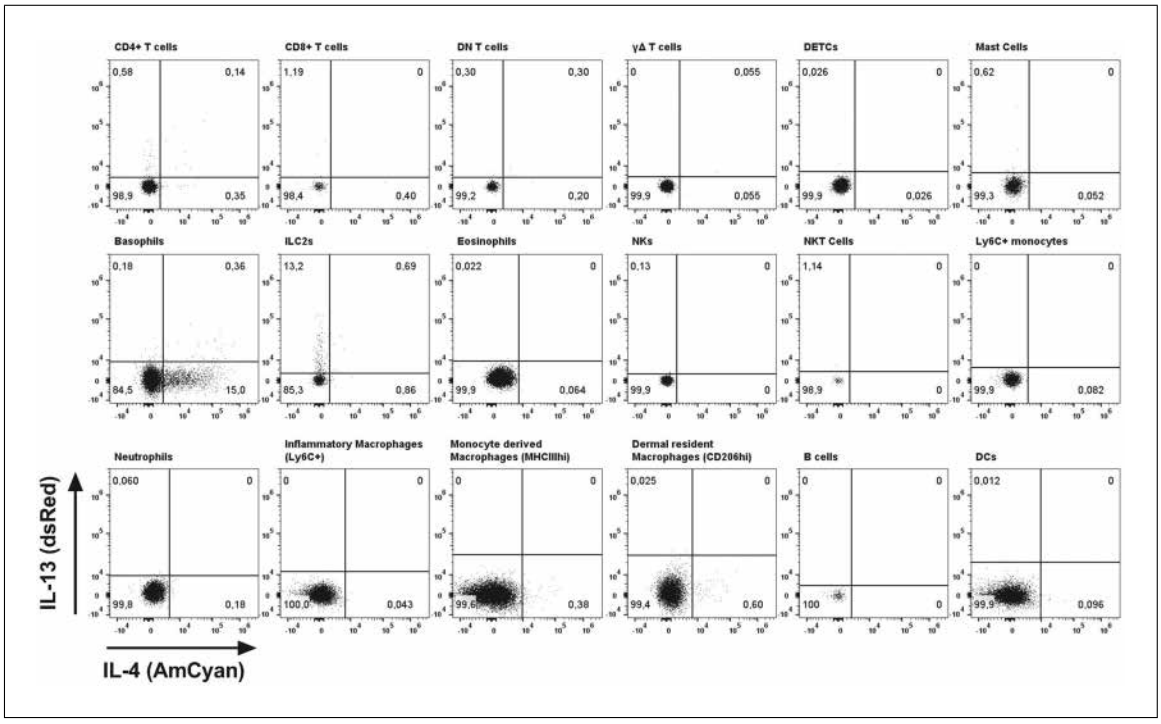

Figure 9 Expression of type 2 cytokines by skin leukocytes. Basoph8 × 4C13R or Basoph8 × C57BL/6 mice were treated for 10 days with topical MC903. Ear-skin leukocytes were analyzed for their expression of the readout markers IL-4 (AmCyan) and IL-13 (dsRed). Quadrant gates were defined independently for each population as positivity <0.1% by using treated Basoph8 × C57BL/6 samples as fluorescence-minus-one samples.

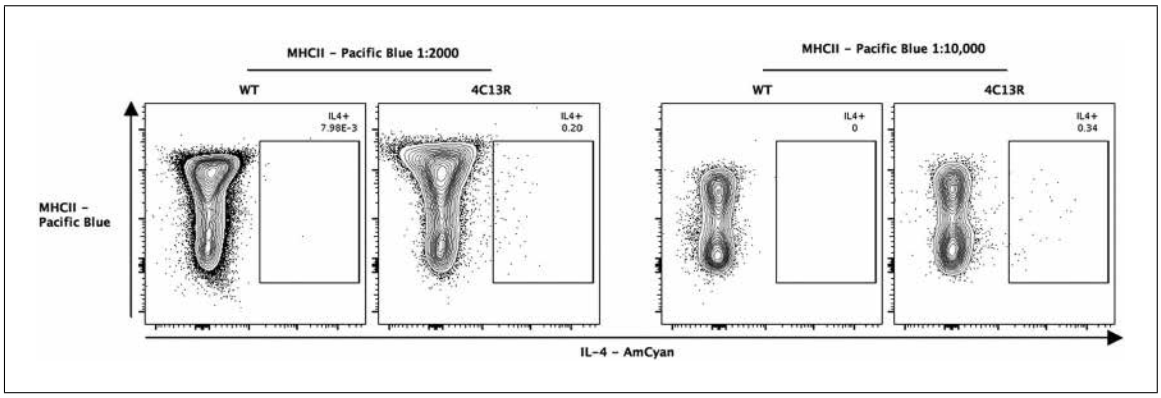

Figure 10 Spreading error of MHCII–Pacific Blue in the AmCyan channel. Analysis of MC903-treated wild-type (WT) ear skin revealed that the high expression of MHCII by CD45$^+$ CD64$^+$ CD11b$^+$ macrophages was impeding detection of IL-4-AmCyan in the reporter mouse. Reducing the concentration of the anti-MHCII–Pacific Blue antibody from a 1:2000 dilution (left panel) to a 1:10,000 dilution (right panel) did improve detection of IL-4 by reducing the spreading error of Pacific Blue into the AmCyan channel.

concentration of MHCII–Pacific Blue from 1:2000 to 1:10,000. This change considerably improved the resolution of IL-4 expression on macrophages, without impairing our ability to detect other MHCII$^+$ cell types, such as dendritic cells (Fig. 10).

Time Considerations

Designing, validating, and analyzing high-dimensional spectral flow cytometry panels takes significantly more time than running the actual experiment. It can take between 2 weeks and 1 month to design a well-optimized panel. It is therefore advisable to develop certain key panels that can be applied to several experimental questions and models. The following is a typical timeline:

- Week 1: Panel design and antibody ordering.
- Week 2: Antibody titrations, acquisition of single-stained cells and FMO controls (if needed), and panel review.
- Week 3: Second or third iteration of the panel if changes in fluorophore(s) or titer(s) have to be made.

Acknowledgments

This work was enabled by the Hugh Green Cytometry Centre, and we wish to thank the Hugh Green Foundation for their ongoing generosity and support. This research has also been funded by an independent research organization grant from the Health Research Council of New Zealand and by the Marjorie Barclay Trust. The authors are also very grateful to Kathy Muirhead, Katherine Woods, Joanne Lannigan, and Janelle Shook for their expert opinions and for reviewing the manuscript.

Literature Cited

Ashhurst, T. M., Smith, A. L., & King, N. J. C. (2017). High-dimensional fluorescence cytometry. *Current Protocols in Immunology*, *119*, 5.8.1–5.8.38. doi: 10.1002/cpim.37.

Bao, K., & Reinhardt, R. L. (2015). The differential expression of IL-4 and IL-13 and its impact on type-2 immunity. *Cytokine*, *75*, 25–37. doi: 10.1016/j.cyto.2015.05.008.

Brummelman, J., Haftmann, C., Núñez, N. G., Alvisi, G., Mazza, E. M. C., Becher, B., & Lugli, E. (2019). Development, application and computational analysis of high-dimensional fluorescent antibody panels for single-cell flow cytometry. *Nature Protocols*, *14*, 1946–1969. doi: 10.1038/s41596-019-0166-2.

Chen, F., Wu, W., Millman, A., Craft, J. F., Chen, E., Patel, N., … Gause, W. C. (2014). Neutrophils prime a long-lived effector macrophage phenotype that mediates accelerated helminth expulsion. *Nature Immunology*, *15*, 938–946. doi: 10.1038/ni.2984.

Cossarizza, A., Chang, H.-D., Radbruch, A., Akdis, M., Andrä, I., Annunziato, F., … Zimmermann, J. (2017). Guidelines for the use of flow cytometry and cell sorting in immunological studies. *European Journal of Immunology*, *47*, 1584–1797. doi: 10.1002/eji.201646632.

Dittrich, W., & Göhde, W. (1969). [Impulse fluorometry of single cells in suspension]. *Zeitschrift fur Naturforschung. Teil B, Chemie, Biochemie, Biophysik, Biologie und verwandte Gebiete*, *24*, 360–361. Retrieved from http://www.ncbi.nlm.nih.gov/pubmed/4389205.

Futamura, K., Sekino, M., Hata, A., Ikebuchi, R., Nakanishi, Y., Egawa, G., … Tomura, M. (2015). Novel full-spectral flow cytometry with multiple spectrally-adjacent fluorescent proteins and fluorochromes and visualization of in vivo cellular movement. *Cytometry A*, *87*, 830–842. doi: 10.1002/cyto.a.22725.

Grégori, G., Patsekin, V., Rajwa, B., Jones, J., Ragheb, K., Holdman, C., & Robinson, J. P. (2012). Hyperspectral cytometry at the single-cell level using a 32-channel photodetector. *Cytometry Part A*, *81A*, 35–44. doi: 10.1002/cyto.a.21120.

Hulspas, R. (2010). Titration of fluorochrome-conjugated antibodies for labeling cell surface markers on live cells. *Current Protocols in Cytometry*, *54*, 6.29.1–6.29.9. doi: 10.1002/0471142956.cy0629s54.

Johansson, U., & Macey, M. (2014). Tandem dyes: Stability in cocktails and compensation considerations. *Cytometry Part B: Clinical Cytometry*, *86*, 164–174. doi: 10.1002/cytob.21154.

Keenan, M. R., Timlin, J. A., Van Benthem, M. H., & Haaland, D. M. (2002). Algorithms for constrained linear unmixing with application to the hyperspectral analysis of fluorophore mixtures. *Proceedings of the SPIE*, *4816*, 193–202. doi: 10.1117/12.451662.

Lawrence, W. G., Varadi, G., Entine, G., Podniesinski, E., & Wallace, P. K. (2008). Enhanced red and near infrared detection in flow cytometry using avalanche photodiodes. *Cytometry. Part A : The Journal of the International Society for Analytical Cytology*, *73*, 767–776. doi: 10.1002/cyto.a.20595.

Le Roy, C., Varin-Blank, N., Ajchenbaum-Cymbalista, F., & Letestu, R. (2009). Flow cytometry APC-tandem dyes are degraded through a cell-dependent mechanism. *Cytometry A*, *75A*, 882–890. doi: 10.1002/cyto.a.20774.

Mahnke, Y. D., & Roederer, M. (2007). Optimizing a multicolor immunophenotyping assay. *Clinics in Laboratory Medicine*, *27*, 469–485. doi: 10.1016/j.cll.2007.05.002.

Monici, M. (2005). Cell and tissue autofluorescence research and diagnostic applications. In R. M. El-Gewely (Ed.), *Biotechnology Annual Review* (pp. 227–256). Amsterdam, the Netherlands: Elsevier Science. Retrieved from https://linkinghub.elsevier.com/retrieve/pii/S1387265605110072.

Nguyen, R., Perfetto, S., Mahnke, Y. D., Chattopadhyay, P., & Roederer, M. (2013). Quantifying spillover spreading for comparing instrument performance and aiding in multicolor panel design. *Cytometry Part A*, *83A*, 306–315. doi: 10.1002/cyto.a.22251.

Nolan, J. P., & Condello, D. (2013). Spectral flow cytometry. *Current Protocols in Cytometry*, *63*, 1.27.1–1.27.13. doi: 10.1002/0471142956.cy0127s63.

Nolan, J. P., Condello, D., Duggan, E., Naivar, M., & Novo, D. (2013). Visible and near infrared fluorescence spectral flow cytometry. *Cytometry Part A*, *83A*, 253–264. doi: 10.1002/cyto.a.22241.

Pellefigues, C., Mehta, P., Prout, M. S., Naidoo, K., Yumnam, B., Chandler, J., … Le Gros, G. (2019). The Basoph8 mice enable an unbiased detection and a conditional Depletion of Basophils. *Frontiers in Immunology*, *10*, 2143. doi: 10.3389/fimmu.2019.02143.

Perfetto, S. P., Chattopadhyay, P. K., & Roederer, M. (2004). Seventeen-colour flow cytometry: Unravelling the immune system. *Nature Reviews Immunology*, *4*, 648–655. doi: 10.1038/nri1416.

Robinson, J. P. (2019). Spectral flow cytometry—Quo vadimus? *Cytometry A*, *95*(8), 823–824. doi: 10.1002/cyto.a.23779.

Robinson, J. P., Rajwa, B., Gregori, G., Jones, J., & Patsekin, V. (2005). Multispectral cytometry of single bio-particles using a 32-channel detector. *Advanced Biomedical and Clinical Diagnostic Systems III*, *5692*, 359.

Roederer, M., De Rosa, S., Gerstein, R., Anderson, M., Bigos, M., Stovel, R., … Herzenberg, L. (1997). 8 color, 10-parameter flow cytometry to elucidate complex leukocyte heterogeneity. *Cytometry*, *29*, 328–339. doi: 10.1002/(SICI)1097-0320(19971201)29:4%3c328::AID-CYTO10%3e3.0.CO;2-W.

Roediger, B., Kyle, R., Yip, K. H., Sumaria, N., Guy, T. V., Kim, B. S., … Weninger, W. (2013). Cutaneous immunosurveillance and regulation of inflammation by group 2 innate lymphoid cells. *Nature Immunology*, *14*, 564–573. doi: 10.1038/ni.2584.

Schmutz, S., Valente, M., Cumano, A., & Novault, S. (2016). Spectral cytometry has unique properties allowing multicolor analysis of cell suspensions isolated from solid tissues. *PLOS ONE*, *11*, e0159961. doi: 10.1371/journal.pone.0159961.

Steinkamp, J. A., Orlicky, D. A., & Crissman, H. A. (1979). Dual-laser flow cytometry of single mammalian cells. *The Journal of Histochemistry and Cytochemistry: Official Journal of the Histochemistry Society*, *27*, 273–276. doi: 10.1177/27.1.374585.

Sun, B., Zhu, L., Tao, Y., Sun, H.-X., Li, Y., Wang, P., … Zhao, Y. (2018). Characterization and allergic role of IL-33-induced neutrophil polarization. *Cellular & Molecular Immunology*, *15*, 782–793.

Tario, J. D., & Wallace, P. K. (2014). Reagents and cell staining for immunophenotyping by flow cytometry. In *Pathobiology of human disease* (pp. 3678–3701). San Diego, CA: Elsevier. Retrieved from: https://linkinghub.elsevier.com/retrieve/pii/B9780123864567071045.

Vantourout, P., & Hayday, A. (2013). Six-of-the-best: Unique contributions of γδ T cells to immunology. *Nature Reviews Immunology*, *13*, 88–100. doi: 10.1038/nri3384.

von Bubnoff, D., Andrès, E., Hentges, F., Bieber, T., Michel, T., & Zimmer, J. (2010). Natural killer cells in atopic and autoimmune diseases of the skin. *Journal of Allergy and Clinical Immunology*, *125*, 60–68. doi: 10.1016/j.jaci.2009.11.020.

Wade, C. G., Rhyne, R. H., Woodruff, W. H., Bloch, D. P., & Bartholomew, J. C. (1979). Spectra of cells in flow cytometry using a vidicon detector. *The Journal of Histochemistry and Cytochemistry: Official Journal of the Histochemistry Society*, *27*, 1049–1052. doi: 10.1177/27.6.110874.

Method for DNA Ploidy Analysis Along with Immunophenotyping for Rare Populations in a Sample using FxCycle Violet

Prashant Tembhare,[1] Yajamanam Badrinath,[1] Sitaram Ghogale,[1] and Papagudi Ganesan Subramanian[1]

[1]Hematopathology Laboratory, Advanced Centre for Treatment Research and Education in Cancer, Tata Memorial Centre, Navi Mumbai, India

The clinical use of flow cytometric DNA ploidy assay has been extended towards stratifying the risk of diseases, such as monoclonal gammopathies or B cell acute lymphoblastic leukemia, and to detect circulating tumor cells, both of which require detection of minute cell populations. This unit describes a protocol for determining DNA ploidy in fixed samples with simultaneous surface immunophenotyping. It is an easy method for simultaneous 6- to 8-color immunophenotyping and DNA content analysis using FxCycle Violet (FCV; DAPI) dye. This protocol is a one-step modification of routine multicolor immunophenotyping that includes surface staining followed by fixation and then DNA staining with FCV. It utilizes mature lymphocytes from the sample as an internal control for determination of DNA index. It is a sensitive method that allows DNA-ploidy determination and cell cycle analysis in a rare tumor population as low as 100 events, as well as DNA ploidy determination in various subsets of hematopoietic cells in the same sample based on their immunophenotype.

Keywords: DNA ploidy • FxCycle Violet • DAPI • flow cytometry • 6- to 8-color immunophenotyping

SIGNIFICANCE STATEMENT

Current literature describes several methods for flow cytometric DNA ploidy analysis including those for simultaneous evaluation of surface immunophenotyping and DNA content analysis. However, these methods are either technically complicated (involve multiple steps), time-consuming (need prolong incubation), difficult to reproduce or limited to only 2- to 3-color immunophenotyping. Six to eight color immunophenotyping allows adequate separation of various subsets of different cell lineages (e.g., T cells, B cells, stem cells, granulocytes, etc.), as well as identify tumor cells (even a rare population) in the background rich in its normal counterpart and other hematopoietic cells. The present protocol describes a very simple and easy method of simultaneous 6- to 8-color immunophenotyping and DNA ploidy determination using FxCycle Violet, a dye excited with a violet laser.

Current Protocols in Cytometry 6.38.1-6.38.15, April 2017
Published online April 2017 in Wiley Online Library (wileyonlinelibrary.com).
doi: 10.1002/cpcy.15

Flow cytometric (FC) DNA content (DNA ploidy) determination is an easy and rapid method to study DNA content and to estimate proportion of cells present in different phases of the cell cycle. It is widely used in the research, as well as in the clinical management of many solid tumors and hematolymphoid malignancies (Vago, 1995; Yuan et al., 2004; Darzynkiewicz, 2010a).Many methods are described to determine DNA ploidy and cell cycle analysis in the samples containing relatively large number of tumor cells (Darzynkiewicz, 2010b). However, it is challenging to evaluate DNA ploidy or cell cycle analysis in samples with minimal tumor involvement having a minute or rare tumor population in the background rich in normal cells from different lineages [e.g., clonal plasma cells in bone marrow aspirate (BM) of monoclonal gammopathies (MGs) or, minimal residual disease (MRD) in BM or circulating tumor cells in peripheral blood]. In samples like bone marrow aspirate, peripheral blood or body fluids with minimal involvement, the tumor cells are very few and other normal or reactive cells are present in the large number. In these situations, simultaneous evaluation of multicolor immunophenotyping and DNA ploidy assessment is the best way to adequately identify and separate the tumor cells with characteristic immunophenotype using four or more markers (≥4-color) and then to determine its DNA ploidy.

In this unit, we describe an easy method for simultaneous 6- to 8-color immunophenotyping and DNA ploidy analysis using a novel dye "FxCycle Violet" (FCV) from Invitrogen (cat. no. F10347; *http://www.lifetechnologies.com/order/catalog/product/F10347)*. FCV (another name = DAPI: 4′, 6-diamidino-2-phenylindole, dihydrochloride) is a DNA selective dye that is excited with a 405/407-nm laser (violet laser) with emission collected in the 450/50 BP filter or equivalent. FCV preferentially stains double-stranded DNA (Kapuściński and Skoczylas, 1978); it appears to be associated with AT clusters in the minor groove (Kubista et al., 1987). Thus, using this dye, the spectrum for colors excited with a blue and red laser is spared for simultaneous surface immunophenotyping up to eight markers. The use of six to eight markers along with DNA staining easily isolates small tumor cell population within the background of its normal counterpart, as well as other hematopoietic cells. In this method, the methodology routinely used for surface marker staining for immunophenotyping is used with an additional step of sample incubation with FCV after fixation. Hence, this method does not affect the results of surface immunophenotyping. Thus, this method is very easy and simple to perform 6- to 8-color surface immunophenotyping (antibodies conjugated with fluorochromes excited with ablue and red laser) along with DNA ploidy analysis in hematolymphoid neoplasms (Tembhare et al., 2016). Moreover, use of 6- to 8-color immunophenotyping allows differentiation of rare tumor cell population co-existing with its normal counterpart like BCPALL MRD with hematogones or clonal plasma cells with normal plasma cells and ploidy can be analyzed in this rare cell population.

Briefly, in this protocol, the cells are processed for surface markers using routine method for immunophenotyping and then cells are fixed for 15 min followed by FCV/DAPI staining for 30 min. Then, the intensity of cellular fluorescence is measured by a flow cytometer with violet laser and data are analyzed using any flow cytometry software.

Materials

Sample to be processed: Any unfixed sample like peripheral blood (PB), bone marrow aspirate (BM), fine needle aspirate (FNA), body fluids within 24 to 48 hr of collection can be processed for the DNA-ploidy using this method (this protocol has been standardized using EDTA anticoagulated bone marrow aspirate and peripheral blood samples)

Red cell lysing reagent (see recipe)

Phosphate buffer saline (PBS) solution with 0.5% albumin (PBS-A; see recipe)

Table 6.38.1 Details for Antibodies Used for B cell Precursor Acute Lymphoblastic Leukemia (B-ALL) and Multiple Myeloma (MM)[a]

Fluorochrome		FITC	PE	ECD/PE-CF594	PC5.5	PC7	APC	APC-Alexa Fluor 700	APC-Alexa Fluor 750
B cell precursor acute lymphoblastic leukemia antibody and DNA ploidy panel									
Antibody/ reagent	FxCycleViolet	CD58	CD86	CD25	CD34	CD10	CD19	CD45	CD38
Catalog number	F_10347	IM1218U	555658	562 403	347 203	A46527	IM2470	A71117	A86049
Clone		*AICD58*	*2331(FUN-1)*	*M-A251*	*8G12*	*ALB1*	*J3-119*	*J.33*	*LS198-4-3*
Isotype control		IgG2a	IgG1	IgG1	IgG1	IgG1	IgG1	IgG1	IgG1
Company	Invitrogen	BC	BD	*BD*	BD	BC	BC	BC	BC
Multiple Myeloma and DNA ploidy panel									
Antibody/ reagent	FxCycle Violet	x	CD81	CD19	CD27	CD56	CD138	CD45	CD38
Catalog number	F_10347	x	IM2579	A07770	B21444	A 51078	A87787	A71117	A86049
Clone	x	*x*	*JS64*	*J3-119*	*1A4CD27*	*N901 (HLD-A6)*	*B-A38*	*J.33*	*LS198-4-3*
Isotype control	x	x	M IgG1	M IgG1	M IgG1	M IgG1	M IgG1	M IgG1	M IgG1
Company	Invitrogen	x	BC	BC	BC	BC	BC	BC	BC

[a]Abbreviations: BC, Beckman Coulter; BD, BD Biosciences.

Antibodies: Antibodies conjugated with fluorochromes that can be excited with blue and red laser depending upon the instrument; antibodies conjugated with fluorochromes excited with violet laser should be avoided due to significant spectral overlap with FCV (see Table 6.38.1 for details on the antibodies used)
Medium-A of Fix and Perm kit (Invitrogen, cat. no. GAS002S100)
Reconstituted FCV (see recipe)
Instrument quality control beads and set up beads: CS&T Beads (Becton Dickinson, cat. no. 642412), flowcheck beads (BC instrument, cat. no. A63493), and SPHERO Rainbow Calibration Particles (Spherotech, cat. no. RCP-30-5A)

12 × 75–mm polystyrene tubes
15-ml polypropylene tubes (Tarsons, cat. no. 546021)
Centrifuge
Pipets
Vortex
Neubauer chamber
Flow cytometer equipped with a 405-nm violet laser, 488-nm argon-ion lasers, and a 635-nm red laser, as a fluorescence excitation source like FACS Canto-II (BD), Navios (BC): this protocol has been used on both the instruments.
Flow cytometry analysis software: e.g., Kaluza, version 1.3 (Beckman Coulter)

Cell preparation, staining, and acquisition

This protocol uses red cell lysis followed by antibody staining and washing technique, which is commonly used for immunophenotyping.

Red cell lysis

Red cell lysis is performed using NH_4Cl-based RBC lysing reagent as per the procedure described below.

1. Aspirate 400 µl of sample into a 12 ×75–mm polystyrene tube (falcon tube or equivalent). For the rare event studies, aspirate 1 ml of sample into a 15-ml polypropylene centrifuge tube.

2. Add 4 ml red cell lysing reagent to the sample (sample to lysing reagent ratio: 1:10). For the rare event studies, add 10 ml RBC lysing reagent and mix well by gentle vortexing. Incubate the mixture of sample and lysing solution for 7 min at room temperature.

3. Centrifuge the sample for 2 min at 540 × *g*, room temperature, and then discard the supernatant by inverting the tube or using a pipet without disturbing the pellet.

Perform washes

4. Break the pellet by tapping the tube or by vortexing for 5 to 10 sec. Add 3 ml of PBS-A and mix well by gentle vortexing. Centrifuge it for 2 min at 540 × *g*, room temperature, and then discard the supernatant by inverting the tube or using a pipet without disturbing the pellet.

5. Repeat the wash procedure one more time and discard the supernatant.

Cells suspension and counting

6. Add 2 ml PBS-A to the pellet and mix well by gentle vortexing. Count the cells on a Neubauer chamber. Adjust the cell counts to get a cell concentration of 1 to 2 million cells per 50 µl.

Surface staining for immunophenotyping

Surface staining is done using the antibody panel to isolate a rare population of interest as per assay or experiment. This protocol describes the procedure for staining for plasma cells of plasma cell neoplasms.

7. Label a new 5-ml falcon or equivalent tube with proper identifier. Add appropriate volume of cell surface antibody cocktails/individual antibodies as determined by titration as described in *UNIT 6.29* (Hulspas, 2010).

8. Pipet 50 µl of cell suspension prepared in step 6 in this new tube with antibody cocktail and mix gently. Incubate for 20 min at room temperature protected from light. Vortex the tube for 5 to 10 sec to resuspend the cells.

9. Wash the cells by adding 2 ml PBS-A and mixing gently. Centrifuge for 2 min at 540 × *g*, room temperature, and discard the supernatant by inverting the tube or using a pipet without disturbing the pellet.

Fixation

10. Break the pellet by tapping the tube gently. Add 100 µl Medium-A of Fix & Perm kit and incubate it for 15 min at room temperature protected from light.

11. Wash the cells by adding 2 ml PBS-A and mixing gently. Centrifuge for 2 min at 540 × *g*, room temperature, and discard the supernatant by inverting the tube or using a pipet without disturbing the pellet.

FxCycle Violet (FCV) staining

12. Resuspend the above-stained cells in 500 µl PBS-A and vortex for 5 to 10 sec. Improper vortexing can result in partial staining of cells with FCV.

13. Add 5 µl of reconstituted FCV and then incubate it for 30 min at room temperature protected from light.

    NOTE: Do not wash the cells after staining with FCV.

14. Now the sample is ready for acquisition.

Cell fluorescence acquisition

Perform instrument quality measurement tests as per laboratory procedure or the manufacturer's guidelines. Optimize the instrument by running routine calibration microbeads. For FACS Canto-II (BD Biosciences): perform daily quality control measures using CS & T beads, as per the manufacturer's recommendations. For Navios (Beckman Coulter, BC): perform daily quality control measures using flow check beads as per the manufacturer's recommendations and check linearity using SPHERO Rainbow Calibration Particles. The steps for creating an acquisition protocol are described here with an example in a sample of multiple myeloma (MM). One can prepare a similar protocol for any hematolymphoid neoplasms.

NOTE: In the Navios instrument, "Area" is indicated by "Integral," "Height" is by "Peak" and "Width is by "Time of light (TOF)."

15. Create an acquisition experiment using normal peripheral blood sample as shown in Figure 6.38.1.
16. FCV is excited with a 405/407-nm laser (violet laser) and emission collected in the 450/50 BP filter or equivalent (FL-9 channel). Hence, set up the FL-9 (in case of Navios) or FL-7 (in case of FacsCanto II) with a linear scale for area, height, and width.
17. Adjust the compensation for all parameters (FL1 to FL10) as per the standard laboratory procedure.
18. Take a SSC-height linear versus FSC-height linear bivariate plot and adjust the PMT voltages to ensure that all cells are being acquired, and to eliminate unnecessary acquisition of debris (Fig. 6.38.1i).
19. Create a bivariate plot of CD45 versus side scatter-linear. Gate the mature lymphocytes (CD45 bright and low side scatter) with "CD45Lym" gate(Fig. 6.38.1ii).
20. Take bivariate plots for the assessment of expression pattern of various markers used for immunophenotyping of various cell populations including tumor or target cells. For the remaining FL1-FL8 parameters, acquire events in log scale as per standard surface staining procedure (Fig. 6.38.1iii to vi). Gate the tumor cells (Fig. 6.38.1 shows plasma cells in a BM sample of multiple myeloma) using expression pattern of relevant markers.
21. Create a "CD45Lym" gated histogram FL-9 with a linear scale for area to illustrate relative DNA content. For Navios, adjust the voltages for FL9 to get normal G0-G1 peak between channel numbers 300-350 (Fig. 6.38.1vii) and for FACS Canto-II, adjust the voltages for FL7 to get a normal G0-G1 peak at about the 50th channel of a 256-channel scale on FL7-Area linear scale.
22. Create a "tumor cell or cells of interest" gated (e.g., "plasma cells" gated) histogram with FL-9-Area in linear scale to illustrate relative DNA content (Fig. 6.38.1viii**).**
23. Acquire preferably 500 events (minimum of 100 events) tumor (target) cells and a minimum 200 mature lymphocytes with the acquisition software available with a flow cytometer. Use low flow rate for acquisition (approximately 100 to 200 events/second).

Analysis of DNA ploidy and surface staining

DNA ploidy and surface staining analysis can be performed with any software used for flow cytometric data analysis. For example, Kaluza software (Beckman Coulter), Diva (BD), Flow Jo, FCS Express, etc. Gating approach for DNA ploidy and surface staining

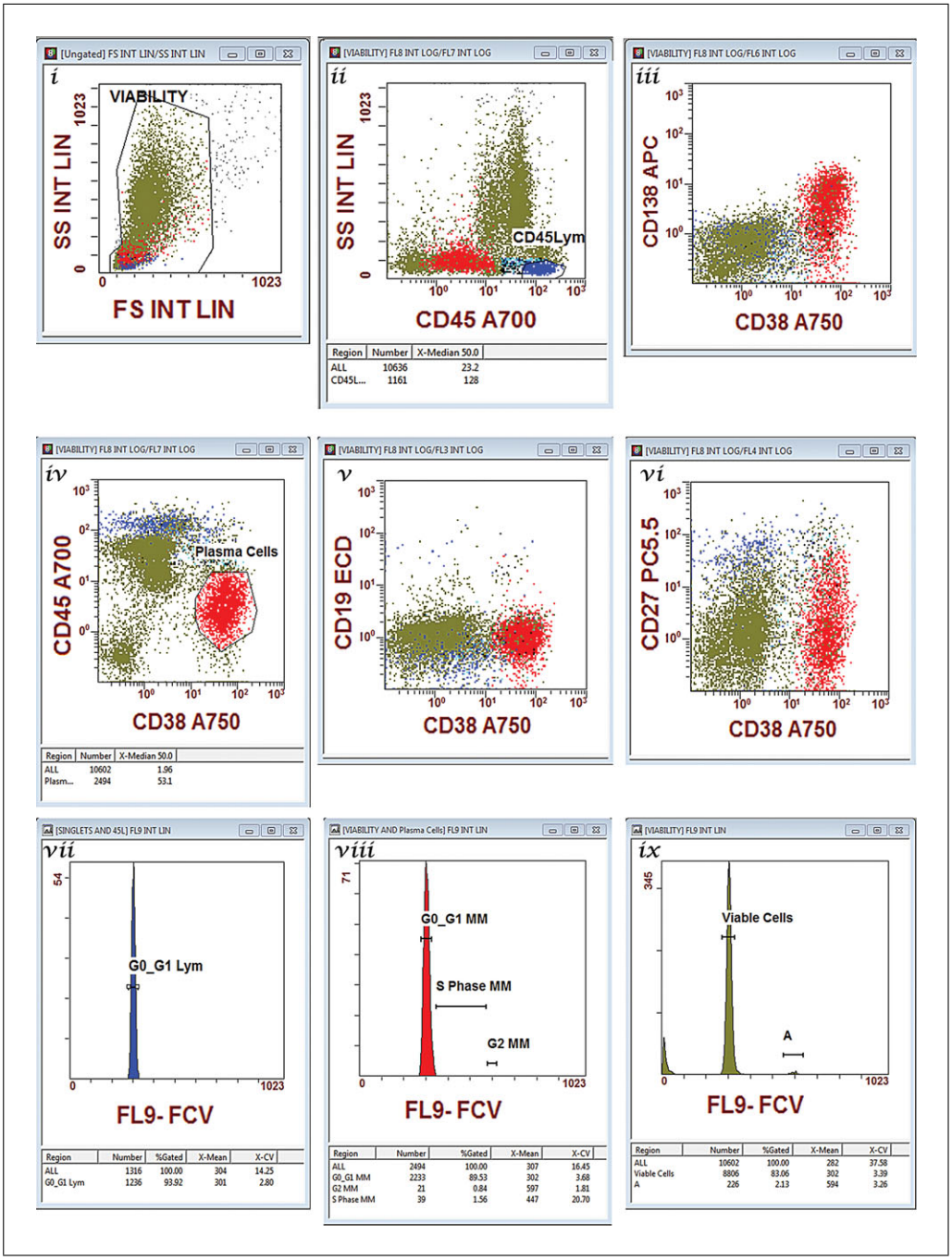

Figure 6.38.1 Demonstrates the acquisition protocol for multi-color immunophenotyping and DNA ploidy assessment using FxCycle Violet (FCV) with an example of bone marrow sample involved by multiple myeloma. Bivariate plot-i showed gating of viable cells of all ungated events with "VIABILITY" gate that was further applied on bivariate plots "ii, iii, iv, v, vi". In bivariate plot ii, the mature lymphocytes were gated (CD45Lym-gate) using strong CD45 expression and low side scatter property. Plots "ii, iii, iv, v, and vi" revealed the expression of various surface markers used in this panel i.e. CD45, CD38, CD138, CD19, and CD27. Based on the expression pattern of these markers, tumor cells (in this example "plasma cells") were gated in the plot iv. Histograms "vii, viii, and ix" showed FCV staining in mature lymphocytes, tumor cells i.e. plasma cells and all viable cells demonstrating their G0/G1 phase, S-phase, and G2 phase peaks.

analysis is described in Figure 6.38.2 using an example of DNA-ploidy analysis in the bone marrow aspirate sample of MM.

24. Take a bivariate-plot side scatter-linear versus forward scatter-linear (Fig. 6.38.2, bivariate-plot "a"). Draw a "Viability" gate in this bivariate plot to exclude the debris and apoptotic cells. Draw another mononuclear cell "MNC" gate to exclude the granulocytes from the analysis as the hematolymphoid tumor cells typically fall in the mononuclear cell region.

25. Create "Viability" gated FL9-FCV-Height versus FL9-FCV-Area density-plot (Fig. 6.38.2, density-plot "b") and exclude the doublets carefully using a "FCV A-H singlets" gate. It is important to extend the gate on left lower side to include the events up to channel number 100 channel less than that of "G0/G1" cluster of lymphocytes (which was set at channel number 300) and to include events G2 region.

26. Create "FCV A-H singlets" gated three to four bivariate plots displaying cell phenotype with markers (Fig. 6.38.2, bivariate plot "c, d, e, f") used in the panel. Based on the strong expression of CD45 and low side scatter, create a "CD45Lym" gate to select mature lymphocytes (Fig. 6.38.2, bivariate plot "d", gate "45Lym"). Similarly, based on the expression pattern of the surface of markers used in the panel, identify the tumor cells or cells of interest. In this example, MM, cells of interest to tumor cells, are plasma cells gated based on the strong CD38 and CD138expression, heterogeneous expression of CD27, weak expression of CD45 and negative expression of CD19 (Fig. 6.38.2, bivariate plot "e", gate "FCV PCs") present in the sample.

27. Analyze the cell cycle phases of mature lymphocytes and tumor cells or cells of interest and create two histograms with FCV-Area on the *x*-axis, first gated with mature lymphocytes (Fig. 6.38.2, histogram "g") and the second gated with tumor cells (e.g., FCV PCs in Figure 6.38.2, histogram "h"). Gate the events in G0/G1 phase with "G0/G1" gate, events in S-phase with "S" gate, and events in G2 phase with "G2" gate. Display coefficient of variation (CV) and geometric mean (GM) of "G0/G1" gated events in the statistic-section of histograms.

28. Determine the DNA Index (DI) of tumor population by calculating the ratio of GM of FCV of tumor cells in PC-G0/G1 phase to GM of FCV of mature lymphocytes G0/G1 phase. DNA Ploidy is categorized as diploidy, hypodiploidy, and hyperdiploidy for DI >0.95 to <1.06, ≤ 0.95, ≥ 1.06, respectively. The percentages of cells in S-phase are enumerated by the percentages of events in the "S" gate.

    The difference between the DNA content of mature lymphocytes and tumor cells or cells of interest can be further demonstrated in the overlay-plot (Fig. 6.38.2"K") or bivariate-plot with FCV-Area (log scale) versus side scatter (Fig. 6.38.2"l")

    Figure 6.38.2 demonstrates plasma cells with hyperdiploidy with DNA index (DI) of 1.34.

REAGENTS AND SOLUTIONS

Use distilled, deionized water in all recipes.

Phosphate-buffered saline with albumin (PBS-A), pH 7.2

Ingredients	Working solution	5× PBS
NaCl	8.0 g/liter	40.0 g/liter
$Na_2HPO_4 \cdot 2H_20$ (mol. wt. 277)	2.6 g/liter	13.0 g/liter
Albumin	2.0 g/liter	10.0 g/liter
KCl	2.0 g/liter	10.0 g/liter
KH_2PO_4	0.2 g/liter	1.0 g/liter
NaN_3	0.2 g/liter	1.0 g/liter

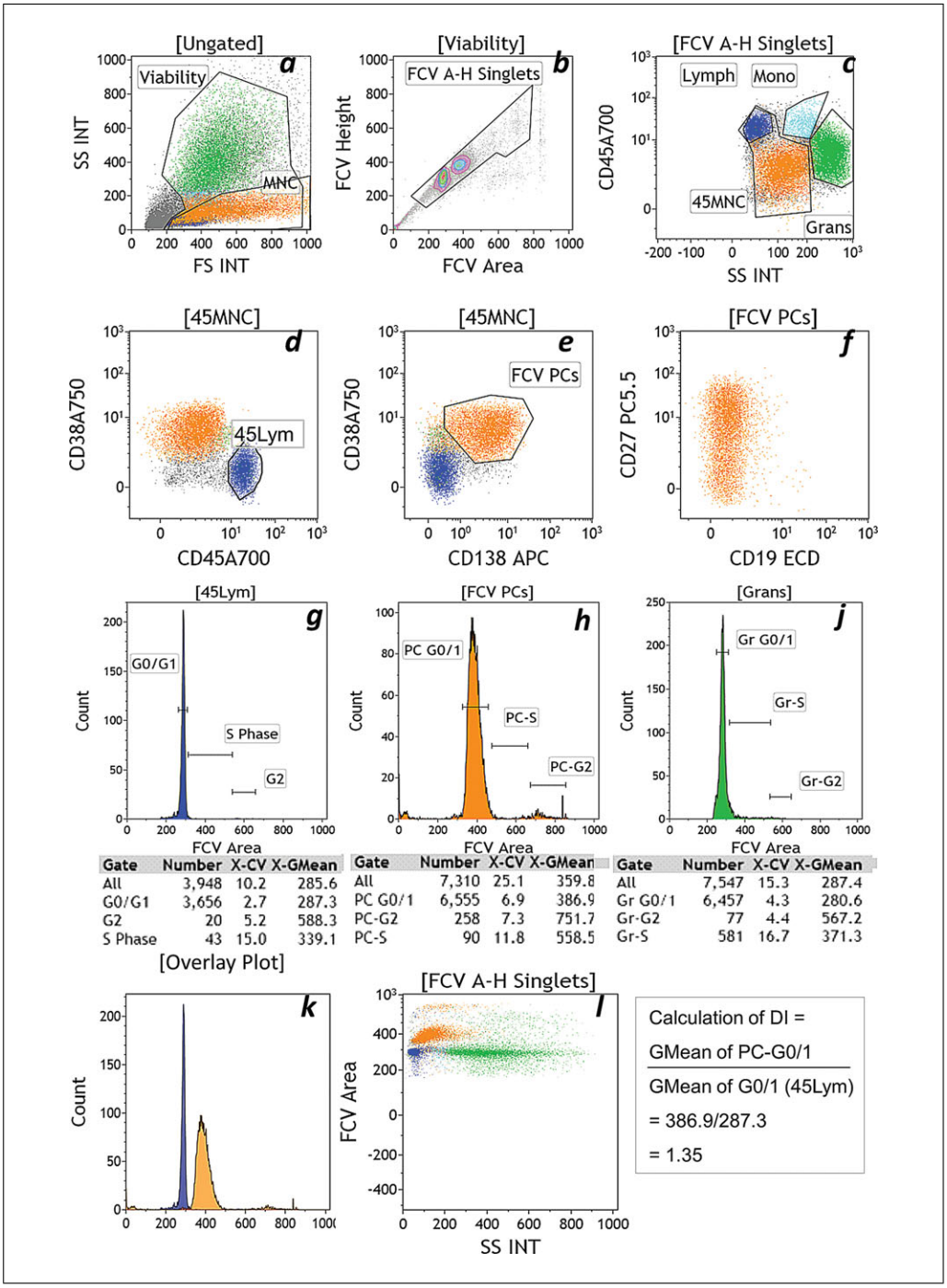

Figure 6.38.2 Demonstrates the analysis approach for multi-color immunophenotyping and DNA ploidy assessment using FxCycle Violet (FCV) with an example in bone marrow sample involved by multiple myeloma with hyperdiploidy. Bivariate plot "a" showed gating of viable cells out of all ungated events with "Viability" gate that excluded the cell debris (gray dots). Bivariate plot "b," showed exclusion of apoptotic and or FCV unstained cells using FCV A-H Singlets gate. On the basis of the expression pattern of various surface markers used in this panel (CD45, CD38, CD138, CD19, CD20, and CD27), bivariate plots "c, d, e, and f" demonstrated the gating of mature lymphocytes (blue dots) and tumor cells (in this example, plasma cellsorange dots) and granulocytes (green dots). Histograms "g, h, and j" showed FCV staining in mature lymphocytes, tumor cells i.e. plasma cells and granulocytes demonstrating their G0/G1 phase, S-phase, and G2 phase peaks. Plot "k" demonstrated the overlay of G0/G1 phase in FCV staining of normal mature lymphocytes and tumor cells (plasma cells) showing higher FCV staining in tumor cells as compared to normal lymphocytes which indicated "hyperdiploidy". Similarly, bivariate plot "l" showed higher staining of FCV in tumor cells as compared to lymphocytes and granulocytes. DNA index of tumor cells was found to be 1.35.

Mix all the above constituents in distilled water to make up the volume to 1000 ml

Working 1× buffer prepared when needed: Take 100 ml of 5× PBS (see recipe) and adjust volume to 500 ml using distilled/deionized water. Adjust pH between 7.0 and 7.5 using 1 N hydrochloric acid or 1 N sodium hydroxide solution, if required. Store up to 24 to 48 hr at room temperature.

Phsophate-bufferd saline (PBS)

0.23 g NaH_2PO_4 (anhydrous; 1.9 mM)
1.15 g Na_2HPO_4 (anhydrous; 8.1 mM)
9.00 g NaCl (154 mM)
Add H_2O to 900 ml
If needed, adjust to desired pH (usually 7.2 to 7.4) with 1 M NaOH or 1 M HCl
Add H_2O to 1 liter
Filter sterilize
Store indefinitely at 4°C

Reconstituted "FxCycle Violet" (FCV) stock solution

To prepare a stock solution of FCV stain, add 500 µl deionized water to one vial of the FCV (Invitrogen or Thermo Fisher Scientific, cat. no. F10347) stain. Mix well. Store this solution at 2° to 6°C, protected from light. When stored as directed, the stock solution is stable for at least 6 months.

Red cell lysing reagent

Ingredients	Working	5× PBS (see recipe)
NH_4Cl	8.26 g/liter	41.3 g/liter
$KHCO_3$	1.0 g/liter	5.0 g/liter
Tetra Sodium EDTA	0.037 g/liter	0.185 g/liter

Mix all the above components and dissolve them in 1000 ml distilled water

Working 1× lysing reagent prepared when needed: Take 40 ml of 5× lysing reagent and adjust volume up to 200 ml.

Store at 4° to 8°C

COMMENTARY

DNA ploidy determination is commonly used in the risk stratification of hematolymphoid neoplasms like B cell precursor acute lymphoblastic leukemia (BCPALL), multiple myeloma (MM) (Zhan et al., 2006; Kenney et al., 2008; O. Basu et al., 2009; Lopez-Otero et al., 2010). In addition, its application has been expanded in the prognostication of many nonhematological cancers (Danielsen et al., 2016). DNA ploidy analysis is clinically relevant in the risk stratification of hematological conditions with rare or minute tumor cells like precursor conditions of MM, i.e., smoldering (asymptomatic) myeloma and monoclonal gammopathies of undermined significance (MGUS) or circulating sezary cells in Mycosis Fungoides or in BCPALL MRD detection (Wang et al., 2004; Perez-Persona et al., 2007; Swerts et al., 2007).

Several methods for DNA ploidy and cell cycle analysis are available including DNA analysis with simultaneous immunophenotyping, but these methods harbor limitations especially in samples with small tumor cell population with a background rich with other normal hematopoietic cells. These limitation are described below. Propidium iodide (PI) based FC DNA ploidy analysis method is commonly used in many types of research, as well as clinical settings, which give high staining linearity independent of DNA conformational status and very low CV (Almeida et al., 1999). However, it is laborsome due to multiple steps, error prone, as it involves many reagents, and is time-consuming (few protocols require overnight incubation), as well as pH sensitive (Nowak et al., 1994). In addition, the broad emission spectrum of PI prevents the concomitant use of other adjacent channels like PE, APC (Corver et al., 2000) limiting its use for multicolor surface staining. Since PI stains double-stranded RNA similar as DNA, analysis of the later requires pre-incubation with RNase, or inclusion of RNase into the staining solution. It should be noted that, dyes like 7-AAD

and DRAQ5 can be used simultaneously along with surface staining with antibodies conjugated with FITC, PE and APC provided that the compensation adjustment is done adequately (Zelenin et al., 1984; Yuan et al., 2004). Unfortunately, 7-AAD may show staining variation due to heterogeneous chromatin packaging and cross-linking of DNA and/or of DNA-histones (Darzynkiewicz et al.,1984; Telford et al., 1992; Linden et al., 1997). Maurizio Carbonari et al. improved this method using acetone-based fixation and integral hot staining (IHS) technique (Carbonari et al., 2001). However, IHS can alter the levels of expression-pattern of surface antigens, if performed as a part of simultaneous immunophenotyping and moreover, it demands prolonged incubation for better DNA staining quality, with low CV (Mancaniello and Carbonari, 2008). Hence, it cannot be a method of choice useful in clinical samples with rare tumor population. DRAQ5, a far red-fluorescing agent with an excitation maximum around 650 nm and an emission spectrum ranging from 665 nm to beyond 780 nm, is another DNA dye shown to be useful in simultaneous immunophenotyping and ploidy analysis. Yuan C et al. and others evaluated and showed the successful use of DRAQ5 along with surface staining in hematological samples (Smith et al., 2004; Yuan et al., 2004; Swerts et al., 2007; Allan et al., 2008). Nevertheless, these studies are limited to maximum three-color immunophenotyping, which may not sufficiently separate a rare tumor population from its normal counterpart cells. For instance, in MGUS or smoldering myeloma (SMM) samples, in which abnormal plasma cells (PCs) coexist with normal polyclonal PCs in BM or in B-ALL post-induction BM samples with a residual disease where leukemic blasts coexist with normal B cell precursors or sezary cells from CD4+ T-cells in peripheral blood. In such situations, a multiparametric approach with a combination of four or more markers is required to differentiate tumor cells from its normal counterpart.

Advancements in the flow cytometry instruments with provision of three to four lasers and recent availability of wide spectrum of fluorochromes easily allow up to the ten-color immunophenotyping in clinical samples for the detection of rare tumor cells (Wood, 2006; Denys et al., 2013; Stacchini et al., 2014) and make it is possible to identify a minute tumor population such as MRD detection and detail characterization of the precursor diseases like MGUS, SMM. There are three major advantages of the present DNA ploidy protocol over the earlier published methods:

1. It uses a FCV-dye that utilizes violet-color excitation spectrum and hence, the emission spectra from green to the far red region is totally available for the surface marker staining with antibodies conjugated with fluorochromes excited with blue and red lasers. Thus, it allows simultaneous up to seven-color immunophenotyping and DNA ploidy analysis.
2. This protocol does not alter the routinely used surface staining protocol with a minor modification. It simply adds only one extra step of incubation of cells with FCV after surface immunophenotyping and fixation. Thus, it does not impose the cells for alteration of physical characteristics or surface marker expression patterns.
3. In this protocol, FCV incubation is just for 30 min after the surface staining and fixation, which makes it very simple to add to daily flow cytometry work list even in the laboratories with a heavy workload.

Therefore, this protocol makes it very easy to perform DNA ploidy analysis along with 6- to 8-color immunophenotyping in samples with rare tumor population. An additional benefit of this protocol is that it also permits analysis of the DNA content in the left-over cells after acquisition for routine immunophenotyping in leukemia or multiple myeloma. For example, if there are 4×10^5cells in the tube stained with surface antibodies (conjugated with fluorochromes excited with laser other than violet-laser) for acute leukemia and out of it, if 3×10^5 cells are acquired for immunophenotyping, then the remaining 1×10^5 cells can be further fixed and stained with FCV. Although the architecture of the cells remains well maintained, the CV of G0/G1 peak cells measured by FCV can be somewhat higher than that based on PI-staining technique (approximately 4% to 5%) due to auto fluorescence of certain cells, such as plasma cells.

Critical Parameters

Choice of fixative: Medium A-fixative by Invitrogen gives the best results with a low coefficient of variation (CV) of G0/G1 peak and a minimum number of unstained cells. Other fixatives like in-house prepared 0.5% paraformaldehyde and Medium-A from Fix and Perm kit (Dako, cat. no. K2311) result in the higher CV and low staining ability of FCV. Hence, it is critical to fix the cells using Medium-A from Fix and Perm kit (Invitrogen) to get low CV of G0/G1 peak in

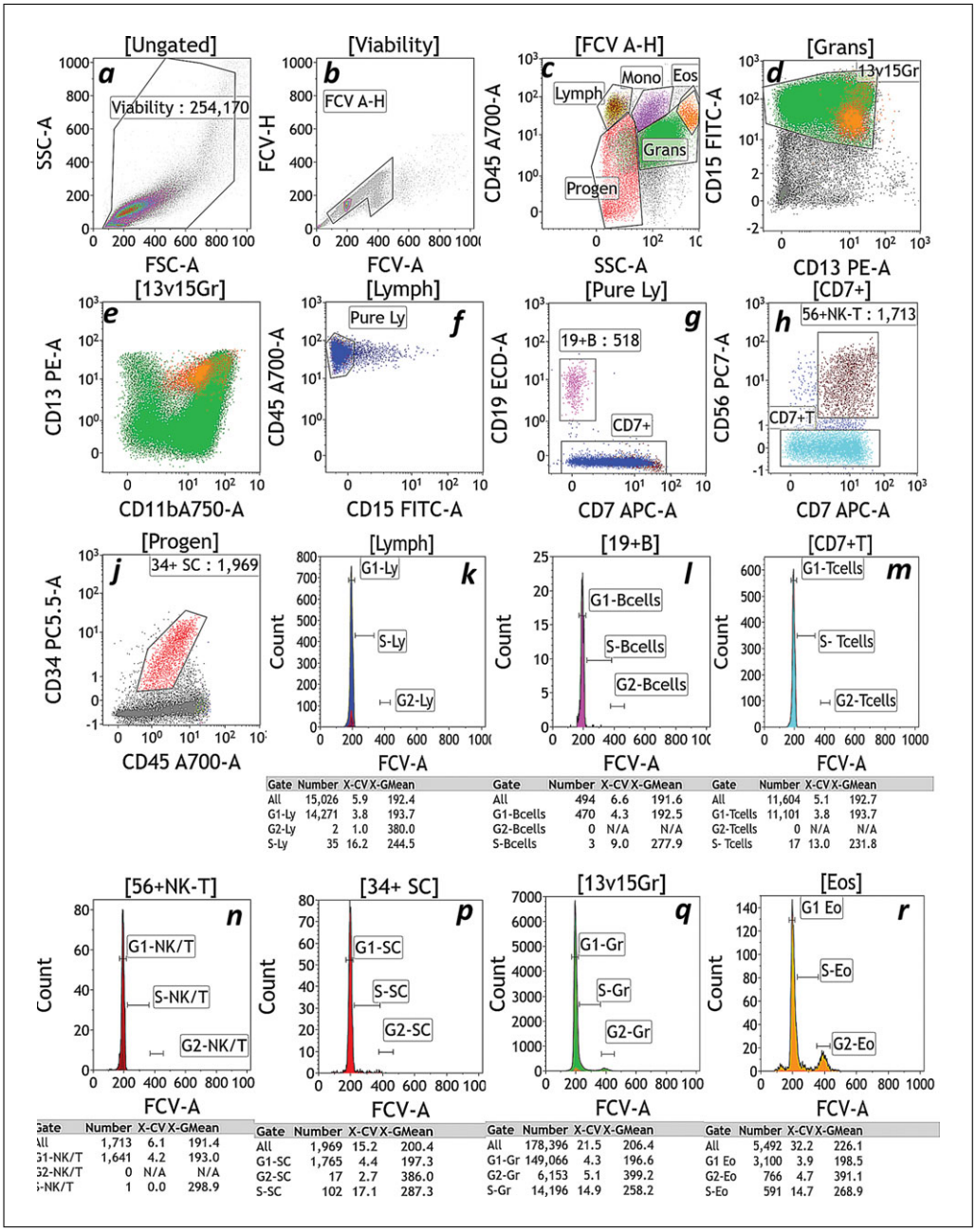

Figure 6.38.3 Demonstrates the simultaneous 8-color surface immunophenotyping and DNA ploidy analysis of different subsets of hematopoietic cells in a BM sample. Bivariate plots "d to j" various subsets of hematopoietic cells which included lymphocytes (CD45 strong/low side scatter), granulocytes (CD13+/CD15+), eosinophils (high side scatter/strong CD45), B cells (CD19+), T cells (CD7+), NK/T cells (CD7+/CD56+), and CD34+ stem cells. Bivariate plot "e" demonstrated maturation pattern of granulocytes with CD13 versus CD11b expression. Histograms "k to r" showed DNA content analysis with FCV staining of all these populations.

DNA-staining with FCV. (*NOTE*: We have not tried any alcohol-based fixative.)

Selection of fluorochromes: It is critical to avoid another marker conjugated with fluorescence excited with a violet laser due to the remarkable spectral overlap of FCV.

Reconstitution of FCV: It is critical to reconstitute FCV in deionized water only and mix properly. It should not be reconstituted in PBS. If it is reconstituted in PBS it does not stain the DNA optimally.

The concentration of cell suspension and speed of cell acquisition: Like any other ploidy assays, it is critical to have similar cell densities (similar DNA per FCV content ratio) in the comparable samples (Darzynkiewicz, 2010a) and maintain low acquisition rate i.e., <200 cells/second. The higher rate of

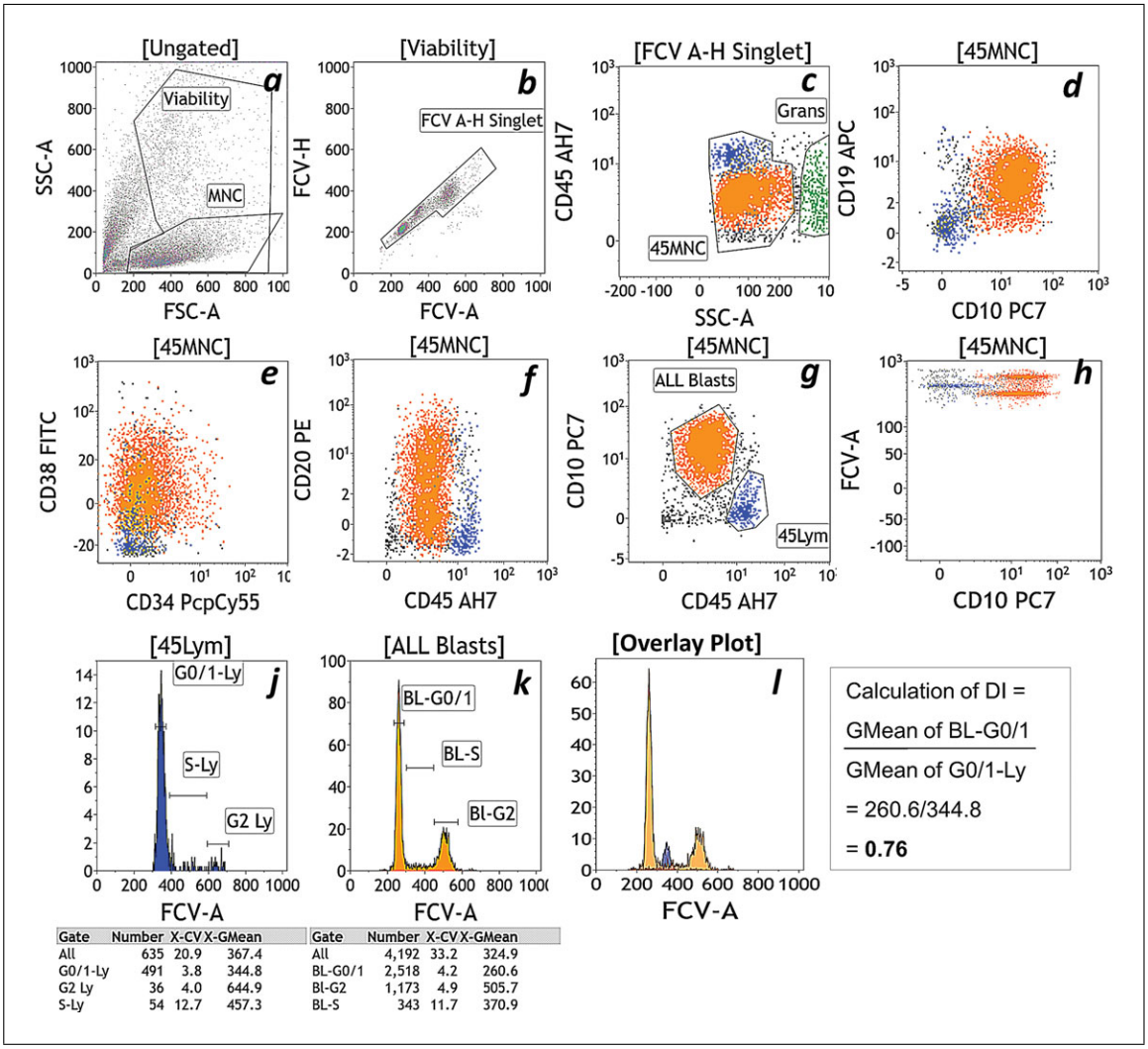

Figure 6.38.4 Demonstrates an example in hypodiploidy in a B cell acute lymphoblastic leukemia. Bivariate plot "a" showed gating of viable cells out of all ungated events with "Viability" gate that excluded the cell debris (gray dots). Bivariate plot "b" showed exclusion of apoptotic and or FCV unstained cells using FCV A-H Singlets gate. B-ALL blasts were gated on the basis of the expression pattern of various surface markers (CD10+, CD19+, CD20-/+, CD34-, CD38-/+, and CD45-/+). The bivariate plots "c to f" demonstrated the gating of mature lymphocytes (blue dots) and BALL blasts (orange dots). Histograms "j and k" showed FCV staining in mature lymphocytes, and BALL blasts demonstrating their G0/G1 phase, S-phase and G2 phase peaks. Plot "l" showed the overlay of G0/G1 phase in FCV staining of lymphocytes and BALL blasts revealing lower FCV staining in BALL blasts as compared to normal lymphocytes, which indicated "hypodiploidy."

acquisition can result in higher CV of G0/G1 peak in DNA analysis. Similarly, even if the acquisition speed is low but if the cell concentration is higher than one million cells/ 0.5 ml, this also leads to the acquisition of more than the recommended cells/second. Hence, it is critical to maintain the cell concentration and acquisition speed to the optimal levels.

Troubleshooting

Usually, the percentage of FCV-unstained cells is <10% of total gated cells. FCV-unstained cells more than 10% of the gated cells indicates suboptimal staining with FCV. The suboptimal staining with FCV can result from three main reasons:

1. *Inadequate reconstitution of FCV dye, low concentration of reconstituted FCV, or inadequate delivery of the dye due to improper pipetting:* To prevent pipetting errors caused by smaller volumes of liquid, it is advisable to reconstitute the FCV stain in 0.5 ml of deionized water such that 5 µl of the stain stock solution is added to the cell suspension.

2. *Insufficient FCV incubation time:* Although, in this protocol we have a standardized incubation period for 30 min, optimization may be required in order to address

variation in staining results caused by differences in batches of the FCV dye.

3. *Inconsistent staining of cells:* An important consideration for this method is the mixing of cells with PBS-A after the washing step following fixation. We have observed that in inexperienced hands this is a common mistake. Since the reconstituted FCV-dye is delivered directly to the cells resuspended in the PBS-A after fixation, the inadequate mixing of the PBS-A and cells prior to the addition of FCV-dye does not allow the FCV staining of all the cells present in the sample. Another issue that can affect the results of DNA ploidy assay is higher CV G0/G1 peak of gated cells. The presence of small cell clumps in the sample may broaden the axis of cell focus in front of the laser beam, which also can result in higher CV G0/G1 peak.

Anticipated Results

Simultaneous assessment of 6- to 8-color immunophenotyping and DNA ploidy analysis using FCV provides freedom of DNA ploidy and cell cycle analysis in multiple cell population present in the samples like BM, PB, or body fluids. This protocol literally allows isolating many cell subsets (e.g., lymphocytes, many subsets of lymphocytes, monocytes, eosinophils basophils, different stages of granulocytes, stem cells and its subsets, etc.) even if they are present as low as 200 events. Since multicolor immunophenotyping adequately differentiates abnormal cells from its normal counterpart cells (e.g., clonal plasma cells and normal plasma cells), it is easily possible to compare the DNA ploidy results between the two compartments. This protocol uses the normal mature lymphocytes from the same person as reference cells, which makes it is easy to calculate the DNA index and reduces the error in the result due to individual variation in the A-T regions and cell stainability with the fluorochrome.

Figure 6.38.3 demonstrates the simultaneous 8-color surface immunophenotyping and DNA ploidy analysis of different subsets of hematopoietic cells in a BM sample acquired in Cytoflex (Beckman Coulter). In this instrument,the G0/G1 peak of lymphocytes was adjusted to be at channel number 200, and as is seen, many subsets of hematopoietic cells (plot d to j) that include lymphocytes (CD45 strong/low side scatter), granulocytes (CD13+/CD15+), eosinophils (high side scatter/strong CD45 and dim expression of CD11b), B cells (CD19+), T cells (CD7+), NK/T cells (CD7+/CD56+), and CD34+ stem cells can be identified. Histograms "k to r" showed DNA content analysis with FCV staining of these populations.

Figure 6.38.4 demonstrates the simultaneous 6-color surface immunophenotyping and DNA ploidy analysis in a case of B cell acute lymphoblastic leukemia (B-ALL) showing hypodiploidy acquired in FACS Canto-II (BD). In this example, BALL-blasts were gated with the expression pattern of CD19, CD10, CD20, CD34, CD38, and CD45 (plots "d to g"). B-ALL blasts gated in plot "g" revealed hypodiploidy with DNA contents lower than lymphocytes (plots h and l) and DNA index of 0.75.

Time Considerations

This method only adds 30 min to the routine surface staining processing time, which is usually 60 to 90 min depending on the protocol. Hence, it is a very simple and quick method of DNA ploidy and cell cycle analysis.

Literature Cited

Allan, R.W., Ansari-Lari, M.A., and Jordan, S. 2008. DRAQ5-based, no-lyse, no-wash bone marrow aspirate evaluation by flow cytometry. *Am. J. Clin. Pathol.* 129:706-713. doi: 10.1309/D2M6Q7BYHWAM1FYQ.

Almeida, J., Orfao, A., Ocqueteau, M., Mateo, G., Corral, M., Caballero, M.D., Blade, J., Moro, M.J., Hernandez, J., and San Miguel, J.F. 1999. High-sensitive immunophenotyping and DNA ploidy studies for the investigation of minimal residual disease in multiple myeloma. *Br. J. Haematol.* 107:121-131. doi: 10.1046/j.1365-2141.1999.01685.x.

Carbonari, M., Tedesco, T., and Fiorilli, M. 2001. A unified procedure for conservative (morphology) and integral (DNA and immunophenotype) cell staining for flow cytometry. *Cytometry* 44:120-125. doi: 10.1002/1097-0320(20010601)44:2%3c120::AID-CYTO1090%3e3.0.CO;2-7.

Corver, W.E., Koopman, L.A., van der Aa, J., Regensburg, M., Fleuren, G.J., and Cornelisse, C.J. 2000. Four-color multiparameter DNA flow cytometric method to study phenotypic intratumor heterogeneity in cervical cancer. *Cytometry* 39:96-107. doi: 10.1002/(SICI)1097-0320(20000201)39:2%3c96::AID-CYTO2%3e3.0.CO;2-X.

Danielsen, H.E., Pradhan, M., and Novelli, M. 2016. Revisiting tumour aneuploidy—the place of ploidy assessment in the molecular era. *Nat. Rev. Clin. Oncol.* 13:291-304. doi: 10.1038/nrclinonc.2015.208.

Darzynkiewicz, Z. 2010a. Critical aspects in analysis of cellular DNA content. *Curr.*

*Protoc. Cytom.*56:7.2.1-7.2.8. doi: 10.1002/0471142956.cy0702s56.

Darzynkiewicz, Z. 2010b. Cytometry of the cell cycle: In search for perfect methodology for DNA content analysis in tissue specimens. *Cell Cycle* 9:3395-3396. doi: 10.4161/cc.9.17.13015.

Denys, B., van der Sluijs-Gelling, A.J., Homburg, C., van der Schoot, C.E., de Haas, V., Philippe, J., Pieters, R., van Dongen, J.J., and van der Velden, V.H. 2013. Improved flow cytometric detection of minimal residual disease in childhood acute lymphoblastic leukemia. *Leukemia* 27:635-641. doi: 10.1038/leu.2012.231.

Hulspas, R. 2010. Titration of fluorochrome-conjugated antibodies for labeling cell surface markers on live cells. *Curr. Protoc. Cytom.* 54:6.29.1-6.29.9. doi: 10.1002/0471142956.cy0629s54.

Kapuściński, J. and Skoczylas, B. 1978. Fluorescent complexes of DNA with DAPI 4′,6-diamidine-2-phenyl indole, 2HCl or DCI 4′,6-dicarboxyamide-2-phenyl indole. *Nucleic Acids Res*. 5:3775-3799.

Kenney, B., Zieske, A., Rinder, H., and Smith, B. 2008. DNA ploidy analysis as an adjunct for the detection of relapse in B-lineage acute lymphoblastic leukemia. *Leuk. Lymphoma* 49:42-48. doi: 10.1080/10428190701760052.

Kubista, M., Akerman, B., and Norden, B. 1987. Characterization of interaction between DNA and 4′,6-diamidino-2-phenylindole by optical spectroscopy. *Biochemistry* 26:4545-4553. doi: 10.1021/bi00388a057.

Linden, E., Skoglund, P., and Rundquist, I. 1997. Accessibility of 7-aminoactinomycin D to lymphocyte nuclei after paraformaldehyde fixation. *Cytometry* 27:92-95. doi: 10.1002/(SICI)1097-0320(19970101)27:1%3c92::AID-CYTO12%3e3.0.CO;2-N.

Lopez-Otero, A., Ruiz-Delgado, G.J., Hernandez-Arizpe, A., Ruiz-Arguelles, A., and Ruiz-Arguelles, G.J. 2010. The flow-cytometric DNA content of the plasma cells of patients with multiple myeloma is a prognostic factor: A single institution experience. *Hematology* 15:378-381. doi: 10.1179/102453310X12719010991669.

Mancaniello, D. and Carbonari, M. 2008. Immunophenotyping and DNA content analysis of acetone-fixed cells. *Curr. Protoc. Cytom.* 46:9.26.1-9.26.11. doi: 10.1002/0471142956.cy0926s46.

Nowak, R., Oelschlagel, U., Hofmann, R., Zengler, H., and Huhn, R. 1994. Detection of aneuploid cells in acute lymphoblastic leukemia with flow cytometry before and after therapy. *Leuk. Res.* 18:897-901. doi: 10.1016/0145-2126(94)90101-5.

O. Basu, F.Z., Uma Devi, P., and Streffer, C. 2009. DNA-Ploidy—Aprognostic factor of acute lymphoblastic leukemia (ALL) in childhood. *Asian J. Exp. Sci.* 23:33-38.

Perez-Persona, E., Vidriales, M.B., Mateo, G., Garcia-Sanz, R., Mateos, M.V., de Coca, A.G., Galende, J., Martin-Nunez, G., Alonso, J.M., de Las Heras, N., Hernandez, J.M., Martin, A., Lopez-Berges, C., Orfao, A., and San Miguel, J.F. 2007. New criteria to identify risk of progression in monoclonal gammopathy of uncertain significance and smoldering multiple myeloma based on multiparameter flow cytometry analysis of bone marrow plasma cells. *Blood* 110:2586-2592. doi: 10.1182/blood-2007-05-088443.

Smith, P.J., Wiltshire, M., and Errington, R.J. 2004.DRAQ5 labeling of nuclear DNA in live and fixed cells. *Curr. Protoc. Cytom.* 28:7.25.1-7.25.11. doi: 10.1002/0471142956.cy0725s28.

Stacchini, A., Demurtas, A., and Aliberti, S. 2014. Immunophenotyping of paucicellular samples. *Curr. Protoc. Cytom.* 68:9.46.1-9.46.14. doi: 10.1002/0471142956.cy0946s68.

Swerts, K., Van Roy, N., Benoit, Y., Laureys, G., and Philippe, J. 2007. DRAQ5: Improved flow cytometric DNA content analysis and minimal residual disease detection in childhood malignancies. *Clin. Chim. Acta* 379:154-157. doi: 10.1016/j.cca.2006.12.008.

Telford, W.G., King, L.E., and Fraker, P.J. 1992. Comparative evaluation of several DNA binding dyes in the detection of apoptosis-associated chromatin degradation by flow cytometry. *Cytometry* 13:137-143. doi: 10.1002/cyto.990130205.

Tembhare, P., Badrinath, Y., Ghogale, S., Patkar, N., Dhole, N., Dalavi, P., Kunder, N., Kumar, A., Gujral, S., and Subramanian, P.G. 2016. A novel and easy FxCycle violet based flow cytometric method for simultaneous assessment of DNA ploidy and six-color immunophenotyping. *Cytometry A* 89:281-291. doi: 10.1002/cyto.a.22803.

Vago, P. 1995. Clinical flow cytometric DNA analysis of human solid tumors. *Bull. Cancer* 82:122-128.

Wang, S., Li, N., Heald, P., Fisk, J.M., Fadare, O., Howe, J.G., McNiff, J.M., and Smith, B.R. 2004. Flow cytometric DNA ploidy analysis of peripheral blood from patients with sezary syndrome: Detection of aneuploid neoplastic T cells in the blood is associated with large cell transformation in tissue. *Am. J. Clin. Pathol.* 122:774-782. doi: 10.1309/8B849FC6PHAP8FDD.

Wood, B. 2006. 9-color and 10-color flow cytometry in the clinical laboratory. *Arch. Pathol. Lab. Med.* 130:680-690. http://www.lifetechnologies.com/order/catalog/product/F10347.doi: 10.1043/1543-2165.

Yuan, C.M., Douglas-Nikitin, V.K., Ahrens, K.P., Luchetta, G.R., Braylan, R.C., and Yang, L. 2004. DRAQ5-based DNA content analysis of hematolymphoid cell subpopulations discriminated by surface antigens and light scatter properties. *Cytometry B Clin. Cytom.* 58:47-52. doi: 10.1002/cyto.b.20000.

Zelenin, A.V., Poletaev, A.I., Stepanova, N.G., Barsky, V.E., Kolesnikov, V.A., Nikitin, S.M., Zhuze, A.L., and Gnutchev, N.V. 1984. 7-Amino-actinomycin D as a specific fluorophore

for DNA content analysis by laser flow cytometry. *Cytometry* 5:348-354. doi: 10.1002/cyto.990050410.

Zhan, F., Huang, Y., Colla, S., Stewart, J.P., Hanamura, I., Gupta, S., Epstein, J., Yaccoby, S., Sawyer, J., Burington, B., Anaissie, E., Hollmig, K., Pineda-Roman, M., Tricot, G., van Rhee, F., Walker, R., Zangari, M., Crowley, J., Barlogie, B., and Shaughnessy, J.D. Jr. 2006. The molecular classification of multiple myeloma. *Blood* 108:2020-2028. doi: 10.1182/blood-2005-11-013458.

CYTOMETRY
Journal of Quantitative Cell Science PART A

OMIP-063: 28-Color Flow Cytometry Panel for Broad Human Immunophenotyping

Kathryn Payne,[1†] Wenyan Li,[2†] Robert Salomon,[2,3] Cindy S. Ma[1,4*]

[1]Immunology Theme, Garvan Institute of Medical Research, Sydney, New South WalesAustralia

[2]Garvan Weizmann Centre for Cellular Genomics, Garvan Institute of Medical Research, Sydney, New South WalesAustralia

[3]Institute for Biomedical Materials and Devices (IBMD), School of Mathematical and Physical Sciences, University of Technology, Sydney, New South WalesAustralia

[4]St Vincent's Clinical School, Faculty of Medicine, UNSW Sydney, New South WalesAustralia

Received 27 March 2019; Revised 20 January 2020; Accepted 2 March 2020

Grant sponsor: National Health and Medical Research Council of Australia, Grant number1124681, Grant number1127157, Grant number1138359, Grant number1139663, Grant number1139865; Grant sponsor: Office of Health and Medical Research of the New South Wales State Government

Additional Supporting Information may be found in the online version of this article.

*Correspondence to: Cindy S. Ma, Immunology Theme, Garvan Institute of Medical Research, 384 Victoria St, Darlinghurst, New South Wales 2010, Australia Email: c.ma@garvan.org.au

†These authors contributed equally to this work.

Published online 16 April 2020 in Wiley Online Library (wileyonlinelibrary.com)

DOI: 10.1002/cyto.a.24018

Purpose

A 28-color panel was developed to screen for a range of lymphocyte subsets in human peripheral blood mononuclear cells (PBMCs), particularly in patients with primary immunodeficiency (PID). Using this panel, we are able to avoid running the sample over multiple screening panels while still deeply phenotyping a diverse range of lymphocyte subsets including innate like lymphocytes ($\gamma\delta$, mucosal-associated invariant T [MAIT], natural killer [NK], and NKT cells), as well as multiple subsets of naïve and memory $CD4^+$ and $CD8^+$ T cells, and B cells. Specifically, naïve, central memory (cmem) and effector memory (emem) $CD4^+$ T cells, naïve, cmem, emem and $CD45RA^+$ revertant memory (TEMRA) $CD8^+$ T cells, regulatory (Tregs), T follicular helper (Tfh) and T helper (Th) 1, and Th17 $CD4^+$ T cells, and transitional, naïve, memory, and $CD21^{lo}$ B cells.

Background

Primary immunodeficiencies (PIDs) are caused by monogenic mutations that compromise the development, maturation, differentiation and/or function of immune cells (1,2). Consequently, individuals with PIDs are highly susceptible to infection by a wide range of pathogens. One of the first steps to understanding the underlying cause of the clinical presentation of patients with PID is to identify any developmental or functional lymphocyte defects that may be present. This is important because several instances have been described where, despite the genetic lesion being determined, the mechanism by which defects in the affected gene result in disease pathogenesis are unknown. Thus, the establishment of "immune cell signatures" for different PID cohorts by flow cytometric-based profiling of immune cell populations in the peripheral blood of PID patients will aid in the diagnosis of these patients and reveal potential cellular defects that may contribute to disease in affected individuals (3). By way of example, patients with heterozygous dominant-negative mutations in *STAT3* present with an autosomal dominant form of hyper IgE syndrome (AD-HIES) characterized by recurrent opportunistic Candida (fungal) and staphylococcal (bacterial) infections and compromised antibody responses. Over the years, we and others have established that patients with AD-HIES display a distinctive lymphocyte signature including reduced MAIT and NKT, but normal $\gamma\delta$ T cells (4), reduced $CD4^+CCR6^+$ T helper (Th) 17 and $CD4^+CXCR5^+$ circulating T follicular helper (cTfh) cells (5–7), and reduced $CD20^+CD27^+$ memory B cells (3,8). Moreover, the failure to generate Th17 cells in AD-HIES directly accounts for increased susceptibility to fungal infections, while decreased memory B cells and Tfh cells explain the poor antibody responses in these individuals.

Previously, this type of screening process would be performed using five different 7–10-color flow cytometric panels (Online Table 3). However, this can be time-consuming and requires more of each sample for a reliable readout. This is especially

Table 1. Summary table for application of OMIP-063

Purpose	Phenotyping of human immune cell populations
Species	Human
Cell types	Peripheral blood mononuclear cells
Cross-references	OMIP 021 (Innate like lymphocytes), OMIP 030 (T cell subsets), OMIP 033 (limited T cell and B cell subsets), OMIP 050 (T cell subsets and markers such as PD1), and OMIP 051 (B cell and DCs)

true when dealing with infrequent cell populations such as the innate like lymphocytes NKT, MAIT, and $\gamma\delta$ T cells. Furthermore, access to a large number of PBMCs is not always feasible when dealing with rare patient samples. Hence, there is a currently unmet need for the establishment of a multiparameter panel to enable detection of different lymphocyte populations in human peripheral blood using a single panel.

In this OMIP, a flow cytometric panel that incorporates 28 different markers has been developed and optimized for the efficient screening of patients presenting with PIDs. The panel focuses on identifying the main subsets of B, $CD4^+$ and

Table 2. Antibodies used for OMIP-063

SPECIFICITY	ALTERNATIVE NAME	FLUOR	AB CLONE	PURPOSE
Viability stain		Zombie UV	NA	Exclusion of dead cells
Innate like lymphocytes				
CD56	NCAM	BB790	NCAM16.2	NK cells and some memory $CD8^+$ T cells
CD161	NKR-P1A, NK1.1, KLRB1	BV786	DX12	MAIT, NK, NKT, and a subset of $CD8^+$ T cells
TCR Vγδ		BV711	11F2	T cell receptor for γδ T cells
TCR Vα24/JαQ		BV605	6B11	Invariant T cell receptor for NKT cells
TCR Vα7.2		APC-Cy7	3C10	T cell receptor for MAIT cells
B cells				
CD20		BUV805	2H7	B cells
CD19		BV750	SJ25C1	B cells
CD21	Complement receptor 2	BUV563	B-Ly4	Down-regulated on atypical/aged memory B cells
CD10	CALLA, NEP, gp100	BV650	HI10a	Transitional B cells
IgD		BV480	IA6-2	Naive B cells and expressed at low levels on IgM memory B cells
IgM		APC- R700	G20-127	Naïve B cells and IgM^+ memory B cells
CD27	TNFRSF7	BB515	M-T271	Memory B cells; naïve and cmem $CD4^+$ and $CD8^+$ T cells
IgG		BB660	G18-145	IgG+ Isotype switched memory B cells
IgA1/A2		PE-Cy5	G20-359	IgA+ Isotype switched memory B cells
T cells				
TCR Vαβ		BUV737	T10B9.1A-31	T cell receptor expression for conventional αβ T cells
CD4		BUV661	SK3	T helper cells
CXCR5	CD185	BUV615	RF8B2	Tfh cells
CD8		BUV496	RPA-T8	Cytotoxic T cells
CD45RA		BUV395	HI100	Marker for naïve and revertant effector (TEMRA) T cells
CD3		BV570	UCHT1	T cells
CXCR3	CD183	BV421	1C6	Th1 cells
CD127	IL7 receptor α chain	BB700	HIL-7R-M21	Down-regulated on Tregs
CCR6	CD196	BB630	11A9	Th17 cells
CD27	TNFRSF7	BB515	M-T271	Memory B cells; naïve and cmem T cells
CCR7	CD197	PE-Cy7	G043H7	Naïve T and cmem T cells
PD1	CD279	PE- CF594	EH12.1	Activation marker
CD25	IL-2 receptorα chain	BYG584	2A3	Tregs
KLRG1	CLEC15A	APC	2F1/KLRG1	Marker of senescence on $CD8^+$ T cells

Table 3. 28-Color panel used to detect major lymphocyte populations in human PBMCs

B cells ($CD3^-CD20^+$)	Transitional ($CD10^+CD27^-$)	
	Naïve ($CD27^-CD10^-$)	
	Memory ($CD27^+CD10^-$)	IgM^+ memory B cells ($IgM^+IgA^-IgG^-$)
		Switched memory B cells ($IgM^-IgG^+IgA^-$ and $IgM^-IgG^-IgA^+$)
	Atypical/aged memory B cells ($CD19^{high}CD21^{low}$)	
T cells ($CD3^+CD20^-$)	$CD4^+$ Helper T cells ($CD4^+CD8^-$)	Naive ($CCR7^+CD45RA^+$)
		Central memory (cmem; $CCR7^+CD45RA^-$)
		Effector memory (emem; $CCR7^-CD45RA^-$)
		Tregs ($CD25^{high}CD127^{low}$)
		Th1 ($CD25^{low/-}CXCR5^-CD45RA^-CXCR3^+CCR6^-$)
		Th17 ($CD25^{low/-}CXCR5^-CD45RA^-CXCR3^-CCR6^+$)
		cTfh ($CD25^{low/-}CXCR5^+CD45RA^-$)
		Other Th cells including Th2 and Th9 cells ($CD25^{low/-}CXCR5^-CD45RA^-CXCR3^-CCR6^-$)
	$CD8^+$ Cytotoxic T cells ($CD4^-CD8^+$)	Naive ($CCR7^+CD45RA^+$)
		Central memory ($CCR7^+CD45RA^-$)
		Effector memory ($CCR7^-CD45RA^-$)
		Effector revertant memory (TEMRA; $CCR7^-CD45RA^+$)
Unconventional T cells ($CD3^+CD20^-$)	MAIT ($CD161^+TCRV\alpha7.2^+$)	
	NKT cells ($TCR\ V\alpha24J\alpha Q^+$)	
	$\gamma\delta$ T cells ($TCR\ V\alpha\beta^-\ TCR\ V\gamma\delta^+$)	
NK Cells ($CD3^-CD56^+$)		

$CD8^+$ T cells and NK cells as well as NKT, $\gamma\delta$ and MAIT cells present in peripheral blood (Tables 1–3). In such a way, this panel can detect and quantify the major lymphocyte subsets in addition to determining their maturation status.

For initial broad characterization, we have separated the B and T cell lineages by CD20 and CD3, respectively. Within the CD3 positive compartment, the T cells are then further divided into $CD4^+$ and $CD8^+$ subsets to allow for recognition of the distinct subsets of helper and cytotoxic T cells, respectively. Within the $CD4^+$ and $CD8^+$ T cell populations, the panel includes monoclonal antibodies to numerous markers to enable determining the maturation, differentiation and activation status of these T cells (Figure 1).

CCR7 and CD45RA are included to delineate $CD4^+$ and $CD8^+$ T cells into naïve ($CCR7^+CD45RA^+$), central memory ($CCR7^+CD45RA^-$), effector memory ($CCR7^-CD45RA^-$) and effector memory revertant ($CCR7^-CD45RA^+$) populations (9). Naïve $CD4^+$ T cells have the ability to differentiate into different helper subsets that have specific roles in immune responses to specific pathogens. For instance, Th1, Th2 and Th17 cells are essential for host defense against viruses and intracellular pathogens, extracellular pathogens, and fungi, respectively. Furthermore, $CD4^+$ regulatory T cells (Tregs) are necessary to maintain immune homeostasis and to guard against autoimmunity, and Tfh cells are essential for the induction of antibody-mediated immunity and long-lived serological memory (10–12). To distinguish between these Th cell populations, we have used the surface receptors CD25, CD45RA, CD127, CXCR5, CXCR3 and CCR6 to identify Tregs ($CD25^{hi}CD127^{lo}$), Th1 ($CD45RA^-CXCR3^+CCR6^-$), Th17 ($CD45RA^-CXCR3^-CCR6^+$), Tfh ($CD45RA^-CXCR5^+$), and other Th cells including Th2 and Th9 cells ($CD45RA^-CXCR3^-CCR6^-$) (11). In regards to $CD8^+$ T cells, the inclusion of killer cell lectin like receptor G1 (KLRG1) has the added benefit of detecting T cell senescence in memory and effector $CD8^+$ T cells (9).

B cells ($CD20^+$) develop in the bone marrow and have the important function of producing antibodies and are thus critical for intact humoral immune responses. Cell surface molecules have been used to identify distinct stages of B cell maturation and differentiation. As such, CD10, CD21, CD27, IgD, IgM, IgG and IgA can be used to resolve transitional ($CD10^+CD27^-$), naïve

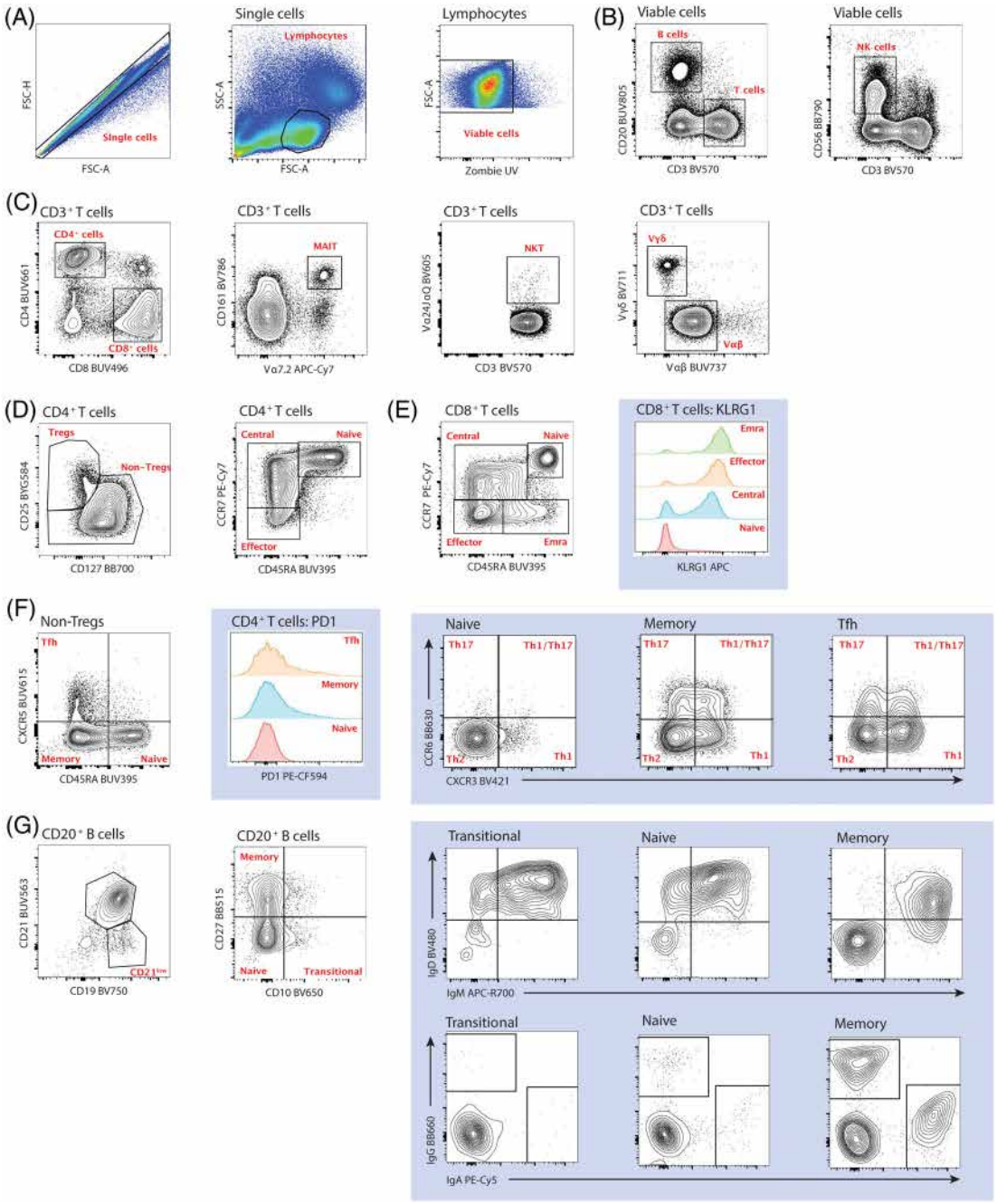

Figure 1. Overview of gating strategy for the 30-parameter panel (including forward and side scatter) on PBMCs. (**A**) Viable cells were determined by firstly gating FSC-A versus FSC-H for single cells, followed by lymphocytes based on FSC-A and SSC-A, and lastly Zombie UV-negative cells. (**B**) From viable cells, T cells ($CD3^+CD20^-$), B cells ($CD20^+CD3^-$), and natural killer (NK) cells ($CD3^-CD56^+$) can be determined. (**C**) Within the $CD3^+$ T cell compartment $CD4^+$ T cells and $CD8^+$ T cells can be identified as well as MAIT cells ($CD161^+V\alpha7.2^+$), NKT cells ($CD3^+V\alpha24J\alpha Q^+$), and $V\alpha\beta^+$ and $V\gamma\delta^+$ T cells. (**D**) $CD4^+$ T cells can be further divided into regulatory T cells (Tregs; $CD25^{high}CD127^{low}$) and "non-Tregs" ($CD25^{low}CD127^{+/-}$), based on CD25 and CD127 expression, as well as naïve ($CCR7^+CD45RA^+$), central memory (cmem; $CCR7^+CD45RA^-$), and effector memory (emem; $CCR7^-CD45RA^-$) populations based on differential expression of CCR7 and CD45RA. (**E**) Similarly, $CD8^+$ T cells can also be divided into naïve ($CCR7^+CD45RA^+$), cmem ($CCR7^+CD45RA^-$), emem ($CCR7^-CD45RA^-$), as well as revertant memory (TEMRA; $CCR7^-CD45RA^+$) subsets. KLRG1 expression can be visualized on these different $CD8^+$ T cell subsets. (**F**) Other $CD4^+$ T helper (Th) populations can be identified. Non-Tregs were further gated into naïve ($CD45RA^+CXR5^-$), T follicular helper (Tfh; $CXCR5^+CD45RA^-$), and "memory non-Tfh" ($CXCR5^-CD45RA^-$) cells based on CD45RA versus CXCR5 expression. PD1 expression can be examined on these $CD4^+$ T cell subsets. Furthermore, memory non-Tfh cells were further examined for CCR6 and CXCR3 expression to determine Th1 ($CXCR3^+CCR6^-$), Th17 ($CXCR3^-CCR6^+$), Th1/Th17 double positive ($CXCR3^+CCR6^+$), and other Th cells including Th2 and Th9 cells ($CXCR3^-CCR6^-$). (**G**) Total $CD20^+$ B cells were examined for CD19 and CD21 expression to identify $CD19^{hi}CD21^{low}$ B cells, and for CD10 and CD27 expression to identify transitional ($CD10^+CD27^-$), naïve ($CD10^-CD27^-$), and memory ($CD10^-CD27^+$) B cells. IgD, IgM, IgG and IgA expression were then examined transitional, naïve and memory B cell populations. [Color figure can be viewed at wileyonlinelibrary.com]

($CD10^-$ $CD27^-$), IgM^+ memory ($CD10^-CD27^+IgM^+IgG^-IgA^-$), and IgG ($CD10^-CD27^+IgM^-IgG^+IgA^-$) and IgA ($CD10^-CD27^+IgM^-IgG^-IgA^+$) isotype switched memory B cells (13–16). In a lot of instances, we can also detect a population of atypical or aged memory B cells ($CD19^{high}CD21^{low}$) that have been proposed to have multiple functions in health and disease, including being plasmablast precursors during anamnestic immune responses, harboring self-reactive specificities in the setting of Ab-mediated autoimmune disease, and being dysfunctional in the setting of chronic infection (e.g., HIV, malaria, Hepatitis B) and thus pathogenic due to an inability to clear these pathogens (17,18).

Finally, we have included additional markers to distinguish subsets of NK cells and innate-like T cells. These include $\gamma\delta$ T (TCR $V\alpha\beta^-V\gamma\delta^+$), NK ($CD3^-CD56^+$) NKT (TCR $V\alpha24J\alpha Q^+$), and MAIT (TCR $V\alpha7.2^+CD161^+$) cells (19). We have also included the PD1 and KLRG1 as markers of activation and senescence, respectively.

Following the outline above, we have defined the various immune cells subsets using this 28-color panel (Table 3).

The gating strategy used to determine these cells is shown in Figure 1 following standard FSC/SSC, singlet, and live cell gating. Using this broad phenotyping panel, differences in the main lymphocyte subpopulations between healthy donors and patients with immune dysregulatory conditions are easily identified. Differences in a particular population can then be further studied using refined, more specific staining panels.

Similarity to Other Published OMIPs

This panel includes a few T cell subsets and differentiation markers used in OMIPs 009, 013, 017, 018, 025, 030, 033, 036, 042, 050; and B cell markers used in OMIP 003, 033, 043, 047, and 051 and innate like populations in OMIP 019, 021, and 046. While some panels such as OMIP 033 and 042 included a few different subsets of lymphocytes, and OMIP 044, OMIP 050 and OMIP 051 are previously published 30-parameter panels with broad phenotyping, there is currently no OMIP that allows for an extensive immunophenotyping of different human lymphocytes as described here.

Acknowledgments

We thank Dr. Andrew Lim of BD Biosciences for providing custom conjugated test antibodies and advice on panel fluorochrome design, Drs John Wotherspoon and Bob Balderas for providing assistance and reagents to assist with instrument characterization and Prof. Stuart G. Tangye for critical review of this manuscript. R.S. is supported by the ISAC shared Resource Laboratory emerging leader program 2014–2018. C.S.M. is supported by grants and fellowships awarded by the National Health and Medical Research Council of Australia (1138359, 1139663, 1139865, 1127157, 1124681) and the Office of Health and Medical Research of the New South Wales State Government of Australia.

Literature Cited

1. Casanova J-L. Severe infectious diseases of childhood as monogenic inborn errors of immunity. Proc Natl Acad Sci 2015;112(51):E7128–E7137.
2. Picard C, Bobby Gaspar H, al-Herz W, Bousfiha A, Casanova JL, Chatila T, Crow YJ, Cunningham-Rundles C, Etzioni A, Franco JL, et al. International Union of Immunological Societies: 2017 primary immunodeficiency diseases committee report on inborn errors of immunity. J Clin Immunol 2018;38(1):96–128.
3. Ma CS and Tangye SG. Flow cytometric-based analysis of defects in lymphocyte differentiation and function due to inborn errors of immunity. Front Immunol 2019; 10:1–13.
4. Wilson RP, Ives ML, Rao G, Lau A, Payne K, Kobayashi M, Arkwright PD, Peake J, Wong M, Adelstein S, et al. STAT3 is a critical cell-intrinsic regulator of human unconventional T cell numbers and function. J Exp Med 2015;212(6):855–864.
5. Ma CS, Avery DT, Chan A, Batten M, Bustamante J, Boisson-Dupuis S, Arkwright PD, Kreins AY, Averbuch D, Engelhard D, et al. Functional STAT3 deficiency compromises the generation of human T follicular helper cells. Blood 2012; 119(17):3997–4008.
6. Ma CS, Chew GYJ, Simpson N, Priyadarshi A, Wong M, Grimbacher B, Fulcher DA, Tangye SG, Cook MC. Deficiency of Th17 cells in hyper IgE syndrome due to mutations in STAT3. J Exp Med 2008;205(7):1551–1557.
7. Ma CS, Wong N, Rao G, Avery DT, Torpy J, Hambridge T, Bustamante J, Okada S, Stoddard JL, Deenick EK, et al. Monogenic mutations differentially affect the quantity and quality of T follicular helper cells in patients with human primary immunodeficiencies. J Allergy Clin Immunol 2015;136(4):993–1006.e1.
8. Avery DT, Deenick EK, Ma CS, Suryani S, Simpson N, Chew GY, Chan TD, Palendira U, Bustamante J, Boisson-Dupuis S, et al. B cell-intrinsic signaling through IL-21 receptor and STAT3 is required for establishing long-lived antibody responses in humans. J Exp Med 2010;207(1):155–171.
9. Appay V, van Lier RAW, Sallusto F, Roederer M. Phenotype and function of human T lymphocyte subsets: Consensus and issues. Cytometry 2008;73A(11):975–983.
10. Deenick EK, Ma CS, Brink R, Tangye SG. Regulation of T follicular helper cell formation and function by antigen presenting cells. Curr Opin Immunol 2011;23(1): 111–118.
11. Sallusto F. Heterogeneity of human $CD4^+$T cells against microbes. Annu Rev Immunol 2016;34(1):317–334.
12. Tangye SG, Ma CS, Brink R, Deenick EK. The good, the bad and the ugly—TFH cells in human health and disease. Nat Immunol 2013;13(6):412–426.
13. Carsetti R, Rosado MM, Wardmann H. Peripheral development of B cells in mouse and man. Immunol Rev 2004;197(1):179–191.
14. Klein U, Rajewsky K, Küppers R. Human immunoglobulin (Ig)M^+IgD^+ peripheral blood B cells expressing the CD27 cell surface antigen carry somatically mutated variable region genes: CD27 as a general marker for somatically mutated (memory) B cells. J Exp Med 1998;188(9):1679–1689.
15. Tangye SG, Liu YJ, Aversa G, Phillips JH, de Vries JE. Identification of functional human splenic memory B cells by expression of CD148 and CD27. J Exp Med 1998; 188(9):1691–1703.
16. Tangye SG, Tarlinton DM. Memory B cells: Effectors of long-lived immune responses. Eur J Immunol 2009;39(8):2065–2075.
17. Isnardi I, Ng YS, Menard L, Meyers G, Saadoun D, Srdanovic I, Samuels J, Berman J, Buckner JH, Cunningham-Rundles C, et al. Complement receptor $2/CD21^-$ human naive B cells contain mostly autoreactive unresponsive clones. Blood 2010;115(24):5026–5036.
18. Warnatz K, Wehr C, Dräger R, Schmidt S, Eibel H, Schlesier M, Peter HH. Expansion of CD19(hi)CD21(lo/neg) B cells in common variable immunodeficiency (CVID) patients with autoimmune cytopenia. Immunobiology 2002;206(5):502–513.
19. Godfrey DI, Uldrich AP, McCluskey J, Rossjohn J, Moody DB. The burgeoning family of unconventional T cells. Nat Immunol 2015;16(11):1114–1123.

ISAC CYTOMETRY Journal of Quantitative Cell Science PART A

MIFlowCyt

OMIP-064: A 27-Color Flow Cytometry Panel to Detect and Characterize Human NK Cells and Other Innate Lymphoid Cell Subsets, MAIT Cells, and γδ T Cells

Nina Hertoghs,[1*] Katharine V. Schwedhelm,[2] Kenneth D. Stuart,[1] Margaret Juliana McElrath,[2] Stephen C. De Rosa[2]

[1]Center for Global Infectious Disease Research, Seattle Children's Research Institute, Seattle, Washington

[2]Vaccine and Infectious Disease Division, Fred Hutchinson Cancer Research Center, Seattle, Washington, 98109,

Received 18 September 2019; Revised 20 February 2020; Accepted 5 March 2020

Grant sponsor: Center for AIDS Research, University of Washington, Grant numberAI027757; Grant sponsor: Division of Intramural Research, National Institute of Allergy and Infectious Diseases, Grant number5U19AI128914-04, Grant numberUM1 AI068618

Additional Supporting Information may be found in the online version of this article.

*Correspondence to: Nina Hertoghs, Center for Global Infectious Disease Research, Seattle Children's Research Institute, Seattle, WA Email: nina.hertoghs@seattlechildrens.org

Published online 16 May 2020 in Wiley Online Library (wileyonlinelibrary.com)

DOI: 10.1002/cyto.a.24031

Abstract

This 27-color flow cytometry panel was developed in order to assess immunological changes over the course of an immunization and challenge regimen in two experimental malaria vaccine trials. The aim of the study was to find correlates of vaccine-induced protection. Several studies have indicated that protection against malaria appears to involve immune responses at various immunological sites, with liver-resident responses playing an essential role. As it is not feasible to monitor the immune responses within the liver in humans, this panel is developed with the aim to thoroughly characterize the immune responses over time in blood in addition to detecting changes that might reflect what happens in other immunological sites like the liver. The focus of this panel is to detect several innate lymphoid cell populations, including NK cells and their activation status. Moreover, unconventional T cells like mucosal associated invariant T cells and γδ T cells are assessed in the panel. © 2020 International Society for Advancement of Cytometry

Key terms

flow cytometry; human PBMC; γδ T cells; NK cells; T cells; MAIT cells; innate lymphoid cells.

Background

Malaria is still a major health threat, with 200 million cases and approximately 400,000 deaths annually, mostly among children under 5 (1–3). The disease is caused by mosquito-transmitted*Plasmodium*parasites that have a complicated lifecycle which occurs in multiple sites of the body, including the liver and the blood. Although efforts to design a potent anti-malaria vaccine have been ongoing for nearly a century, there is still no vaccine that confers adequate durable immunity to infection. Furthermore, naturally occurring sterilizing immunity to malaria is rare, despite repeated infections (4,5). Immunization with radiation-attenuated sporozoites (RAS), which are parasites that have retained their ability to infect the liver, has been shown to confer sterilizing protection. However, the mechanism behind this protection is incompletely understood (1,6–9). Remarkably, the occurrence of natural infection seems to inhibit the development of protective sterilizing immunity, as clinical trials in nonendemic regions consistently report higher vaccine efficacies than those in malaria-endemic regions (10). It has been suggested that tolerogenic responses, immune exhaustion, and senescence play a role (11). Identifying the underlying immune mechanisms of anti-malarial immunity or the lack thereof will aid the development of a protective vaccine that is suitable for mass distribution. High parameter multicolor flow cytometry enables thorough characterization of immune responses against pathogens. Here we describe a 27-color panel that aims to detect immune responses that correlate with protection

Table 1 Summary table for application of OMIP-064

Purpose	Extensive phenotyping
Species	Human
Celltype	PBMC
Cross-references	OMIP-029, OMIP-039, OMIP-044, OMIP-055, OMIP-056, and OMIP-058

in experimental malaria vaccine trials, in addition to comparing responses in individuals from malaria endemic regions with those from nonendemic regions. This panel was developed for use with three other panels, in order to extensively phenotype the immune responses triggered by RAS-immunizations. The other panels we developed focus on T and B cells and we used a dendritic/monocyte panel published as an optimized multicolor immunofluorescence panel (OMIP) (Table 1) (12).

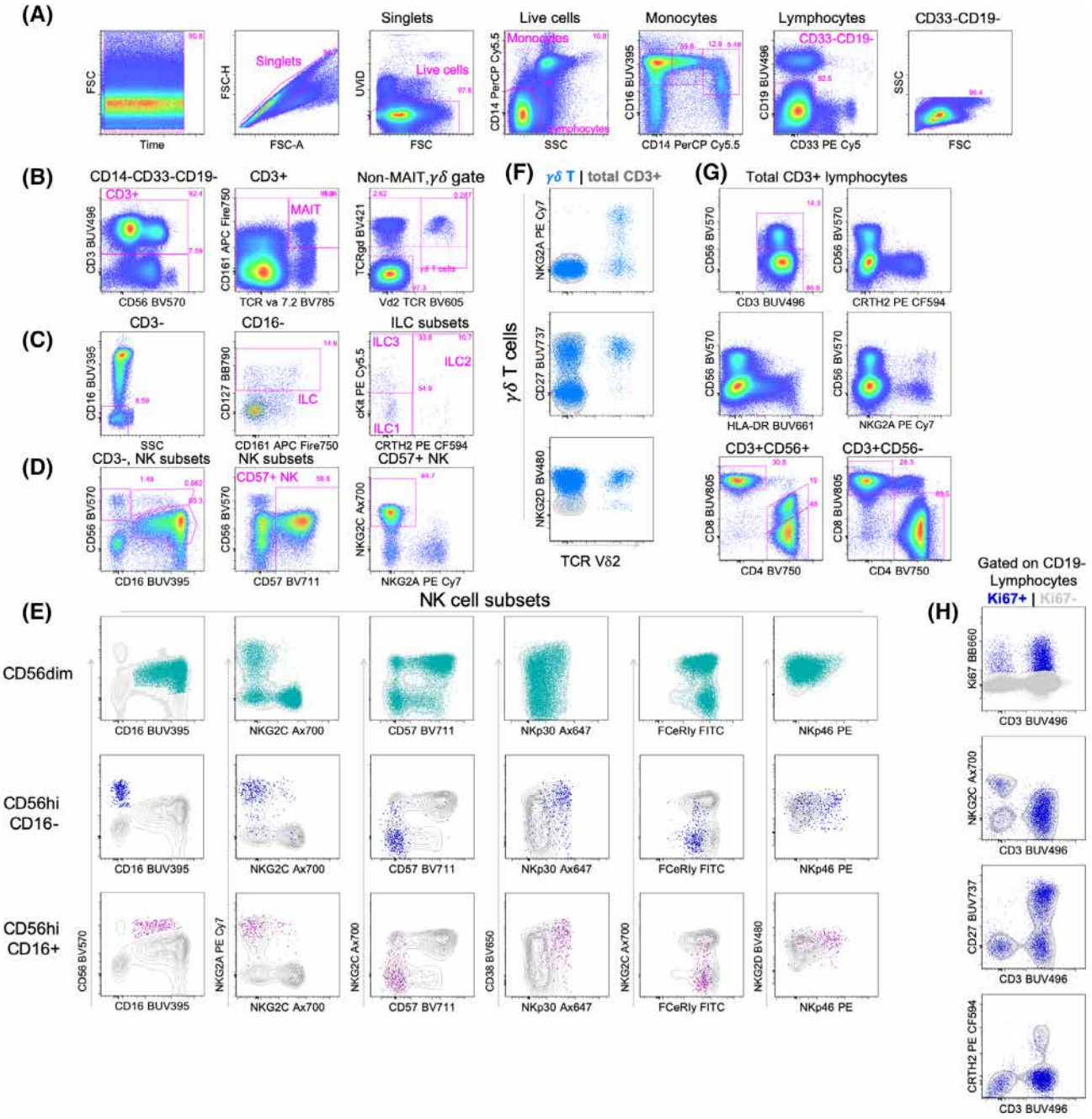

Fig 1. Legend on next page.

The panel described here is developed with a focus on innate lymphoid cells (ILCs), conventional NK cells and their activation status, γδ T cells, mucosal associated invariant T (MAIT) cells in addition to the major lineages including T cells, B cells and monocytes, both for exclusion of other lineages and to characterize potential expression of NK-relevant markers in these other cell types. All the reagents are listed in Table 2. The panel includes lineage markers CD14 and CD33 to gate out monocytes, dendritic cells, and granulocytes and CD19 for the exclusion of B-cells. For the gating of T cells, CD3, CD4, and CD8 are used to identify the conventional T cell subsets, although these markers can be expressed on several other cell types detected by this panel, such as NK cells. CD161 and TCRvα7.2 are included to gate on MAIT cells. These cells are detected in peripheral blood, although they are more abundant at mucosal sites and in the liver. Their role in the protection against malaria infection is unknown, although MAIT cells were observed to contract and then expand in a controlled human malaria-infection(CHMI) study (13).

Another unconventional T cell subset that has generated attention in the malaria immunology field is the subset of T cells expressing the γδ T cell receptor (TCR). These γδ T cells have been shown to be expanded in acute malaria infection, and a recent study showed that the Vδ2 subset was found to correlate with protection in a large cohort of healthy, malaria-exposed individuals that were immunized with a RAS-vaccine (14). In addition, their relevance to malaria has also been demonstrated in animal models, for example, γδ T cells are required for the induction of sterile immunity in a rodent model (14). We have therefore included antibodies detecting the γδ TCR and Vδ2 to identify γδ T cells and the Vδ2 subset.

Animal models have helped elucidate some of the mechanisms needed for protective immune responses in the liver, and NK cells have previously been shown to be important in the immune responses during the early phases of liver stage infection. NK cells likely contribute through the production of IFNγ and potentially through direct cytolysis of infected hepatocytes (15,16).

In humans, NK cells have been shown to play a role in malaria disease, both as having protective effects against the pathogen in addition to contributing to pathology in cerebral malaria (17). We have included several markers to extensively characterize NK phenotypes, in which maturation status, differentiation, and activation markers are included. To phenotype NK cells, we used CD56 in combination with CD16 to delineate different NK subsets. An extensive set of NK cells markers were included to monitor maturation and differentiation, which can also indirectly indicate the functionality of these NK subsets. Recently, so-called adaptive NK cells that lack FCεRI-γ were associated with protective effects in a large cohort of seasonal malaria transmission monitoring (18). This marker is combined with NKG2C, CD57 and a lack of NKG2A expression to identify these adaptive NK cells (19). CD27 has been implicated as another maturation or memory-like marker, and has therefore been included (20). CD27 on NK cells mark mature NK cells with low cytotoxic potential (21). CD27-expressing NK cells were also indicated as being memory-like NK cells in a murine tuberculosis model (22). NKp30, NKp46, and CD38 are included to monitor activation of NK cells. CD38 was recently described to be a key regulator in NK cells that are enhanced in their cytotoxic abilities and cytokine producing potential (23,24). The activating receptor NKG2D was shown to be highly expressed in liver-resident NK cells in a rodent model, and implicated in humans (20,25,26). NKG2D ligands are upregulated in response to type I interferons, which have been shown to be induced in plasmodium-infected hepatocytes in mice, and these cells could therefore be of interest to monitor (15,27). Several of the NK markers in this panel have been shown to be expressed on the conventional and unconventional T cells detected by this panel. For instance, NKG2A and CD27 can be detected on γδ T cells as indirect markers for IFNγ-producing γδ T cells (28), and CD57 expression on T cells

FIGURE 1 Example of the gating strategy of the 27-color measurement of cryopreserved PBMCs. (**A**) The cells from a healthy donor were stained and the data were subsequently acquired on a BD FACSymphony instrument. The plot depicting forward scatter (FSC) vs. time is to verify that there are no pressure fluctuations that might affect fluorescent signals. The FSC-Area (A) vs. FSC-Height (H) is to gate on single cells and to exclude doublets. Next, the UViD-negative events are gated to exclude dead or damaged cells. CD14 vs. Side scatter (SSC)-A is used to gate monocytes (CD14+ and SSChi) vs. lymphocytes (CD14- and SSClo), and CD14 and CD16 are used to gate on the different monocyte subsets. In parallel, CD19 and CD33 are used as exclusion channels, to gate out B cells and granulocytes. Another clean-up gate for lymphocytes is included based on FSC and SSC. (**B**) The negative fraction is then plotted for CD3 to gate on T cell subsets. First, MAIT cells are gated as CD3+ TCRγδ- CD161+ and TCRva7.2+. The non-MAIT cells are then used to gate γδ T cells, as CD3+ and TCRγδ+. The vδ2 T cells are double positive for TCRγδ+ and the vδ2TCR. The negative fraction is then used to gate on conventional T cells that are either CD4+ or CD8+. (**C**) The CD3-gate is use for further delineation of ILCs. The ILC subsets are gated as CD3-CD16-CD127 + CD161+, although ILC1 and LTi have been shown to lack CD161 expression, so ILCs can be gated on without this marker as well. Further differentiation between ILC1, ILC2, and ILC3 can be done with CRTH2 and cKit, with CRTh2-CKit- cells gated as ILC1, CRTh2+ cells gated on as ILC2 and ILC3 are cKit+. (**D**) The CD3-fraction is alternatively gated as CD56 vs. CD16 for NK subsets. The second plot in this row shows that CD57 is mainly expressed on CD56dim NK cells. These cells are then plotted as NKG2A vs. NKG2C, the latter of which are adaptive NK cells. (**E**) The 3 NK subsets as shown in the left plot in each row are plotted separately for the remaining NK subset markers (CD57, NKG2A, NKG2C, NKG2D, NKp30, and NKp46), overlaid on the total CD3- population in gray. Also the expression of FCεRIγ is measured, "adaptive NK cells" have a low expression of this marker (36). (**F**) Depiction of the γδ T cells (blue overlay) and NKG2A, NKG2D and CD27 against vδ2.The background depicts total CD3+ cells, in gray. (**G**) A subset of CD3+ cells is positive for CD56 and these will include NK T cells. The expression of CRTH2, HLA-DR, and NKG2A is plotted vs. CD56 to demonstrate several phenotypic differences between the CD56+ and CD56- populations. The two plots in the third row show the CD4 versus CD8 pattern and how the CD56+ CD3+ cells have a CD4+ population that dimly expressed CD8. (**H**) Ki67+ is used as a proliferation marker and plotted against CD3+ on all CD14-CD33-CD19- lymphocytes, and shown as overlay combined with several markers that are different between the CD3+ and CD3− populations. [Color figure can be viewed at wileyonlinelibrary.com]

Table 2 Reagents used for OMIP-0

MARKER	ANTIBODY CLONE	FLUOROCHROME	PURPOSE
CD16	3G8	BUV395	NK, monocyte, ILC gating
Viability	NA	Fixable blue	Dead cell dump
CD3	UCHT1	BUV496	T cells
CD19	SJ25C1	BUV563	B cells
HLA-DR	G46-6	BUV661	Activation
CD27	L128	BUV737	NK phenotyping
CD8	SK1	BUV805	CD8+ T cells
TCRγδ	11F2	BV421	Pan-γδ T cells
NKG2D	1D11	BV480	NK phenotyping
CD56	HCD56	BV570	NK phenotyping
Vδ2 TCR	B6	BV605	γδ T cell subset vδ2
CD38	HB-7	BV650	Activation
CD57	HNK-1	BV711	NK phenotyping
CD4	SK3	BV750	CD4+ T cells
TCRvα7.2	3C10	BV786	MAIT cells
FCεRIγ	poly	FITC	NK phenotyping
Ki-67	Ki67	BB660	Proliferation
CD14	MΦP9	PerCP-Cy5.5	Monocytes
CD127	HIL-7R-M21	BB790	ILC phenotyping
NKp46	9E2/NKp46	PE	NK phenotyping
CRTh2	BM16	PE-CF594	ILC phenotyping
CD33	WM53	PE-Cy5	Granulocyte/monocyte exclusion
c-kit	104D2	PE-Cy5.5	ILC phenotyping
NKG2A	Z199	PE-Cy7	NK phenotyping
CD337/Nkp30	AF29-4D12	APC	NK phenotyping
NKG2C	134,591	Ax700	NK phenotyping
CD161	HP-3G10	APC-Fire750	MAIT cells/ILC phenotyping

can be used as an exhaustion marker, previously shown to be upregulated in *Plasmodium falciparum* infection (11).

The markers CD16, CD161, CD127 c-kit, and CRTH2 can together be used to differentiate the ILC subsets, which are found in low abundance in the blood, although they are more prevalent in tissues (29). The role of ILCs in malaria vaccine responses has not been identified yet, although sparse data indicate that ILCs may have a role in infection. For instance, blood stage infection led to a rapid loss of group 1 ILCs in the blood of subjects participating in a CHMI study (30). Another study suggested that group 2 ILCs were involved in protection against cerebral malaria (31). As an additional marker to phenotype cellular responses, we included Ki67 as a marker for proliferation and recent in vivo activation. Figure 1 shows an example of how these markers can be used to gate on different cell subsets. This panel can be used for preipheral blood mononuclear cells (PBMC), and possibly for other sample types.

Similarity to Published OMIPs

This panel is unique, although there is some overlap with OMIP-056 (32), which also looks at MAIT, γδ T cells, and NK cells (Table 1). However, the focus of that panel is more on functional responses in the context of HIV infection, and does not deeply phenotype subsets of NK cells and unconventional T cells, as in this panel. The 21-marker panel described in OMIP-055 (33) has nine markers in common with this panel, although four of those are lineage markers and all lineage markers are assigned to the same fluorochrome, which limits the depth of the analysis to ILC subsets. OMIP-039 (34) and OMIP-029 (35) describe panels that phenotype NK cells that partly overlap with this panel, although both panels are less elaborate, as they include 14 and 13 colors, respectively, and can therefore not combine both NK cell markers with MAIT and γδ T cells. OMIP-058 also has several markers that overlap with our panel, although the emphasis is on γδ T cells and iNKT cells and the depth of NK subset phenotyping is more limited than the panel we describe here. Overall, our panel is unique because it enables a deep assessment of NK subsets in addition to conventional and unconventional T cells, combined with an extensive set of activation and maturation markers.

Acknowledgments

We would like to thank all the technologists in the HIV Vaccine Trial Network Laboratory for their help with the procedures in the lab and with the use of their instruments. We thank

Dr. Catherine Blish for her advice on the NK markers, and Alicia Annamalay and Jason Carnes for ordering of the reagents.

Conflict of Interest

The authors declare no conflict of interest.

LiteratureCited

1. Hoffman SL, Goh LML, Luke TC, Schneider I, le TP, Doolan DL, Sacci J, de la Vega P, Dowler M, Paul C, et al. Protection of humans against malaria by immunization with radiation-attenuated*Plasmodium falciparum* sporozoites. J Infect Dis 2002;185:1155–1164.
2. Fernandez-Ruiz D, Ng WY, Holz LE, Ma JZ, Zaid A, Wong YC, Lau LS, Mollard V, Cozijnsen A, Collins N, et al. Liver-resident memory CD8+ T cells form a front-line defense against malaria liver-stage infection. Immunity 2016;45:889–902.
3. WHO. Malaria. WHO; 2019. Available at: https://www.who.int/malaria/en/. Accessed June 27, 2019.
4. Hoffman SL, Oster CN, Plowe CV, Woollett GR, Beier JC, Chulay JD, Wirtz RA, Hollingdale MR, Mugambi M. Naturally acquired antibodies to sporozoites do not prevent malaria: Vaccine development implications. Science 1987;237:639–642.
5. Doolan DL, Dobaño C, Baird JK. Acquired immunity to malaria. Clin Microbiol Rev 2009;22:13–36.
6. Goswami D, Minkah NK, Kappe SHI. Designer parasites: Genetically engineered plasmodium as vaccines to prevent malaria infection. J Immunol 2019;202:20–28.
7. Nussensweig RS, van der Berg J, Most H, Orton C. Protective immunity produced by the injection of X-irradiated sporozoites of *Plasmodium berghei*. Nature 1967; 216:160–162.
8. Clyde DF, Most H, McCarthy VC, Van der Berg JP. Immunization of man against sporozoite-induced falciparum malaria. Am J Med Sci 1973;266:169–177.
9. Crompton PD, Moebius J, Portugal S, Waisberg M, Hart G, Garver LS, Miller LH, Barillas-Mury C, Pierce SK. Malaria immunity in man and mosquito: Insights into unsolved mysteries of a deadly infectious disease. Annu Rev Immunol 2014;32:157–187.
10. Beeson JG, Kurtovic L, Dobaño C, Opi DH, Chan JA, Feng G, Good MF, Reiling L, Boyle MJ. Challenges and strategies for developing efficacious and long-lasting malaria vaccines. Sci Transl Med 2019;11:eaau1458.
11. Frimpong A, Kusi KA, Adu-Gyasi D, Amponsah J, Ofori MF, Ndifon W. Phenotypic evidence of T cell exhaustion and senescence during symptomatic *Plasmodium falciparum* malaria. Front Immunol 2019;10:1345. https://doi.org/10.3389/fimmu.2019.01345.
12. Mair F, Prlic M. OMIP-044: 28-color immunophenotyping of the human dendritic cell compartment. Cytometry Part A 2018;93A:402–405.
13. Mpina M, Maurice NJ, Yajima M, Slichter CK, Miller HW, Dutta M, McElrath MJ, Stuart KD, De Rosa SC, McNevin JP, et al. Controlled human malaria infection leads to long-lasting changes in innate and innate-like lymphocyte populations. J Immunol 2017;199:107–118.
14. Zaidi I, Diallo H, Conteh S, Robbins Y, Kolasny J, Orr-Gonzalez S, Carter D, Butler B, Lambert L, Brickley E, et al. γδ T cells are required for the induction of sterile immunity during irradiated sporozoite vaccinations. J Immunol 2017;199:3781–3788.
15. Miller JL, Sack BK, Baldwin M, Vaughan AM, Kappe SHI. Interferon-mediated innate immune responses against malaria parasite liver stages. Cell Rep 2014;7:436–447.
16. Burrack KS, Hart GT, Hamilton SE. Contributions of natural killer cells to the immune response against plasmodium. Malar J 2019;18:1–9.
17. Wolf A-S, Sherratt S, Riley EM. NK cells: Uncertain allies against malaria. Front Immunol 2017;8:212.
18. Hwang I, Zhang T, Scott JM, Kim AR, Lee T, Kakarla T, Kim A, Sunwoo JB, Kim S. Identification of human NK cells that are deficient for signaling adaptor FcRγ and specialized for antibody-dependent immune functions. Int Immunol 2012;24: 793–802.
19. Luetke-Eversloh M, Killig M, Romagnani C. Signatures of human NK cell development and terminal differentiation. Front Immunol 2013;4:1–6.
20. Paust S, Blish CA, Reeves RK. Redefining memory: Building the case for adaptive NK cells. J Virol 2017;91:1–12.
21. Vossen MTM, Matmati M, Hertoghs KML, Baars PA, Gent MR, Leclercq G, Hamann J, Kuijpers TW, van Lier RAW. CD27 defines phenotypically and functionally different human NK cell subsets. J Immunol 2008;180:3739–3745.
22. Choreño Parra JA, Martínez Zúñiga N, Jiménez Zamudio LA, Jiménez Álvarez LA, Salinas Lara C, Zúñiga J. Memory of natural killer cells: A new chance against *Mycobacterium tuberculosis*?Front Immunol 2017;8:1–12.
23. Le Gars M, Seller C, Kay AW, Bayless NL, Sola E, Starosvetsky E, Moore L, Shen-Orr SS, Aziz N, Khatri P, et al. CD38 is a key regulator of enhanced NK cell immune responses during pregnancy through its role in immune synapse formation. bioRxiv 349084; 2018. doi:https://doi.org/10.1101/349084
24. Terhorst C, van Agthoven A, Leclair K, Snow P, Reinherz E, Schlossman S. Biochemical studies of the human thymocyte cell-surface antigens T6, T9 and T10. Cell 1981;23:771–780.
25. Oliviero B, Varchetta S, Paudice E, Michelone G, Zaramella M, Mavilio D, De Filippi F, Bruno S, Mondelli MU. Natural killer cell functional dichotomy in chronic hepatitis B and chronic hepatitis C virus infections. Gastroenterology 2009;137: 1151–1160.
26. Wang Y, Wang W, Shen C, Wang Y, Jiao M, Yu W, Yin H, Shang X, Liang Q, Zhao C. NKG2D modulates aggravation of liver inflammation by activating NK cells in HBV infection. Sci Rep 2017;7:1–11. https://doi.org/10.1038/s41598-017-00221-9.
27. Minkah NK, Wilder BK, Sheikh AA, Martinson T, Wegmair L, Vaughan AM, Kappe SHI. Innate immunity limits protective adaptive immune responses against pre-erythrocytic malaria parasites. Nat Commun 2019;10:3950.
28. D'Ombrain MC, Hansen DS, Simpson KM, Schofield L. γδ-T cells expressing NK receptors predominate over NK cells and conventional T cells in the innate IFN-γ response to *Plasmodium falciparum* malaria. Eur J Immunol 2007;37:1864–1873.
29. Hazenberg MD, Spits H. Human innate lymphoid cells. Blood 2014;124:700–709.
30. Ng SS, Souza-Fonseca-Guimaraes F, Rivera FL, Amante FH, Kumar R, Gao Y, Sheel M, Beattie L, Montes de Oca M, Guillerey C, et al. Rapid loss of group 1 innate lymphoid cells during blood stage plasmodium infection. Clin Transl Immunol 2018;7:e1003.
31. Palomo J, Quesniaux VFJ, Togbe D, Reverchon F, Ryffel B. Unravelling the roles of innate lymphoid cells in cerebral malaria pathogenesis. Parasite Immunol 2018;40 (2):e12502. https://doi.org/10.1111/pim.12502.
32. Dintwe O, Rohith S, Schwedhelm KV, McElrath MJ, Andersen-Nissen E, de Rosa SC. OMIP-056: Evaluation of human conventional T cells, donor-unrestricted T cells, and NK cells including memory phenotype by intracellular cytokine staining. Cytometry Part A 2019;95A:722–725.
33. Bianca Bennstein S, Riccarda Manser A, Weinhold S, Scherenschlich N, Uhrberg M. OMIP-055: Characterization of human innate lymphoid cells from neonatal and peripheral blood. Cytometry Part A 2019;95A:427–430.
34. Hammer Q, Romagnani C. OMIP-039: Detection and analysis of human adaptive NKG2C+ natural killer cells. Cytometry Part A 2017;91A:997–1000.
35. Mahnke YD, Beddall MH, Roederer M. OMIP-029: Human NK-cell phenotypization. Cytometry Part A 2015;87A:986–988.
36. Lee J, Zhang T, Hwang I, Kim A, Nitschke L, Kim MJ, Scott JM, Kamimura Y, Lanier LL, Kim S. Epigenetic modification and antibody-dependent expansion of memory-like NK cells in human cytomegalovirus-infected individuals. Immunity 2015;42:431–442.

CYTOMETRY
Journal of Quantitative Cell Science PART A

OMIP-066: Identification of Novel Subpopulations of Human Group 2 Innate Lymphoid Cells in Peripheral Blood

Yoichiro Ohne*

Bioscience Asthma, Research and Early Development, Respiratory and Immunology, BioPharmaceuticals R&D, AstraZeneca, Gaithersburg, Maryland, USA

Received 25 October 2019; Revised 14 April 2020; Accepted 11 May 2020

Additional Supporting Information may be found in the online version of this article.

*Correspondence to: Yoichiro Ohne, AstraZeneca, One MedImmune Way, Gaithersburg, MD 20878. Email: yoichiro.ohne@astrazeneca.com

Published online 25 June 2020 in Wiley Online Library (wileyonlinelibrary.com)

DOI: 10.1002/cyto.a.24046

- **Purpose and Appropriate Sample Types**

This 14-color flow cytometry panel was designed to identify newly described subpopulations within human group 2 innate lymphoid cells (ILC2s) and other ILC subsets. This panel also allowed to identify recently reported subpopulations of peripheral blood CRTH2$^-$ c-Kit$^+$ ILCs. We validated this panel mostly in human peripheral blood but also confirmed that the same panel and gating strategy works well in human tonsillar cells. The panel contains a few markers indicating the activation status of ILCs. In addition, phycoerythrin (PE) channel is available for the markers of interest in each study. In the validation studies described here, PE channel was used to test the expression of some markers. These features make this panel applicable for immunophenotyping of ILCs in various disease states. © 2020 International Society for Advancement of Cytometry

- **Key terms**

innate lymphoid cells; ILC2; innate immunity; human immunology

Background

Innate lymphoid cells (ILCs) are an emerging immune cell population that plays important roles in innate immune responses to pathogens, tissue maintenance, and repair after infection (1). ILCs have been classified into three subsets—ILC1, ILC2, and ILC3s—based on cytokine profile, transcription factors, and receptor expression, and it has been noted that they are functionally similar to T-helper 1 (Th1), Th2, and Th17 cells (1). In light of recent findings of subpopulations with intermediate phenotypes, however, there has been a growing understanding that this classification of ILCs may be oversimplified (2-5). The functional plasticity with which one ILC subset can adopt certain phenotypic aspects of another subset further contributes to the uncertainty surrounding this classification (6-9). Recently, we reported that human ILC2s defined as lineage-negative (Lin$^-$) CD127$^+$ CRTH2$^+$ were still highly heterogeneous (2) and could be divided into subpopulations with different functionalities by using two surface markers, c-Kit and CCR6. The c-Kit$^-$ population (c-Kit$^-$ ILC2s) represents canonical ILC2s expressing higher levels of thymic stromal lymphopoietin receptor (TSLPR) and *IL4*, *IL5*, and *IL13* mRNA at baseline. These cells demonstrated a robust response to IL-33 to produce cytokines IL-5 and IL-13. In contrast, the c-Kit$^+$ CCR6$^+$ population (c-Kit$^+$ ILC2s) represented an atypical subpopulation with moderate expression of ILC3 signature genes, such as *RORC* which encodes transcription factor RORγt, and the ability to differentiate into IL-17–producing ILC3s in addition to having the basic characteristic of ILC2s (2, 3). We further identified a third subpopulation that expressed skin homing receptor CCR10 (CCR10$^+$ ILC2s) within c-Kit$^+$ ILC2s, which seemed to represent a precursor of skin ILC2s while exhibiting ILC3-like features (2).

Peripheral blood CRTH2$^-$ c-Kit$^+$ ILCs were once considered to be ILC3s (10), but recent studies have suggested that these populations are highly heterogeneous and contain progenitors for all ILC populations (4, 11). Most recent study showed that an NKp46$^+$ population and a KLRG1$^+$ population within blood CRTH2$^-$ c-Kit$^+$ ILCs represent progenitors biased toward ILC3s or ILC2s, respectively (4).

Given that ILC subpopulations exhibit significant differences in function and plasticity and/or progenitor properties, it is extremely important to have an optimized flow cytometry panel to dissect these subpopulations without concern for cross-contamination. Here, we describe a novel panel to dissect subpopulations within ILCs, especially ILC2s in human peripheral blood (Table 1).

Reagents used in the final panel are described in Table 2. With our panel, the total ILC population was defined as CD45$^+$ Lin$^-$ CD94$^-$ CD127$^+$ cells (Fig. 1A). Lineage markers included CD3, CD4, CD14, CD19, CD34, and CD123. Total ILCs were further divided into CRTH2$^+$ ILC2s, CRTH2$^-$ c-Kit$^+$ ILCs, and CRTH2$^-$ c-Kit$^-$ populations (Fig. 1A).

Table 1. Summary table for application of the panel

PURPOSE	IDENTIFICATION OF HUMAN ILC2 SUBPOPULATIONS IN PERIPHERAL BLOOD
Cell types	Freshly isolated human PBMCs
Cross-references	OMIP-055, −007, −029, and − 038

Notably, the expression of CRTH2 was lower in the c-Kit positive population than in the c-Kit dim/negative population within ILC2s (Online Fig. S2A, red arrow). Thus, suboptimal antibody panels and gating strategies may lead to cross-contamination between a portion of the ILC2s and the CRTH2$^-$ c-Kit$^+$ ILCs. Although the CRTH2$^-$ c-Kit$^-$ population was considered to be ILC1s, there is some controversy on this point (12-15). Natural killer (NK) cells identified as Lin$^-$ CD94$^+$ were further divided into CD56^{int} cytotoxic NK (cNK) and CD56^{bright} NK cells (Fig. 1B) (16).

The ILC2 population was further subdivided into three subpopulations; CCR10$^+$ ILC2s, c-Kit$^+$ ILC2s and c-Kit$^-$ ILC2s, using the expression of CCR10, c-Kit and CCR6 (Fig. 1C). CCR10$^+$ ILC2s were dominantly identified within the c-Kit positive population (Fig. 1C). As described above, c-Kit$^-$ ILC2s expressed TSLPR at higher levels than did other ILC2 subpopulations (Online Fig. S2B). Because TSLPR expression is induced in ILC2s under activating conditions (7), it can also be used as an activation marker for ILC2s. In our panel, additional markers of interest can be assessed in phycoerythrin (PE) channel. In the validation study presented here, we measured the expression of inducible T-cell costimulator (ICOS) in the PE channel. Although ICOS is reported to be expressed in human ILC2s (17), we found significant differences in ICOS expression between ILC2 subpopulations (Online Fig. S2C). For additional validation of the panel, we used the PE channel to test the expression of CD161 and CD7, which have been used as pan-ILC2 markers in previous reports (11, 18) and in OMIP-055 (19). We found

Table 2. Reagents used in the final panel

SPECIFICITY	CLONE	FLUOROCHROME	PURPOSE
CD3	SK7	BV510	Dump/lineage
CD4	RPA-T4	BV510	Dump/lineage
CD14	M5E2	BV510	Dump/lineage
CD19	HIB18	BV510	Dump/lineage
CD34	581	BV510	Dump/lineage
CD123	6H6	BV510	Dump/lineage
CD45	HI30	BUV805	Lymphocyte
CD127	REA614	VioBright515	Total ILC
CRTH2	BM16	AF647	ILC2
c-Kit	104D2	PE/Cy7	CRTH2$^-$ c-Kit$^+$ ILCs and ILC2 subpopulation
CCR6	G034E3	BV421	ILC2 subpopulation
CCR10	1B5	BUV395	ILC2 subpopulation
KLRG1	13F12F2	SuperBright702	CRTH2$^-$ c-Kit$^+$ subpopulations
NKp46	9E2	PE/Dazzle594	CRTH2$^-$ c-Kit$^+$ subpopulations
NKp44	p44-8	BV786	ILC3 in tonsil
TSLPR	1F11	BB700	ILC2 activation
CD94	DX22	APC/Fire750	NK cells
CD56	NCAM16.2	APC/R700	NK cells and CRTH2$^-$ c-Kit$^+$ ILC subpopulations
Dead cells	NA	Live/Dead Fixable Blue	Viability

BV510: Brilliant Violet 510, BV421: Brilliant Violet 421, BV786: Brilliant Violet 786, BUV805: Brilliant Ultraviolet 805, BUV395: Brilliant Ultraviolet 395, BB700: Brilliant Blue 700, AF647: Alexa Fluor 647, PE/Cy7: Phycoerythrin-Cy7 tandem: PE/Dazzle594: Phycoerythrin-Dazzle594 tandem, APC/Fire750: Allophycocyanin-Fire750 tandem, APC/R700: Allophycocyanin-R700 tandem.

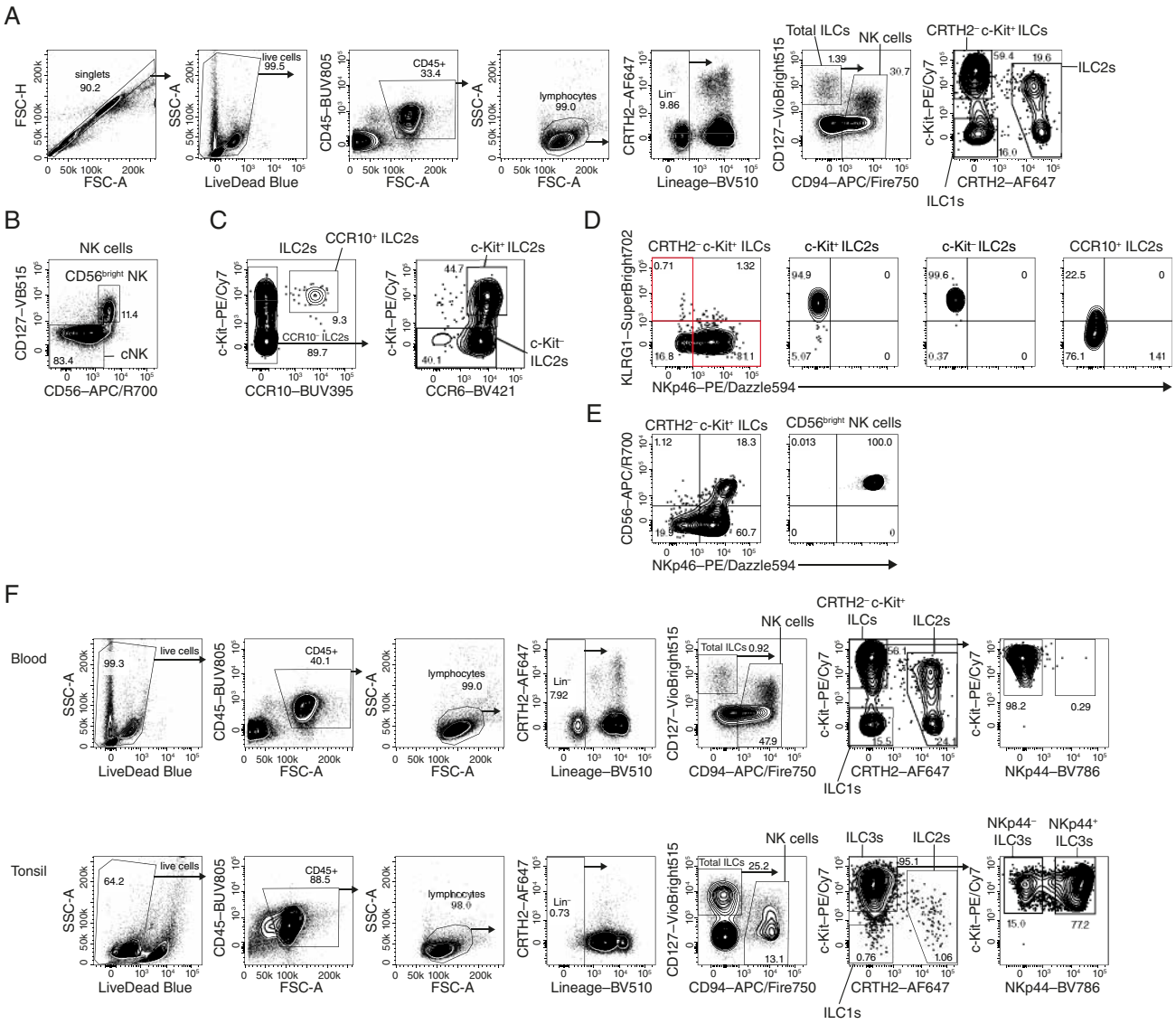

Figure 1. (A) Gating strategy to identify major ILC populations in peripheral blood. After selection of singlet cells (FSC-A vs. FSC-H) and live cells (live/dead blue vs. SSC-A), lymphocytes were selected (FSC-A vs. CD45). After lineage-positive ($CD3^+$, $CD4^+$, $CD14^+$, $CD19^+$, $CD34^+$, and $CD123^+$) cells were excluded (lineage vs. CRTH2), total ILCs were identified as $CD127^+$ $CD94^-$ (CD127 vs. CD94). Total NK cells were identified as $CD94^+$ cells. Among total ILCs, ILC2s, $CRTH2^-$ c-kit^+ ILCs, and ILC1s ($CRTH2^-$ c-kit^-) were gated as indicated (CRTH2 vs c-kit). (B) Identification of NK cell subsets. Within total NK cells gated as in **a**, cytotoxic NK (cNK) cells and $CD56^{bright}$ NK cells were identified as $CD56^+$ $CD127^-$ and $CD56^{hi}$ $CD127^{int}$, respectively. (C) Identification of ILC2 subpopulations. Within ILC2s identified as in **a**, $CCR10^+$ ILC2s were identified from the c-kit positive population (left). The remaining $CCR10^-$ cells were named c-kit^+ ILC2s (c-kit^+ $CCR6^+$) and c-kit^- ILC2s (c-kit^-) as gated (right). (D) Identification of subpopulations within $CRTH2^-$ c-kit^+ ILCs. Within $CRTH2^-$ c-kit^+ ILCs, $NKp46^+$ and $KLRG1^+$ populations were mutually exclusively identified (far left, red rectangles). As a reference, c-kit^+ ILC2s and c-kit^- ILC2s showed high expression of KLRG1 without NKp46 expression. $CCR10^+$ ILC2s expressed KLRG1 at a significantly lower level. (E) CD56 expression in the $NKp46^+$ subpopulation of $CRTH2^-$ c-kit^+ ILCs. Part of the $NKp46^+$ population expressed CD56 (left), but at a lower level than $CD56^{bright}$ NK cells (right). (F) Applying the panel and gating strategy to human tonsils. Following the gating strategy described in **a**, total ILCs were identified in tonsil (bottom) similarly to that in peripheral blood (top). After gating out $CRTH2^+$ ILC2s, $NKp44^+$ ILC3s were identified as c-kit^+ $NKp44^+$ in tonsil but not in peripheral blood. [Color figure can be viewed at wileyonlinelibrary.com]

that CCR10-expressing c-Kit^+ ILC2s expressed a significantly lower level of CD161 and CD7 than did other ILC2 subpopulations (Online Fig. S2D). Because $CCR10^+$ ILC2s are the rarest subpopulation within ILC2s, it is possible that using CD161 or CD7 as surrogate markers for ILC2s might have led to the exclusion of $CCR10^+$ ILC2 populations from the analyses. It is therefore not advisable to use these markers as pan-ILC2s markers.

Although the focus of this study was to identify subpopulations within ILC2s, we also attempted to identify subpopulations within $CRTH2^-$ c-Kit^+ ILCs, using the two markers NKp46 and KLRG1 in the panel. We confirmed that NKp46

and KLRG1 were expressed in a mutually exclusive manner within this population (Fig. 1D). Notably, the frequency of the KLRG1^{+} NKp46^{-} population was significantly less than what has been reported previously (4). Consistent with a previous report (4), the NKp46^{+} population showed heterogeneous expression of CD56, which was slightly weaker than that of CD56^{bright} NK cells (Fig. 1E).

Finally, we tested the panel in human tonsil and confirmed that total ILCs could be identified by following the same gating strategy. Because the panel includes antibody for NKp44, two subsets of ILC3s; NKp44^{+} and NKp44^{-} ILC3s, were identified in tonsil (Fig. 1F, bottom). Although NKp44^{+} ILC3s were not found in peripheral blood from healthy donors (Fig. 1F, top), a prior report showed that this population emerged in peripheral blood of psoriasis patients (20). Thus, this panel can be useful for blood phenotyping of ILC populations in different disease states.

In summary, we report here the first comprehensive flow cytometry panel for identifying newly described human ILC2 subpopulations in peripheral blood. Additionally, given TSLPR as the potential activation marker for ILC2s and NKp44 as a tissue ILC3 marker, as well as the availability of the PE channel for additional markers of interest, this panel can serve as a valuable resource for immunophenotyping of ILC populations in various tissues, such as gut and lung, from multiple diseases.

Similarity to Other Published OMIPs

Whereas OMIP-055 (19) was designed for the simple identification of ILC1, ILC2, and ILC3 subsets in human peripheral blood and cord blood, our panel was designed for identification of subpopulations within ILC2s and CRTH2^{-} c-Kit^{+} ILCs with recently described novel markers (2, 4). Furthermore, with the use of newly developped fluorochromes and careful consideration of the impact of spillover spreading, the panel can provide clear separation between CRTH2^{+} ILC2s and c-Kit^{-} CRTH2^{-} ILCs. Additionally, we made some critical modifications, including removing CD161 and CD7 from the panel, as using this marker can pre-exclude the CCR10^{+} ILC2 subpopulation. By using TSLPR and NKp44, this panel can also assess the activation states of ILCs, which can occur in some disease contexts. Regarding NK cell subsets, OMIP-007, −029, and −038 (21-23) used similar gating strategies.

Acknowledgments

The author thanks AstraZeneca Gaithersburg Cytometry team, especially Chris Groves, for actively introducing new technologies and providing advice for designing the panel. The author appreciates Radhika Rayanki, Rebecca Grady, and Raffaello Cimbro for maintenance and QC of cytometers; Nicole Barnes, Shin Ji Lee, Mary Everett and Kendra Hayden for processing blood samples; and Deborah Shuman of AstraZeneca for providing editorial support.

Conflict of Interest

Yoichiro Ohne is an employee of AstraZeneca and has stock ownership and/or stock interests or options in the company.

Literature Cited

1. Artis D, Spits H. The biology of innate lymphoid cells. Nature 2015;517:293–301.
2. Bernink JH, Ohne Y, Teunissen MBM, Wang J, Wu J, Krabbendam L, Guntermann C, Volckmann R, Koster J, van Tol S, et al. C-kit-positive ILC2s exhibit an ILC3-like signature that may contribute to IL-17-mediated pathologies. Nat Immunol 2019;20:992–1003.
3. Hochdorfer T, Winkler C, Pardali K, Mjosberg J. Expression of c-kit discriminates between two functionally distinct subsets of human type 2 innate lymphoid cells. Eur J Immunol 2019;49:884–893.
4. Nagasawa M, Heesters BA, Kradolfer CMA, Krabbendam L, Martinez-Gonzalez I, de Bruijn MJW, Golebski K, Hendriks RW, Stadhouders R, Spits H, et al. KLRG1 and NKp46 discriminate subpopulations of human CD117(+)CRTH2(−) ILCs biased toward ILC2 or ILC3. J Exp Med 2019;216:1762–1776.
5. Gury-BenAri M, Thaiss CA, Serafini N, Winter DR, Giladi A, Lara-Astiaso D, Levy M, Salame TM, Weiner A, David E, et al. The spectrum and regulatory landscape of intestinal innate lymphoid cells are shaped by the microbiome. Cell 2016;166:1231–1246.
6. Bernink JH, Krabbendam L, Germar K, de Jong E, Gronke K, Kofoed-Nielsen M, Munneke JM, Hazenberg MD, Villaudy J, Buskens CJ, et al. Interleukin-12 and -23 control plasticity of CD127(+) group 1 and group 3 innate lymphoid cells in the intestinal lamina propria. Immunity 2015;43:146–160.
7. Ohne Y, Silver JS, Thompson-Snipes L, Collet M, Blanck JP, Cantarel BL, Copenhaver AM, Humbles AA, Liu Y. IL-1 is a critical regulator of group 2 innate lymphoid cell function and plasticity. Nat Immunol 2016;17:646–655. Erratum in: Nat Immunol 2016;17(8):1005.
8. Silver JS, Kearley J, Copenhaver AM, Sanden C, Mori H, Yu L, Harms Pritchard G, Berlin AA, Hunter CA, Bowler R, et al. Inflammatory triggers associated with COPD exacerbations orchestrate ILC2 plasticity in the lung. Nat Immunol 2016;17:626–635. Erratum in: Nat Immunol. 2016;17:1005.
9. Bal SM, Bernink JH, Nagasawa M, Groot J, Shikhagaie MM, Golebski K, van Drunen CM, Lutter R, Jonkers RE, Hombrink P, et al. IL-1beta, IL-4 and IL-12 control the fate of group 2 innate lymphoid cells in human airway inflammation in the lungs. Nat Immunol 2016;17:636–645.
10. Hazenberg MD, Spits H. Human innate lymphoid cells. Blood 2014;124:700–709.
11. Lim AI, Li Y, Lopez-Lastra S, Stadhouders R, Paul F, Casrouge A, Serafini N, Puel A, Bustamante J, Surace L, et al. Systemic human ILC precursors provide a substrate for tissue ILC differentiation. Cell 2017;168:1086–1100.
12. Bernink JH, Mjosberg J, Spits H. Human ILC1: To be or not to be. Immunity 2017;46:756–757.
13. Roan F, Ziegler SF. Human group 1 innate lymphocytes are negative for surface CD3ε but express CD5. Immunity 2017;46:758–759.
14. Simoni Y, Fehlings M, Kloverpris HN, McGovern N, Koo SL, Loh CY, Lim S, Kurioka A, Fergusson JR, Tang CL, et al. Human innate lymphoid cell subsets possess tissue-type-based heterogeneity in phenotype and frequency. Immunity 2017;46:148–161.
15. Simoni Y, Newell EW. Toward meaningful definitions of innate-lymphoid-cell subsets. Immunity 2017;46:760–761.
16. Cooper MA, Fehniger TA, Caligiuri MA. The biology of human natural killer-cell subsets. Trends Immunol 2001;22:633–640.
17. Maazi H, Patel N, Sankaranarayanan I, Suzuki Y, Rigas D, Soroosh P, Freeman GJ, Sharpe AH, Akbari O. ICOS:ICOS-ligand interaction is required for type 2 innate lymphoid cell function, homeostasis, and induction of airway hyperreactivity. Immunity 2015;42:538–551.
18. Mjosberg JM, Trifari S, Crellin NK, Peters CP, van Drunen CM, Piet B, Fokkens WJ, Cupedo T, Spits H. Human IL-25- and IL-33-responsive type 2 innate lymphoid cells are defined by expression of CRTH2 and CD161. Nat Immunol 2011;12:1055–1062.
19. Bianca Bennstein S, Riccarda Manser A, Weinhold S, Scherenschlich N, Uhrberg M. OMIP-055: Characterization of human innate lymphoid cells from neonatal and peripheral blood. Cytometry A 2019;95:427–430.
20. Villanova F, Flutter B, Tosi I, Grys K, Sreeneebus H, Perera GK, Chapman A, Smith CH, Di Meglio P, Nestle FO. Characterization of innate lymphoid cells in human skin and blood demonstrates increase of NKp44+ ILC3 in psoriasis. J Invest Dermatol 2014;134:984–991.
21. Eller MA, Currier JR. OMIP-007: Phenotypic analysis of human natural killer cells. Cytometry A 2012;81A:447–449.
22. Mahnke YD, Beddall MH, Roederer M. OMIP-029: Human NK-cell phenotypization. Cytometry A 2015;87A:986–988.
23. Smolen KK, Cai B, Kollmann TR. OMIP-038: Innate immune assessment with a 14 color flow cytometry panel. Cytometry A 2017;91A:966–968.

Received: 9 February 2021 | Revised: 14 July 2021 | Accepted: 16 July 2021

DOI: 10.1002/cyto.a.24490

OMIP

MIFlowCyt

ISAC CYTOMETRY Journal of Quantitative Cell Science PART A

OMIP 078: A 31-parameter panel for comprehensive immunophenotyping of multiple immune cells in human peripheral blood mononuclear cells

Takuto Nogimori[1,2] | Yuko Sugawara[1,3] | Masaya Higashiguchi[1,4] | Hirotomo Murakami[1,4] | Hirofumi Akita[1,4] | Shokichi Takahama[1] | Satoshi Tanaka[1,3] | Takuya Yamamoto[1,2,5,6]

[1]Laboratory of Immunosenescence, National Institutes of Biomedical Innovation, Health and Nutrition, Osaka, Japan

[2]Research Institute for Microbial Diseases, Osaka University, Osaka, Japan

[3]BD Biosciences, Nippon Becton Dickinson Company, Ltd, Tokyo, Japan

[4]Department of Gastroenterological Surgery, Graduate School of Medicine, Osaka University, Osaka, Japan

[5]Laboratory of Aging and Immune Regulation, Graduate School of Pharmaceutical Sciences, Osaka University, Osaka, Japan

[6]Joint Research Center for Human Retrovirus Infection, Kumamoto University, Kumamoto, Japan

Correspondence
Takuya Yamamoto, Laboratory of Immunosenescence, National Institutes of Biomedical Innovation, Health and Nutrition, 7-6-8, Saito-Asagi, Ibaraki City, Osaka 567-0085, Japan.
Email: yamamotot2@nibiohn.go.jp

Funding information
Japan Society for the Promotion of Science, Grant/Award Numbers: Challenging Exploratory Research/JP19k21601, Scientific Research (B)/JP20H03728: Research Activity Start-up/ JP20K22774; Japan Agency for Medical Research and Development, Grant/ Award Numbers: JP20fk0410023, JP21fk0210057, JP20fk0108141, JP21fk0410040, JP21wm0325015; Collaborative research with Nippon Becton Dickinson Company, Ltd

Abstract

This 31-parameter panel was developed for simultaneously measuring multiple immune cell populations including T cells, B cells, natural killer cells, dendritic cells, monocytes, and hematopoietic progenitor cells in human peripheral blood mononuclear cells. This panel enables the capture of individual immune dynamics and assessments of single-cell changes in the immune system that are associated with aging and diseases. This panel includes markers to separate the differentiation status of each cell population and might be applicable to studies of infectious and autoimmune diseases, as patient samples are usually limited in volume and require an analysis system that provides a relatively large amount of information.

KEYWORDS
aging, immune cells, multi-color flow cytometry

1 | BACKGROUND

The human immune system, a defense mechanism against infectious pathogens and tumors, is composed of a large number of diverse cell types involved in innate and adaptive immunity. The immune response to pathogens is orchestrated by the complex cell–cell interactions and activities of immune cells. The immune system also undergoes dramatic changes in response to various environmental

factors, as well as aging. For example, naive T cells have consistently been shown to decline with age [1]. More recently, it has been shown that $CD34^+$ hematopoietic progenitor cells in the blood decline with age and that telomere length and telomerase activity in HPCs from elderly donors are reduced [2]. These age-related changes in the immune system are referred to as "immunosenescence." Whereas immunosenescence has been extensively investigated in recent years, its underlying mechanisms have yet to be understood.

TABLE 1 Summary table for application of this study

Purpose	Comprehensive immunophenotyping of multiple immune cell subsets in human PBMCs
Species	Human
Cell types	PBMCs
Cross references	OMIP-033, OMIP-034, OMIP-042, OMIP-063, OMIP-064, OMIP-069

Abbreviation: PMBC, peripheral blood mononuclear cell.

Multicolor flow cytometric analysis is a powerful technique that can be used to better understand immunosenescence. This complex immunophenotyping technique involves measuring the expression levels of multiple surface markers and intracellular proteins simultaneously and assessing single-cell changes in the immune system that are associated with aging and diseases. Recently, fluorescence-based multicolor flow cytometry was shown to simultaneously measure up to 29 fluorescence parameters [3, 4], offering deeper insights into human immunology. The combination of conjugated antibody panels improves analyses of high-dimensional cytometric data [5]. In analyzing high-dimensional data, it is difficult to capture individual characteristics using a manual gating strategy, and computational approaches such as clustering and dimensionality reduction are required [6] (Table 1).

Here, we selected the major immune cell lineage markers listed in Table 2 to establish a multicolor panel for the comprehensive immunophenotyping of human samples. First, we titrated all antibodies to maximize separation between positive and negative cell populations and to

TABLE 2 Reagents used in this study

Specificity	Fluorophore	Clone	Purpose
Viability	Ax700	N/A	Viability
CD57	FITC	NK-1	T cell differentiation
CD127	BB630	HIL-7R-M21	T cell differentiation
CD38	BB660	HIT2	B cell differentiation
CD34	BB700	8G12	HPC lineage
CD1c	BB755	F10/21A3	Dendritic cell lineage
IgM	BB790	G20-127	B cell differentiation
CD133	PE	W6B3C1	HPC lineage
CD11c	PE-CF594	3.9	Dendritic cell differentiation
CD56	PE-Cy5	B159	NK cell activation
CD4	PE-Cy5.5	SK3	CD4 T cell lineage
CD27	PE-Cy7	M-T271	T and B cell differentiation
IgD	APC	IA6-2	B cell differentiation
CD3	APC-Cy7	SP34-2	T cell lineage
CD303	BV421	V24-785	Dendritic cell differentiation
CD123	BV480	7G3	Plasmacytoid dendritic cell lineage
CD45RO	BV570	UCHL1	T cell differentiation
CD138	BV605	MI15	B cell differentiation
CD16	BV650	3G8	Monocyte and NK cell differentiation
CD19	BV711	SJ25C1	B cell lineage
CD24	BV750	ML5	B cell differentiation
PD-1	BV786	EH12.1	T cell inhibitory receptor
CD11b	BUV395	ICRF44	Monocyte lineage
CD45	BUV496	Hi30	Leukocytes
CD8	BUV563	RPA-T8	CD8 T cell lineage
CD141	BUV615	1A4	Dendritic cell differentiation
HLA-DR	BUV661	G46-6	Activation marker
IgG	BUV737	G18-145	B cell differentiation
CD14	BUV805	M5E2	Monocyte differentiation

Abbreviations: HPC, hematopoietic progenitor cell; NK, natural killer.

minimize potential fluorescence leakages into adjacent channels. Following titration of the antibodies, we used the multicolor panel to stain peripheral blood mononuclear cells (PBMCs) from healthy individuals, and the samples were analyzed by BD FACSymphony. The obtained Flow Cytometry Standard (FCS) files were analyzed using FlowJo software. The representative plots were created, described as follows (Figure 1A). PBMC samples were gated on live $CD45^+$ single cells, and each immune cell subset of the PBMCs was divided based on specific surface markers. Within the lymphocyte gate, T cells were defined as $CD19^-CD14^-CD56^-CD16^-CD133^-CD3^+$ and then separated according to the expression of CD4 and CD8. In addition to providing markers to define T cells, our panel used the expression levels of CD27 and CD45RO to illustrate differentiation statistics, namely pertaining to naive T cells ($CD27^+CD45RO^-$, no. 15 and 18), central memory T cells ($CD27^+CD45RO^+$, no. 16 and 19) and effector/effector memory T cells ($CD27^-$, no. 17 and 20) [7]. Additionally, this panel was capable of further phenotyping T cell subsets based on their expression levels of CD127, CD57, and PD-1. NKT cells were defined as $CD19^-CD14^-CD56^+CD3^+$ (no. 14).

We next defined natural killer (NK) cells as $CD19^-CD14^-CD3^-$ and HPCs as $CD19^-CD14^-CD56^-CD11b^-HLA\text{-}DR^-CD34^+$ (no. 21). We distinguished among four NK cell subsets based on their expression levels of CD56 and CD16 (no. 22, 23, 24, and 25) [8]. Moreover, we were able to distinguish between various subsets of B cells, monocytes, and dendritic cells (DCs) by using the following gating strategy. Within the gate for total cells, B cells were defined as $CD14^-CD56^-CD3^-CD19^+$, DCs were defined as $CD14^-CD3^-CD19^-CD56^-CD11b^-HLA\text{-}DR^+$, and monocytes were defined as $CD3^-CD19^-CD56^-CD8^-CD34^-HLA\text{-}DR^+$. Using surface markers including CD27, CD24, CD38, CD138, IgD, IgM, and IgG, B cells were further divided into various differentiation stages, namely the naive ($CD27^-IgD^+$, no. 1), unswitched memory ($CD27^+IgD^+$, no. 2), memory ($CD27^+IgD^-$, no. 3), IgG^+ memory ($CD27^+IgD^-IgM^-IgG^+$, no. 4), plasma cell ($CD27^+IgD^-IgM^-CD38^+CD138^-$, no. 5), plasmablast ($CD27^+IgD^-IgM^-CD38^+CD138^+$, no. 6), and translational ($CD27^-CD38^+CD24^+$, no. 7) stages [9]. Monocytes were further separated into classical monocytes ($CD14^+CD16^-$, no. 8), intermediate monocytes ($CD14^+CD16^+$, no. 9), and non-classical monocytes ($CD14^-CD16^+$, no. 10) [10]. DCs were separated into plasmacytoid DCs ($CD11c^-CD123^+CD303^+$, no. 13), $CD141^+$ conventional DCs (cDCs; $CD11c^+CD1c^-CD141^+$, no. 12), and $CD1c^+$ cDCs ($CD11c^+CD141^-CD1c^+$, no. 11) [11]. As explained, the multicolor panel designed in this study covered most of the cellular components of human PBMCs.

To obtain an overview of the immune subsets in PBMCs from 10 donors in two different age groups, we next conducted a t-SNE analysis of the immune cell abundance profiles using the concatenated data from all donors and divided the merged t-SNE map based on their age (Figure 1B). These results indicated that our panel was capable of capturing the differences between the young and elderly groups. Subsequently, we obtained clusters based on the FlowSOM algorithm and overlaid them onto the t-SNE map (Figure 1C). Furthermore, we overlaid manually gated cell populations onto the t-SNE map (Figure 1D). The frequency of cluster 16, which displayed a $CD8^+$ T cell phenotype, in elderly donors was significantly lower than that in young donor (Figure 1E). We next conducted further t-SNE analysis on $CD8^+$ T cells. The map resulting from the t-SNE analysis of $CD8^+$ T cells from all donors is shown in Figure S2A. The t-SNE map was divided into young and elderly groups, showing that the number of naive $CD8^+$ T cells ($CD27^+CD45RO^-$) was decreased and that the number of effector/effector memory $CD8^+$ T cells ($CD27^-CD57^{-/+}$) was increased in older $CD8^+$ T cells (Figure S2B). In addition to the t-SNE analysis, we built a reference minimal spanning tree of $CD8^+$ T cells from all donors using FlowSOM and mapped the two age groups onto the reference map (Figure S2C). The background color of the nodes in the FlowSOM maps illustrates meta-clusters and the pie charts indicate the expression levels of surface markers. As with the t-SNE maps, the differences in naive $CD8^+$ T cell (Cluster 5) and effector/effector memory $CD8^+$ T cell (Cluster 6) clusters between young and elderly subjects were visually apparent. Subsequently, to examine whether the difference between two groups was statistically significant, we compared the frequencies of each meta cluster from the FlowSOM algorithm (Figure S2D). The frequency of Cluster 5 in elderly donors was significantly decreased, whereas the frequency of Cluster 6 in elderly donors was significantly increased compared with that in young donors. To further evaluate similarities among donors, we conducted Principal Component Analysis (PCA) based on the frequencies of FlowSOM-meta-clusters (Figure S2E). The resulting PCA map showed that donors were separated into two groups by age. However, further studies are needed, as the sample size was insufficient for confirming that observation.

In conclusion, the panel designed in our study is an effective tool for analyzing age-related changes in each cell subset. This panel might be applicable to studies of infectious and autoimmune diseases, as patient samples are usually limited in volume and require an analysis system that provides a relatively large amount of information. For example, many recent reports have shown that changes in immune responses with aging are involved in the severity and the mortality of COVID-19 [12–15]. It has been reported that the severity of disease in COVID-19 is associated with changes in the number of lymphocytes [16–18], and this panel could be applied to the analysis of immune dynamics against COVID-19 and is potentially useful for the prediction of disease severity. We showed that high-dimensional flow cytometric analyses such as dimensionality reduction and clustering methods are able to detect immune dynamics with high sensitivity. Our comprehensive analysis panel could have potential applications in clinical trials.

2 | SIMILARITY TO PUBLISHED OMIPS

There are many panels that identify major immune cell populations such as OMIP-33, 34, 42, 63, and 69 [19–23]. In particular, this panel overlaps with recent OMIP-69. However, this panel uniquely includes CD34 and CD133 which enable the detection of HPCs. HPCs are scarce cell populations in blood, and being able to analyze them

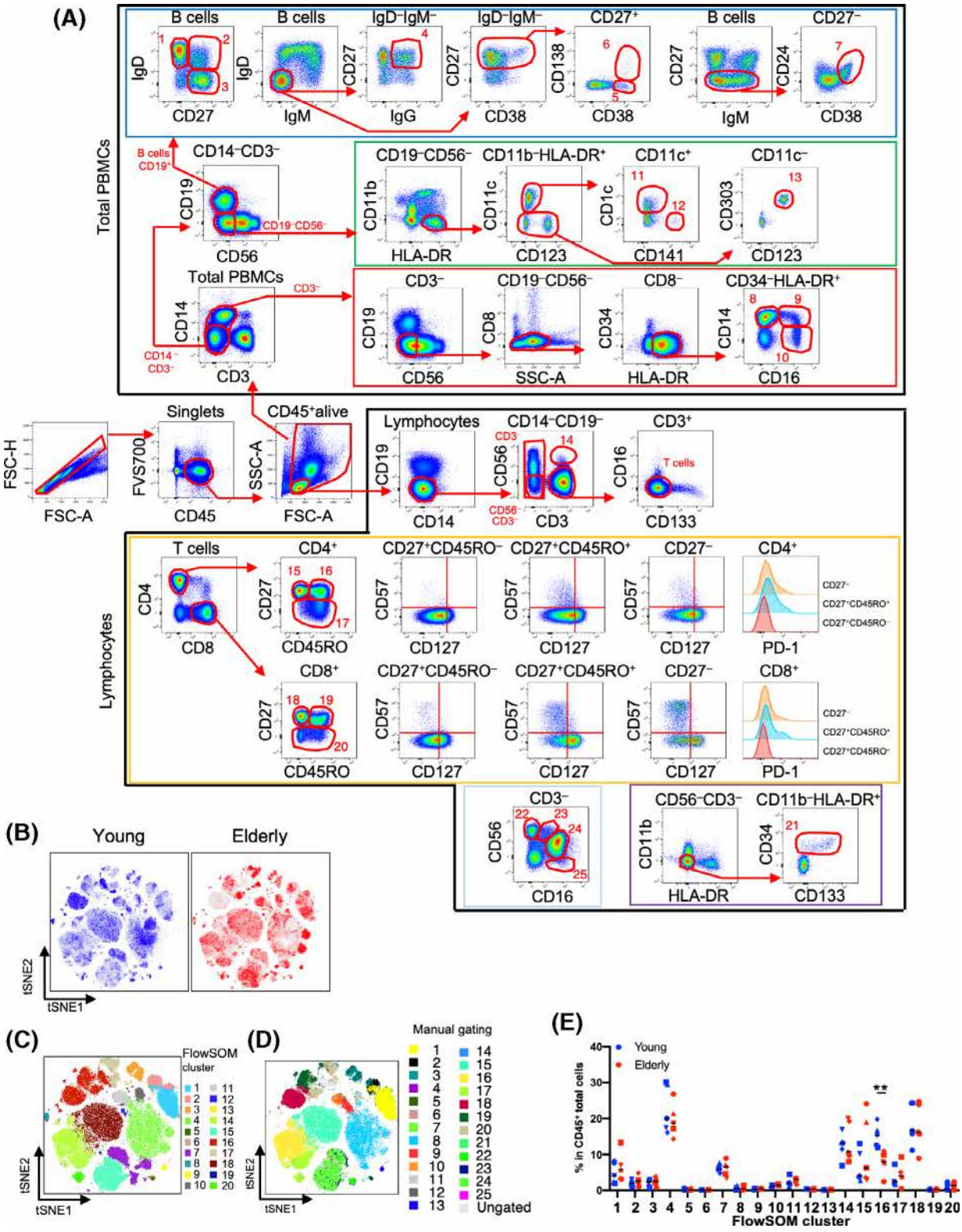

FIGURE 1 Gating strategy of 29-color flow cytometry for detection of immune cell populations in human peripheral blood mononuclear cells (PBMCs). (A) Representative flow cytometric analysis of PBMCs from a young donor demonstrates the gating strategy for identifying immune cell populations. (B) Flow cytometry samples from 10 donors were manually gated on live CD45$^+$ single cells as shown in (A). The live CD45$^+$ single cells were down-sampled to 50,000 cells per donor and concatenated. t-SNE analysis of all donors was performed based on all surface markers except CD45. t-SNE maps of live CD45$^+$ single cells were separated into young (left panel) and elderly (right panel) donors. (C) FlowSOM-based meta clusters were overlaid onto the tSNE map as a color dimension. (D) The resulting t-SNE map was colored according to each manually gated cell subset. (E) The percentage of each FlowSOM-based meta cluster within young (blue) and elderly (red) CD45$^+$ cells. *p*-values were determined using the Mann–Whitney *U*-test. **p* < 0.05, ***p* < 0.01 [Color figure can be viewed at wileyonlinelibrary.com]

simultaneously with other cell populations is important in terms of sample volume limitations.

3 | STATEMENT OF ETHICAL USE OF HUMAN SAMPLES

The study protocol and procedures employed were reviewed and approved by the local institutional ethics committee (National Institutes of Biomedical Innovation, Health and Nutrition, Osaka, Japan) and were followed in compliance with the Declaration of Helsinki 1975; all participants provided written informed consent.

ACKNOWLEDGMENTS

We thank Drs. Robert S. Balderas, Tatsuo Achiwa, Satoshi Takagi, Yoshiyuki Okada, and Keisuke Yuki of BD Biosciences, for providing conjugated test antibodies and advice on high parameter fluorescence flow cytometry through a Cooperative Research and Development Agreement with NIBIOHN. In addition, we would like to acknowledge all of our lab members for their support in writing this manuscript.

AUTHOR CONTRIBUTIONS

Takuto Nogimori: Conceptualization; data curation; formal analysis; investigation; methodology; project administration; validation; writing - original draft. **Yuko Sugawara:** Data curation; formal analysis; methodology; validation. **Masaya Higashiguchi:** Data curation; methodology; resources. **Hirotomo Murakami:** Data curation; methodology; resources. **Hirofumi Akita:** Data curation; resources; supervision; validation. **Shokichi Takahama:** Conceptualization; data curation; methodology; supervision; validation. **Satoshi Tanaka:** Data curation; formal analysis; methodology; supervision; validation. **Takuya Yamamoto:** Conceptualization; data curation; formal analysis; funding acquisition; investigation; methodology; project administration; resources; supervision; validation; writing - original draft.

CONFLICT OF INTEREST

Yuko Sugawara and Shokichi Takahama are employed by Nippon Becton Dickinson Company, Ltd., and Takuya Yamamoto received funding from Nippon Becton Dickinson Company, Ltd. The other authors declare that no other competing interests exist.

PEER REVIEW

The peer review history for this article is available at https://publons.com/publon/10.1002/cyto.a.24490.

ORCID

Takuto Nogimori https://orcid.org/0000-0002-6011-9631
Takuya Yamamoto https://orcid.org/0000-0003-3753-1211

REFERENCES

1. Czesnikiewicz-Guzik M, Lee WW, Cui D, Hiruma Y, Lamar DL, Yang ZZ, et al. T cell subset-specific susceptibility to aging. Clin Immunol. 2008;127:107–18.
2. Fali T, Fabre-Mersseman V, Yamamoto T, Bayard C, Papagno L, Fastenackels S, et al. Elderly human hematopoietic progenitor cells express cellular senescence markers and are more susceptible to pyroptosis. JCI Insight. 2018;3:e95319.
3. Filipovic I, Sönnerborg I, Strunz B, Friberg D, Cornillet M, Hertwig L, et al. 29-color flow Cytometry: unraveling human liver NK cell repertoire diversity. Front Immunol. 2019;10:2692.
4. Liechti T, Roederer M. OMIP-060: 30-parameter flow Cytometry panel to assess T cell effector functions and regulatory T cells. Cytometry A. 2019;95:1129–34.
5. Liechti T, Roederer M. OMIP-051 - 28-color flow cytometry panel to characterize B cells and myeloid cells. Cytometry A. 2019;95:150–5.
6. Chester C, Maecker HT. Algorithmic tools for mining high-dimensional Cytometry data. J Immunol. 2015;195:773–9.
7. Appay V, van Lier RA, Sallusto F, Roederer M. Phenotype and function of human T lymphocyte subsets: consensus and issues. Cytometry A. 2008;73:975–83.
8. Cooper MA, Fehniger TA, Caligiuri MA. The biology of human natural killer-cell subsets. Trends Immunol. 2001;22:633–40.
9. Claes N, Fraussen J, Stinissen P, Hupperts R, Somers V. B cells are multifunctional players in multiple sclerosis pathogenesis: insights from therapeutic interventions. Front Immunol. 2015;6:642.
10. Ziegler-Heitbrock L, Ancuta P, Crowe S, Dalod M, Grau V, Hart DN, et al. Nomenclature of monocytes and dendritic cells in blood. Blood. 2010;116:e74–80.
11. Dzionek A, Fuchs A, Schmidt P, Cremer S, Zysk M, Miltenyi S, et al. BDCA-2, BDCA-3, and BDCA-4: three markers for distinct subsets of dendritic cells in human peripheral blood. J Immunol. 2000;165:6037–46.
12. Rydyznski Moderbacher C, Ramirez SI, Dan JM, Grifoni A, Hastie KM, Weiskopf D, et al. Antigen-specific adaptive immunity to SARS-CoV-2 in acute COVID-19 and associations with age and disease severity. Cell. 2020;183:996–1012.e19.
13. Paschold L, Simnica D, Willscher E, Vehreschild MJ, Dutzmann J, Sedding DG, et al. SARS-CoV-2 specific antibody rearrangements in pre-pandemic immune repertoires of risk cohorts and COVID-19 patients. J Clin Invest. 2021;131:e142966.
14. Mathew D, Giles JR, Baxter AE, Oldridge DA, Greenplate AR, Wu JE, et al. Deep immune profiling of COVID-19 patients reveals distinct immunotypes with therapeutic implications. Science. 2020;369:eabc8511.
15. Akbar AN, Gilroy DW. Aging immunity may exacerbate COVID-19. Science. 2020;369:256–7.
16. Zhang X, Tan Y, Ling Y, Lu G, Liu F, Yi Z, et al. Viral and host factors related to the clinical outcome of COVID-19. Nature. 2020;583:437–40.
17. Cao W, Li T. COVID-19: towards understanding of pathogenesis. Cell Res. 2020;30:367–9.
18. Zheng M, Gao Y, Wang G, Song G, Liu S, Sun D, et al. Functional exhaustion of antiviral lymphocytes in COVID-19 patients. Cell Mol Immunol. 2020;17:533–5.
19. Brodie T, Rothaeusler K, Sospedra M. OMIP-033: a comprehensive single step staining protocol for human T- and B-cell subsets. Cytometry A. 2016;89:629–32.
20. Baumgart S, Peddinghaus A, Schulte-Wrede U, Mei HE, Grützkau A. OMIP-034: comprehensive immune phenotyping of human peripheral leukocytes by mass cytometry for monitoring immunomodulatory therapies. Cytometry A. 2017;91:34–8.
21. Staser KW, Eades W, Choi J, Karpova D, DiPersio JF. OMIP-042: 21-color flow cytometry to comprehensively immunophenotype major lymphocyte and myeloid subsets in human peripheral blood. Cytometry A. 2018;93:186–9.
22. Payne K, Li W, Salomon R, Ma CS. OMIP-063: 28-color flow Cytometry panel for broad human Immunophenotyping. Cytometry A. 2020;97:777–81.

23. Park LM, Lannigan J, Jaimes MC. OMIP-069: forty-color full Spectrum flow Cytometry panel for deep Immunophenotyping of major cell subsets in human peripheral blood. Cytometry A. 2020;97:1044–51.

SUPPORTING INFORMATION

Additional supporting information may be found online in the Supporting Information section at the end of this article.